Technical
University
of Crete

Long-term prediction of temperature data for the assessment of future trends of the building heating and cooling loads

Post Graduate Program Environmental and Sanitary Engineering

Christina Georgatou

Chania 2015

Examination Committee

Dr Denia Kolokotsa, Assistant Professor (supervisor)

School of Environmental Engineering

....

Dr Kostas Kalaitzakis, Professor

School of Electronic and computer engineering

....

Dr Nikolaos Nikolaidis, Professor

School of Environmental Engineering

....

ABSTRACT

The present work focuses on the long term prediction of temperature data employing neural network models. Primarily, a benchmarking auto regressive model is developed. Then, different neural networks are developed regarding the network type, the training function and the training intervals. Temperature predictions are calculated for ten and for five year intervals. Each model's results are compared with the corresponding real temperature data, in terms of mean, maximum and minimum temperature values, cooling degree days and frequency distribution. The best predicted temperature data are used as outdoor temperature for the heating and cooling loads calculations of a typical office building. The building simulation model which is used for the energy demand calculations is the open source ESP-r model. The results indicate a relative accurate potential of the neural networks for the simulation of the mean temperature data and prediction of the cooling degree days. Regarding the high temperature values and the maximum peaks, the neural network models are unable to reach precise values, due to the lack of similar training data. As a result, the cooling loads calculated from neural network predictions are underestimated, while the heating loads prediction is more accurate.

ACKNOWLEDGMENTS

TABLE OF CONTENTS

1. Introduction

1.1 The aim of this study

During the Earth's history climate has varied amongst ages of relative warmth and relative cold. Though, it is evident that the temperature of the earth's surface and lower atmosphere has increased on average by about 0.6 °C over the past 100 years. Climate is the long-term statistical expression of short-term weather. According to NASA's climate research agency, earth has warmed since 1880. The temperature increase has deteriorated since the 1970s, while the 20 warmest years followed in 1981 with all 10 of the warmest years occurring in the past 12 years. Throughout these years, the energy consumption associated with the changes in the outdoor temperature has altered in terms of heating and cooling loads as well as the extent of greenhouse gases in the atmosphere, as a result of the burning of fossil fuels for energy and transportation. These changes have drag with them wider changes in the ecological balances such as land use changes, changes in water resources etc. Recent studies, concerns have grown that the amount of GHG and the temperature increase are partially related. As a result, global warming is nowadays considered most probably to be due to the increases in greenhouse gas emissions.

Regarding those temperature changes occurred in the past, the question arises whether this phenomena will continue to grow in the coming years and if yes, to what extent. This request exists not only because of the curiosity or the fascination of predicting the future. Numerous people work on predictions such as, meteorologists, engineers, business analysts. Long term weather predictions are mainly useful to prevent possible harms or to limit the damages. In the present study long-term prediction of temperature data are examined with the help of neural networks and used for the calculation of the thermal and cooling loads of a typical office building in Crete.

1.2 Methodology

In order to proceed with a long term temperature prediction, real temperature data have been collected from a meteorological station located in Greece, so the data are representative for the Greek-Mediterranean climate. For the purposes of this study, the temperature data are acquired by the Laboratory of Climatology and Atmospheric Environment (LACAE) of NKUA, from the city of Heraklion in Crete. The temperature data have a sampling rate from three to one hour step. The reference period of the temperature data are from year 1970 to year 2010. Firstly, the data are analyzed in daily and yearly means, winter and summer periods, in order to derive a representative overview of the temperature variations of the past forty years. Furthermore, a benchmark simulation model was developed using a seasonal autoregressive model (ARMA). Then, different types of neural networks (NN) have been developed with different training functions and training periods. The NN developed is of one layer type because, as has been observed, increase of the networks complexity

resulted in less accurate data. Predictions are calculated for ten and for five year intervals. The model results are compared in terms of mean, maximum and minimum temperature values, in the cooling degree days and in the frequency distribution (histograms). Subsequently, the predicted outdoor temperature data that are considered as the best results, are used as input to the heating and cooling loads model of a typical office building. The building simulation model used for the building energy demand calculations is the open source ESP-r model. The results revealed a relative potential of the neural networks to accurately simulate the mean temperature data and predict the cooling degree days. Regarding, the high temperatures and the maximum peaks, the neural network models are unable to reach those values, due to the lack of similar training data. This was also reflected in the cooling loads calculations. The results and discussion are presented in Chapter 5.

2. Solar radiation in the atmospheric boundary layer - Temperature

The present work focuses on processes and effects of physical phenomena which occur in the lower boundary of the atmosphere, near the surface of the earth. It is that part of the troposphere that is instantly affected by the surface of the earth and reacts to its forcings within about an hour or less. The lowest part of the atmosphere is where surface effects are most evident. This region is known as the atmospheric boundary layer (ABL) of the earth, and extends from the surface to ca 1 to 2 km high (in mid-latitudes can vary from 100 m to 3 km).

The surface of the earth has many intense effects on the atmosphere that impact our ability to understand and predict its manner of acting. The surface layer of the earth consists of several types and combinations of landscapes and constructions such as mountains, hills, lakes and seas, plants, and manmade structures. Each of the surfaces types differs in how it interacts with the atmosphere. The different interactions between surface and boundary layer are called surface and boundary layer processes. Surface and boundary layer processes define the amount of heat, water, gases; particles are exchanged between the surface and the boundary layer and between the boundary layer and the free atmosphere. In the definitions of fluid mechanics, a boundary layer is the layer of fluid in the immediate vicinity of a bounding surface where the effects of viscosity are significant. In the Earth's atmosphere, the atmospheric boundary layer is the air layer near the ground affected by diurnal heat, moisture or momentum transfer to or from the surface.

For example, more water will typically evaporate from a lake than from a pasture of the same size, and dark barren soil will absorb much more solar radiation than a bright snow surface. Also of interest is how the winds and temperatures within the lower part of the ABL are affected. The temperatures in the ABL reveal diurnal variations unlike the atmosphere above. The earth's surface influences the ABL by friction and by heat fluxes at the ground. The air flow in the ABL is characterized by turbulence, which is generated by wind shear (wind is approximately geostrophic at the top of the ABL but zero at the surface). Temperature gradients can either generate or suppress turbulence. [1]

Table 1. Comparison between Boundary layer and free atmosphere

Property	Boundary Layer	Free Atmosphere
Turbulence	Almost continuously turbulent over its whole depth	Turbulence in convective clouds
Friction	Strong drag against earth's surface. Large energy dissipation	Small viscous dissipation
Dispersion	Rapid turbulent mixing in the vertical and horizontal	Small molecular diffusion. Often rapid horizontal transport by mean wind.
Winds	Near logarithmic wind speed profile in the surface layer and subgeostrophic above.	Nearly geostrophic
Vertical transport	Turbulence dominates	Mean wind and cumulus-scale dominate
Thickness	Varies between 100 m to 3 km in time and space. Diurnal oscillations over land	Less variable. 8-18 km. Slow time variations

It is the layer where nature springs, humans live and all our activities occur and the pollutants disperse affecting the rest of the atmosphere. Furthermore, all meteorological conditions prevail considered for the study or forecasting of the climate changes, and the temperature variations.

During a clear day the boundary layer can be divided into several sublayers, as shown in Figure 1:

1. The roughness sublayer this is the layer of air in which air flows around individual roughness elements

(such as grass, plants, trees or buildings). It is the part in which the present work focuses.

2. The surface layer (formerly known as the constant flux layer) in this layer, typically 100 m thick (or 10%

of the depth of the ABL), the winds, temperature and humidity vary rapidly with altitude, and the characteristics of turbulence are affected by the surface. Vertical fluxes of heat and momentum are approximately constant.

3. The well-mixed layer rising buoyant plumes from the surface layer, and associated turbulence, cause potential temperature and other quantities to be relatively constant with altitude. The earth s rotation becomes important in this layer, and the wind direction veers with height.

4. The capping inversion on a summer s day the convective boundary layer is often capped by a temperature inversion, which inhibits mixing, and confines air and pollution below it to within the boundary layer.

At night a new stable nocturnal boundary layer grows as air is cooled from the surface. The daytime mixed-layer remains as a residual layer while the capping inversion is eroded. Sometimes the ABL is difficult to define; in the vicinity of fronts there is no obvious capping inversion and the ABL structure is more a response to synoptic forcing.
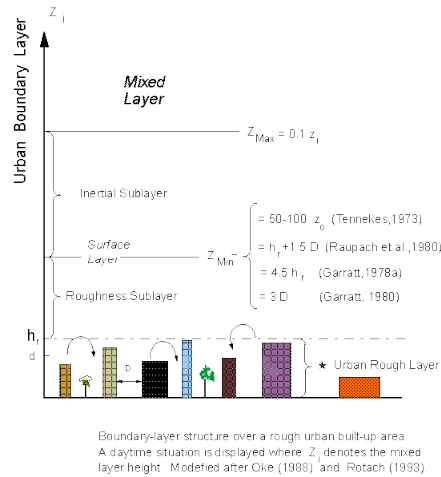
Figure 1. Boundary layer sublayers
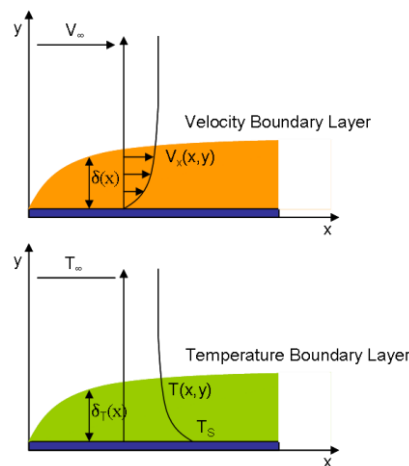
Figure 2. Velocity and temperature boundary layer similarity [2]

The flow of air and the thermal structure of the atmospheric boundary layer is defined by the Earth's surface. In particular, the surface energy balance, the separation of energy at the surface into diverse kinds, and the roughness of surface establish the temperature and the vertical profiles of wind and temperature in the boundary layer. Urban areas alter the material and aerodynamic character of the surface, greatly affecting the surface energy balance as well as the dynamic and thermodynamic nature of the boundary layer. These modifications to the local climate are the core topics of urban meteorology and urban climatology. [3]

The surface energy balance drives the diurnal variation in the ABL. For an infinitely thin surface layer of the ground, we have the following balance (with all terms in W/m^2):

$$R_n - G = H + \lambda E$$

where R_n is the net irradiance (net radiation) into the surface.

G is the ground heat flux density by conduction from the surface layer of the ground into the ground beneath.

H is the sensible heat flux density: the heating of the atmosphere by loss of energy from the surface.

λE is the latent heat flux density: the loss of energy by evaporation (the units of evaporation rate E is kg·$m^{-2} \cdot s^{-1}$ and the specific latent heat of evaporation equals 2.5 106 J kg-1).

The net radiation is the available energy at the earth's surface as it is converted into heat. The relocation of this energy crosswise the surface occurs primarily through three processes. Firstly is the process where heat is transferred from the Earth's surface to the atmosphere by conduction and convection sensible heat flux, Q_h Secondly, latent heat flux, Q_e, moves energy when solid and liquid water are converted into vapour. Finally ground heat flux, Q_g, is the transfer of sensible heat in the soil towards the surface or away from the surface. The following equation describes the partitioning of heat energy at the earth's surface. [4]

$$R_n = Q_h + Q_e + Q_g$$

The nature of the ABL is determined by the balance between H and E (or Q_h and Q_e), which depends on surface moisture availability. A convenient parameter is the Bowen ratio, defined as $B = H / \lambda E$ or

$$B = \frac{Q_h}{Q_e} = \gamma \frac{\Delta T}{\Delta e} \quad \text{with} \quad \gamma = \frac{PC_p}{\varepsilon L_v}$$

where γ is called the psychrometric constant, P is the atmospheric pressure, Cp is the specific heat of air at constant pressure, Lv is the latent heat of vaporization of water, ε is the ratio of the molecular weight of water vapor (Mw) to the molecular weight of air (Ma), T is the temperature, and e is the vapor pressure. The temperature is proportional to the sensible heat flux density Q_h. Hence, ΔT and Δe are the temperature and vapor pressure gradients respectively between the two heights of measurement.

The Bowen ratio is measured as the ratio of the gradients of temperature and vapor pressure across two fixed heights above the surface. All fluxes are positive downward. The Bowen ratio system is applied under the assumption that the turbulent transfer coefficients for sensible heat and water vapor are equal. [5]

Different surfaces are vegetated surfaces, oceans, urban areas, deserts, etc.

The boundary layer over an urban area is of particular interest as it is in this layer of the atmosphere that the majority of routine observations in urban areas are taken. It is therefore important to know what these observations represent. As air flows from one surface to another an internal boundary layer forms. The internal boundary layer is influenced by, but not fully adjusted to, the new surface and deepens with fetch. The internal boundary layer formed over urban areas is the urban boundary layer. The urban boundary layer is however a collection of successive internal boundary layers rather than one internal boundary layer due to the continual changing of building formations and densities across the urban area.
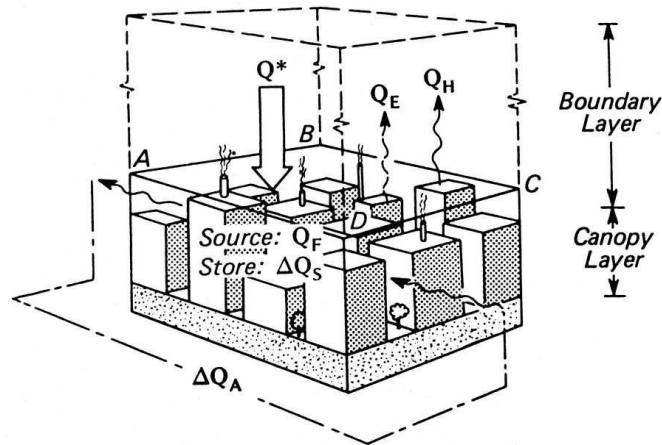
Figure 3. Schematic of the volumetric averaging approach to urban energy balance (after Oke, 1987). The base of the averaging volume is determined as the level across which there is negligible energy transfer on time scales of less than a day. Note the different notation: Q_ is the net radiation; QH the sensible heat flux; QE the latent heat flux; _QS storage; _QA the advective flux; and QF the anthropogenic heat flux.
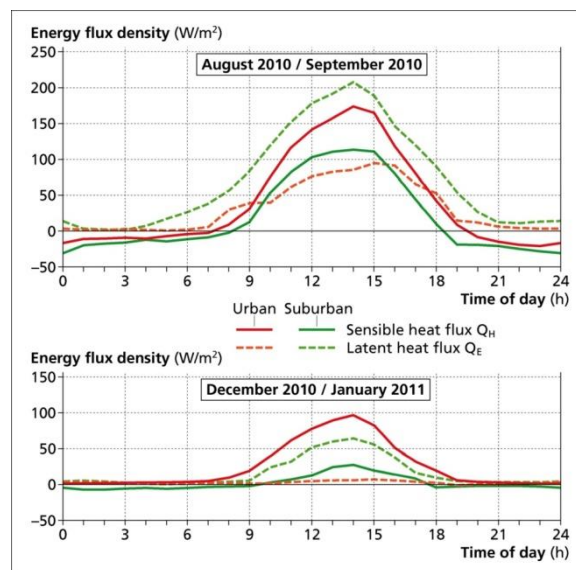

Figure 4. Average diurnal courses of turbulent heat flux densities (Q_H, Q_E) at an urban and suburban site in Oberhausen, Germany (source: Goldbach & Kuttler, 2012) [6]

2.1 Temperature at low altitudes in an urban environment – The Urban Heat Island

The climatic conditions prevailing in large built up areas differ from the climate of its rural surroundings. Unlike rural areas, built up areas denote higher air and surface temperatures, which happen mainly during climate conditions characterized by low winds and limited cloud cover. Urban climates differ in air temperature, humidity, wind speed and direction, as well as in the amount of precipitation. These differences result in large part from the alteration of the natural terrain through the construction of artificial structures and surfaces. Tall buildings, paved surfaces, and parking areas affect wind flow, precipitation runoff, and the energy balance of a

locale. Among other factors (Table 2), high daytime radiation, a negative radiation balance (Q*) in the evening and at night as well as a limited atmospheric exchange guarantee the development of a positive horizontal temperature difference between urban and rural, non-built-up surroundings. This phenomenon is called the urban heat island (UHI).[6] Urban heat islands are caused by development and the changes in radiative and thermal properties of urban infrastructure as well as the impacts buildings can have on the local micro-climate— for example tall buildings can slow the rate at which cities cool off at night. Heat islands are influenced by a city's geographic location and by local weather patterns, and their intensity changes on a daily and seasonal basis. [7]

Table 2. Meteorological and structural factors influencing the UHI (source: Kuttler 2009)

Influencing factor (IF)	Sign of correlation coefficient between UHI and IF
Cloud cover	-
Wind Speed	-
Anthropogenic heat emission	+
Bowen ratio B ($B=Q_H/Q_E$)	+
Population	+
Sky view factor (degree to which the sky is obscured by the surroundings at a given location)	-
Ratio building height/street width (H/W)	+
Surface sealing	+
Green and water surface area/total area	-
Latitude	+

Temperature changes resulting by the built-up setting affect people's health and comfort in addition to energy consumption and air quality. For that reason it is significant for the urban planners to learn about air temperature variations between different land use categories for both extreme situations and during average conditions. [8]. Furthermore is also of great importance to be able to provide accurate predictions in the longer term for the future situation for the study of climatic conditions, when designing a city.

In a built environment, solar energy is absorbed into infrastructure paving, roofs and facades of different materials, causing the increase of the surface temperature of urban structures to become 10 - 20 °C higher than the ambient air temperatures [9]. The albedo is a measure of the quantity of solar energy reflected by a surface In Figure 5 albedo values for different city surfaces can be seen. Low albedo implies higher surface temperatures since the larger amounts of energy are absorbed.

As surfaces throughout an entire community or city become hotter, overall ambient air temperature increases. [10] Buildings and urban constructions have different thermal properties from their natural surroundings. This results to a temperature excess in the build-up areas near-surface air layer. In addition to the UHI, many kinds

of UHIs can be defined. They include those defined according to the target medium, the location and the type of sensor. These UHIs do not appear inevitably in an "island" structure. Therefore in these cases it is more appropriate to talk about the urban temperature field or pattern. The determination of the surface temperature in cities is difficult because of the complex structure of the urban-atmosphere interface [11].
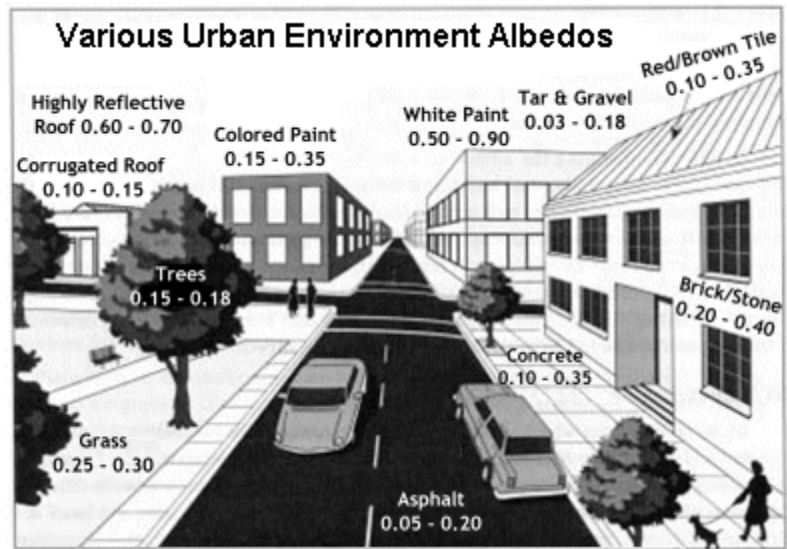

Figure 5. Albedo values for various urban surfaces [10]

Land surface temperature (LST) and its diurnal variation are crucial for the evaluation of the interactions between the urban land surfaces and the atmosphere. Land surface temperature (LST) is one of the key parameters of land-atmosphere energy exchange, climate change, and the global hydrological cycle. The diurnal variations of LST are strongly correlated with solar insolation, wind, and land surface characteristics, e.g. vegetation type, soil moisture, and surface structure [12], [13]. In greater built up areas the surface temperature is generally measured indirectly with the help of distant sense equipment although the sensors or cameras don't capture the total active surface because of the obstructions present on the 3D surface [14]. This study focuses on the air temperature in an urban environment. There are surface and atmospheric urban heat islands. These two types of heat island differ in their formulation, the techniques used to recognize and measure them, their impacts, and to some degree, the methods available to mitigate them. Table 3 summarizes the basic characteristics of each type of heat island [7].

Table 3. Surface and atmospheric UHI basic characteristics

Feature	Surface UHI	Atmospheric UHI
Temporal Development	Present at all times of the day and night Most intense during the day in the summer	May be small or non-existent during the day Most intense at night or predawn and in the winter

	More spatial and temporal variation Day: 10 – 15 ^oC Night: 5 – 0 ^oC	Less variation Day: -1 – 3 ^oC Night: 7 – 12 ^oC
Peak intensity (Most intense UHI conditions)	More spatial and temporal variation Day: 10 – 15 ^oC Night: 5 – 0 ^oC	Less variation Day: -1 – 3 ^oC Night: 7 – 12 ^oC
Typical Identification Method	Indirect measurement: Remote sensing	Direct measurement: Fixed weather stations Mobile traverses
Typical Depiction	Thermal Image	Isotherm map Temperature graph

The air temperature between the city buildings in a city web is affected by the temperatures of both horizontal and vertical surfaces. This compound impact and the individual effects of factors are complicated to be determined. Voogt and Oke (1997) introduced the concept of complete surface temperature which cannot be measured directly, but it can be calculated or estimated as a result of the radiation originating from all of the horizontal and vertical surfaces. [15]

The present study focuses on the field of impact which has an influence on the temperature of the near-surface air temperature.

2.2 Air temperature variations over the last 100 years

People are observing the world's average temperature from the late 19th century where weather stations began to record measurements more steadily. On January 1923 "A period of warm winters in Europe " was published by C. E.P. Brook, stating an abnormal winter warmth in central Europe, during the decade 1911-1920. [16] By the 1930s, observers had accumulated millions of numbers for temperatures at stations around the world and realized there had been a obvious warming trend, at least in eastern North America and western Europe, the only parts of the world where reliable measurements went back so far, while the press began to call awareness to several anecdotes of above-normal temperatures. Experts considered this was simply one phase of a cycle of increasing and decreasing temperatures that probably fluctuated over centuries. Scientists stated, when they referred to a contemporary "*climate change*" this was not an everlasting alter, but a long-term cyclical change "like all other climate fluctuations". Temperature data were such disorderly that with adequate manipulation someone could obtain several forged trends. An English engineer, named Guy Stewart Callendar sorted out data by his effort assessing the average global temperature, and was the first who he announced in 1938 that the mean global temperature between 1890 and 1935 had beyond doubt risen, by close to 0.5°C. Furthermore, reviving an old theory that human emissions of carbon dioxide gas (CO_2) from burning fuel could cause a "greenhouse effect," Callendar said this was the cause of the warming. The climatologist Helmut Landsberg, found also in 1958 a considerable warming in the first half of the century, especially in the northern latitudes at an average 0.8°C.

This fact was amplified by the climate historian Hubert H. Lamb in 1959 who wrote "*Our attitude to climatic 'normals' must clearly change*". During the next decade 1960s and into the 1970s, the average global temperature remained cool while Western Europe in particular suffered some of the coldest winters on record. This observation led many scientists to believe that the global warming reported for the decades before 1940 had been an illusion. To this concept counted the argument that most temperature measurements came from built-up areas. The expansion of the urban limits, led to local temperature increase (a preliminary conception of the UHI idea), which might have given a fake sense of global warming.

Moreover few experts expressed the opinion that human sources pollution, was starting to shade and cool the earths' surface although the more adequate explanation was again that the earth was responding to long-term fluctuations in the Sun's output of energy.

J. Murray Mitchell, an American climatologist published in 1975 a study about atmospheric pollution (carbon dioxide and particulate loading) of long-term changes, and the impact of such changes on the equilibrium temperature of the Earth, where it was assumed that there was really a natural cycle responsible for the cooling in the past decade, only temporarily preventing the greenhouse warming.

Many experts saw at that time no concrete evidence that warming would continue in the future. Trustworthy records covered hardly a century and showed large variations in particular between 1940 and 1970. Most of them expected that evidence would come into sight clearly around the end of the century, but not earlier.

By the late 1990s, numerous kinds of proof indicated a general warming at surface level such as that the spring in the Northern Hemisphere was coming on average a week earlier than in the 1970s. This was confirmed by much more diverse measures as in the earlier years as well measured in satellite pictures. A more essential indicator became the temperature of the upper ocean layers where most of the heat entering the climate system was stored and a serious rise was found in recent decades. By this time, the 1990s were indubitably the warmest decade since thermometers came into common use, and the trend was accelerating. [17]
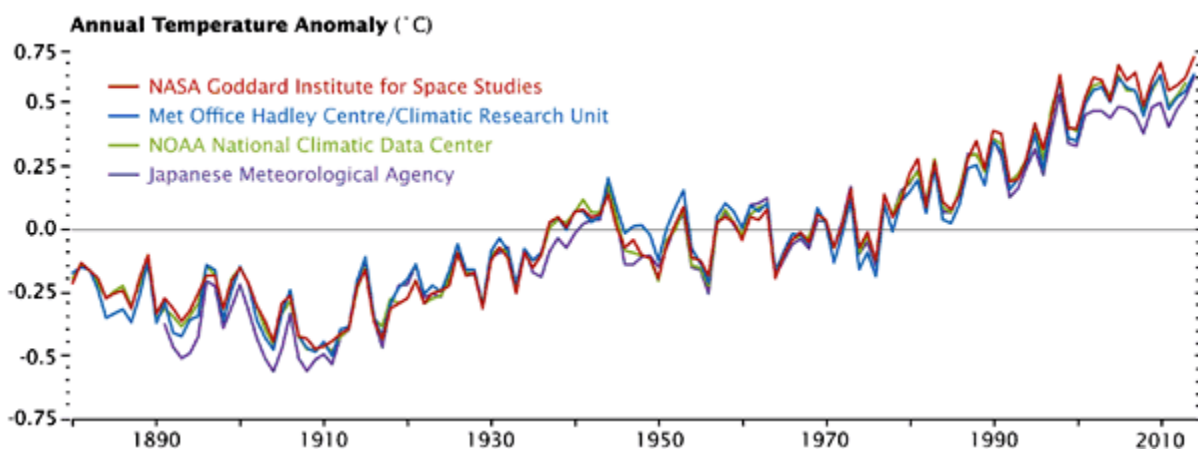

Figure 6. Global temperature 1880-2014 - Average annual surface air temperatures, based on

measurements by meteorological stations, ships and satellites, as analyzed using independent methods by four different groups. (Source: NASA Earth Observatory.)

Through the last decade, research on the earths' mean surface air temperature has shown that its increase relies partially on differential changes in daily maximum and minimum temperatures, leading to a reduction of the diurnal temperature range (DTR). Diurnal temperature range (DTR) is a meteorological indicator independent of internal climate variation and therefore, considered as a signature of observed climate change. It has been observed that global averaged DTR has decreased significantly in the last fifty years. However, the change in DTR has regional and seasonal characteristics.[18] In general, the amplitude of the diurnal air temperature variation is reduced by the presence of vegetation, cloud cover, smoke, haze, and strong winds. If the vegetation is dense or tall, it reduces the incoming radiation by absorption and reflection, and acts as the primary source of radiation during the night. The general effect is that the vegetative surface is subject to much less temperature variations than bare soil. They reveal that there is a seasonal dependence of the diurnal variation of the air temperature amplitude on season and height. These average temperature variations are mainly a consequence of the daily and seasonal change of short-wave radiation, while the diurnal variation for particular cases is also strongly influenced by cloudiness, wind speed, atmospheric stability, etc. [19]

Temperature analysis, using modern weather stations and with a wider coverage of the Southern Hemisphere, show that the DTR is continuing to decrease in most parts of the world, that urban effects on globally and hemispherically averaged time series are insignificant, and that circulation variations in parts of the Northern Hemisphere appear to be related to the DTR. [20] According the *Union of Concerned Scientists Global Warming Effects Around the World* [21] the last decade 2001-2010 was the warmest since 1880. Moreover during the last 50 years a decline of cold days and low temperature records is observed in combination to a rise of hot days and heat waves worldwide. The best projections demonstrate that average global temperatures are likely to increase 1.8-4.0° C by the end of the century depending on the quantity of carbon emissions.

Regarding the Mediterranean area the occurrence of increased temperatures is very strong in South East Mediterranean where recent studies have shown unusual temperature anomalies due to climate change.

In parallel, recent analysis has shown that the heat island phenomenon is present in the major cities of the specific area, while presenting a noteworthy increase in its intensity. [22]

2.3 Temperature and Thermal Energy

So far, measurements of the temperature in the lower surface layer are described as an extent of how hot or cold the air is or as the heat intensity present in the air and expressed according to the scale of Celsius degrees. Microscopically, Kelvin temperature is a measure of the average kinetic energy of the atoms or

molecules in a substance. Temperature is something like a level of agitation that is low when the atoms and molecules are gently oscillating and rotating. It is high when atomic motion becomes hectic and turbulent. The temperature in a body can be compared to the strength of winds in the atmosphere with low values when the leaves rustle, but higher ones when the branches start swinging. Just as high winds can break whole trees, high temperatures can cause atoms to tear away from their bonds. Thermal energy is the total internal energy of the atoms or molecules of a substance. As thermal energy is added to a substance, the motions of the molecules increase, and we say the substance is hotter, i.e. its temperature increases. Temperature is not the same as heat. Heat is energy in transfer. Heat is thermal energy that is being transferred between two places and is measured in the same units as energy. Heat is the kinetic energy of molecules being transferred.

The usual unit of thermal energy is the calorie (c) or the joule (j) or the British thermal unit BTU. The energy E in joules (J) is equal to the power P in watts (W), times the time period t in seconds (s):

$$E(J) = P(W) \times t(s) \quad or \quad J = W \times s$$

In Table 4, the equivalences of the thermal energy units are depicted.

Table 4. Thermal energy units

Thermal Energy Units	Calorie (c)	Joule (J)	BTU	Watt-hour (Wh)
Calorie (c)	1.00	4.18400	0.00396566683	0.00116222222
Joule (J)	0.239005736	1.00	0.00094781712	0.000277778
BTU	252.164401	1 055.05585	1.00	0.29307107
Watthour (Wh)	860.42065	3600	3.41214163	1.00

The *transfer of thermal energy as heat* requires a difference in temperature between the two points of transfer. Heat may be transferred by means of *conduction*, *convection*, or *radiation*.

Conduction is the transfer of thermal energy (heat in transfer) due to collisions between the molecules in the object. Collisions between adjacent atoms and molecules transfer kinetic energy from the warmer to the cooler object. The objects must be in physical contact. How rapidly an object transports thermal energy by conduction depends, in part, on what material the object is made of. This property is known as thermal conductivity (k), a constant indicating how easily heat is transferred through a substance.

$$Heat\ transfer\ Q = \frac{energy\ transfer}{time} = \frac{K \cdot A \cdot (T_{hot} - T_{cold})}{L}$$

Where

K= the thermal conductivity ($\frac{J}{s \cdot m \cdot \,^{o}C}$ or $\frac{BTU}{inch \cdot hour \cdot foot^{2} \cdot \,^{o}F}$)

A = the cross sectional area (m^2 or f^2)

T = temperature (^{o}C or o ^{o}F)

L = thickness (m or in)

Convection is thermal energy transferred by the flow of matter. It is the transfer of thermal energy due to the motion of the substance that contains the thermal energy. Although the conduction process can occur in liquids and gases as well as solids, convection may have a much larger effect in liquids and gases where the molecules are free to migrate.

Radiation is the transfer of energy by electromagnetic radiation. Radiation can travel in a vacuum. In conduction and radiation, an energy transfer occurs without the transfer of mass. It is found that energy can be transferred by radiation from one location to another. No medium, such as air or water, is needed for the radiation to travel and transfer energy. It can pass through a perfect vacuum, as energy from the sun does in reaching earth. If you stand near an open fire such as a campfire, you notice that the side of you facing the fire becomes much warmer than the other side even if no wind is blowing. The explanation is that energy is transferred from the burning material to you via electromagnetic radiation. Of course, a small amount of energy is also transferred as heat via conduction and convection. For a campfire most of the radiant energy is infrared radiation. Thermal resistance (R) is a heat property and a measurement of a temperature difference by which an object or material resists a heat flow. In terms of insulation, the thermal resistance is measured by the R −value. The R-value is a measure of thermal resistance used in the building and construction industry. Under uniform conditions it is the ratio of the temperature difference across an insulator and the heat flux (heat transfer per unit area per unit time,$\dot{Q}_A$). Thermal resistance varies with temperature but it is common practice in construction to treat it as a constant value. An R-value is a unit thermal resistance for a particular material or assembly of materials (such as an insulation panel). The R-value depends on a solid material's resistance to conductive heat transfer. For loose or porous material, the R-value accounts for convective and radiative heat transfer through the material. However it does not account for the radiative or convective properties of the material's surface, which may be an important factor for some applications. R is expressed as the thickness of the material normalized to the thermal conductivity. The unit thermal conductance of a material is the reciprocal of the unit thermal resistance. This can also be called the unit surface conductance. The higher the value of R, the better the building insulation's theoretical effectiveness. R-value is the reciprocal of U-factor. The overall heat transfer coefficient is employed in calculating the rate of heat transfer $\dot{Q}$ from one fluid at an average bulk temperature T_1 through a solid surface to a second fluid at an average bulk temperature T_2 (where $T_1 > T_2$). The defining equation is generally only applicable to an incremental element of heat transfer surface dA for which the heat transfer rate is $\dot{Q}$, and the equation is strictly valid only at steady state conditions and negligible lateral heat transfer in the solid surface, conditions generally true enough in most practical applications. The defining equation is:

$$d\dot{Q} = U(T_1 - T_2)dA$$

where U is referenced to a specific surface (see below).

In the particular situation of heat transfer across a plane wall of uniform thickness, U is related to the individual film heat transfer coefficients, α₁ and α₂, of the two fluids by the equation:

$$U = \frac{1}{\frac{1}{a_1} + \frac{\delta_w}{\lambda_w} + \frac{1}{a_2}}$$

where δ_w is the thickness of the wall and λ_w is the thermal conductivity of the wall.

If there are fouling deposits on the wall, they have a resistance to heat transfer, R₁ and R₂, in units of m² K/W, and these resistances must be added in:

$$U = \frac{1}{\frac{1}{a_1} + R_1 + \frac{\delta_w}{\lambda_w} + R_2 + \frac{1}{a_2}}$$

For the special but very important case of heat transfer through the wall of a plain round tube, the different heat transfer areas on the inside and outside surfaces of the tube need to be considered. Let dAᵢ be the inside incremental area and dA_0 be the outside. Then (including fouling resistances R_{fi} and R_{f0} inside and out):

$$U_0 = \frac{1}{\frac{1}{a_i} + R_{fi} + \frac{r_i \ln(\frac{r_o}{r_i})}{\lambda_w} + R_{f0} + \frac{r_i}{r_0} + \frac{r_i}{a_0 r_0}}$$

where U_0 is termed the "overall heat transfer coefficient referenced to (or based on) the inside tube heat transfer area", and r_i and r_0 the inside and outside radii of the tube. Alternatively, the overall coefficient may be based on the outside heat transfer area, giving:

$$U_0 = \frac{1}{\frac{r_o}{a_i r_i} + R_{fi}\frac{r_0}{r_i} + \frac{r_0 \ln(\frac{r_o}{r_i})}{\lambda_w} + R_{f0} + \frac{1}{a_0}}$$

where U_0 is termed the "overall heat transfer coefficient based on the outside tube heat transfer area." Note that:

$$d\dot{Q} = U_i(T_1 - T_2)dA_i = U_0(T_1 - T_2)dA_0$$

These ideas may be extended to more complicated surfaces such as finned or composite tubes, but it is then necessary to add further resistance terms (and the area ratio corrections) for the fins or imperfect metal-to-metal contact. Generally, in order to use these equations in heat transfer applications, the basic equation must be integrated:

$$A_T = \int_0^{Q_T} \frac{d\dot{Q}}{U \ (T_1 - T_2)'}$$

Where A_T is the total area required to transfer $\dot{Q}_T$ and T_1, T_2 and sometimes U must be expressed as functions of the heat already transferred from one end up to a given point in the heat transfer device. This is the basic design equation for most heat exchangers. The thermal energy that must be supplied to or removed from the interior of a building in order to maintain the desired comfort conditions is described as heating or cooling load.
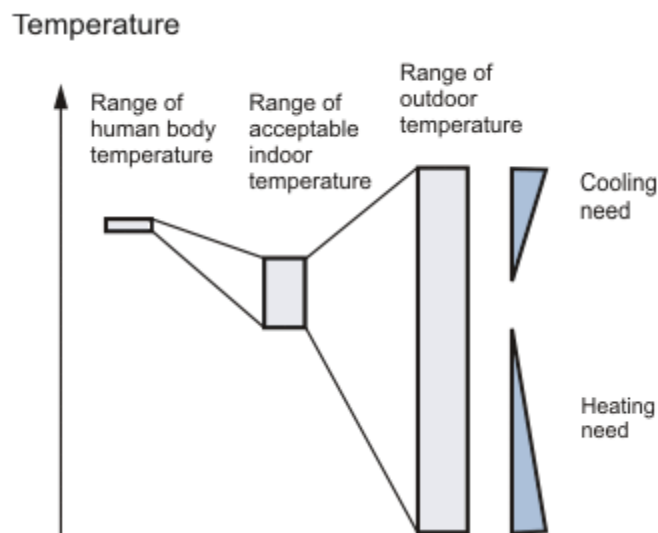
Figure 7. Schematic representation of the heating and cooling needs of a building

Heating and cooling degree days are measures that reflect the amount of energy needed to heat or cool a building to a comfortable temperature, given how cold or hot it is outside. A "degree day" indicates that the daily average outdoor temperature is one degree higher or lower than some comfortable baseline temperature (in our case 18.6 °C for heating or 26 °C for cooling) on a particular day. The sum of the number of heating or cooling degree days over a year is approximately related to the annual amount of energy that would be needed to heat or cool a building in that location.

2.4 Theoretical background investigations linking fluctuations of temperature data with the heating and cooling loads

Nowadays it is evident that the increase of urban temperatures has a serious impact on the energy demand of buildings by increasing significantly the energy consumption for cooling, while decreasing to some extent the energy consumption for heating. Moreover the urban landscape creates a climate which affects, human comfort, air quality and energy consumption. Though, regardless of these facts, climate issues often have low impact on the urban planning process in practice. [23] Investigation on the subtropical climates such as the Mediterranean region have shown an increasing trend of temperature and summer discomfort over the past decades while studies converged on the outcome that temperature increase leads to higher building cooling demand. Higher air conditioning requires more electricity use and thus more carbon emissions which consecutively would deteriorate global warming. Regarding the northern climates where higher temperatures could lower the heating energy, the consequences of climate change on the total requirements on primary energy are doubtful. That is because heating is less ordinary provided by electricity and more likely by oil- or gas-fired boiler plants opposed to electricity-driven air conditioners. Heating and cooling energy requirements as well as their trends and changes are of importance taking into account the national o worldwide energy and environmental perspective. In general these estimations are approached either by calculating the degree days with the appropriate temperature set points (usually for Greece they are 18.6-20°C for heating and 26°C for cooling) or through building energy simulation models.

Moreover, considering buildings with large internal heat gains and non-domestic use, with many visitors, electrical equipment and lighting, the annual energy is larger for cooling than for heating. As a result, regardless the climate zone, the total required building energy would increase mostly in a hot or warmer summer and as well as warm winter periods where building energy use is dominated by cooling requirements.

 Most of the climatic information currently used for building design and energy analysis is historical and there is a need for regular revision and updating taking the prospects of future climate change into consideration, especially the impact of temperature extremes on the selection of outdoor design conditions. More work on a continuing, regular basis is required. [24]

According to Christenson et al. [25] weather data currently used for building design would increasingly lead to an overestimation of heating and underestimation of cooling demand in buildings and, therefore, require

periodic adaptation. Greater attention should be paid in future to the summer thermal behavior of buildings. During 1901–2003, the HDD were found to have decreased by 11–18%, depending on the threshold temperature (8, 10 or 12 °C) and location. For the period 1975–2085, the scenario calculations suggested a further decrease between 13% and 87%. For CDD, accelerating positive trends were found during the 20th and 21st centuries.

Pilli-Sihvola et al. [26] examined the impact on the increasing temperatures in five European countries in alongside a south–north contour with different climates, namely Spain, France, Netherland, Germany and Finland. The results show clear increasing temperature impacts on electricity demand and costs, with a decrease in the required heating energy in the central and northern European regions and an increase in the cooling energy demand in the southern Europe.

Day et al. [27] investigated the CDDs in London stating that by 2030, without control, the increase in active cooling systems in London could lead to a doubling of CO_2 emissions. The emissions raise relies on the increase in building stock, in the cooling systems market share and on climate change. The last of these is difficult to predict, but by itself could add 260,000–360,000 tones of CO_2 emissions by 2030. This increase can be strongly mitigated, or even offset, by improvements in system efficiency. The difference between no efficiency improvements and an assumed 1–3% annual efficiency improvement is around 340,000 tonnes by 2030.

Regarding our Mediterranean region, Cartalis et al. [28] analyzed the HDD and CDD alterations, finding a decline in heating and increase in cooling energy requirements. Furthermore, Mirasgedis et al. [29] investigated the HDDs and CDDs for the mid-term prediction of electricity demand in Greece, estimating an increase of 3.6-5.5% in the annual electricity demand because of the climate change in the 21st century. Santamouris et al. [30], [31] calculated the spatial distribution of the cooling needs of different typical buildings for different urban zones in the city of Athens. Because of the heat island effect, the cooling needs as well as the peak electricity demand for cooling in the affected areas, increased up to 100% compared to the corresponding load in the suburban areas around the city.

As one can observe, the temperature increase affects the building energy demand by several ways depending on the geographical position, the main climate zones as well as on the most established energy use for heating and cooling requirements. In national, European but also worldwide viewpoint the energy and environmental strategies are formed and influenced by those factors. Heating is mostly managed with oil- or gas-fired boiler plants, while cooling systems operate more with electricity. The increasing temperatures, electricity demand and carbon emissions can be investigated with different energy sources, conventional fuels or in order to further investigate, adapt or mitigate the impact of climate change on the energy use in the built environment. For example, in the Mediterranean region, solar-powered cooling is very attractive due to the concurrency of the maximum cooling requirements and solar intensity. Furthermore, regarding large non domestic constructions advanced building energy management systems taking into account the indoor and outdoor environmental parameters and short term predictions can significantly mitigate the building's energy requirements. Nevertheless, additional efforts are required for an adaptive thermal comfort in the current building design guidelines and energy codes and in the existing building stock, engaging socio-economic aspects of building occupant behavior.

2.5 Incentives in long term forecasting

The 21st century projections of the temperature increase combined with the negative effects of the present extreme climate events, results to more investigation on climate adaptation techniques, as well as forecasting in urban areas for the next years.[32] The applied environmental engineering science and urban planners need decision making techniques on climate change adaptation and mitigation strategies. The historical data can become a reliable background however the changing nature of our climate needs a gradual revision taking into account the impact of future increase of temperature. Though this regular revision and recalculation of temperature trends can be implemented with an adequate time step from one minute to decades ahead, depending on the application. For example, a modern building energy management system requires indoor or outdoor temperature predictions of a daily time step or less in order to manage the building energy requirements. On the other hand, decision making on adaptation and mitigation strategies and policies have a time horizon of 5 to 50 years. For example the 2020 Renewable Energy Directive sets regulations for the EU to achieve its 20% renewable target by 2020, the EPDB directive sets rules moving towards new and retrofitted nearly-zero energy buildings by 2020 or the 2050 roadmap for moving to a low-carbon economy, with the suggestion to reduce the emissions around 90% by 2050, when global warming is to be held below 2°C compared to the temperature in pre-industrial times. Moreover, when studying new energy efficient building constructions, or when suggesting rehabilitation actions, one must consider them through the whole lifespan of a building because of the preventive cost of a regular refurbishment or reconstruction. As a result, it is a necessity to be aware of the longer term climatic conditions and temperature data. However, long term projections of such a stochastic physical quantity as temperature can never be reliable, it will always require worldwide monitoring, corrections, forecasting again beyond the time intervals of observation and so forth, and so on, from Guy Stewart Callendar in 1938 till the future scientists.

outdoor temperature prediction can be used as input to indoor conditions predictive algorithms [33] which are used for testing genes of an optimization algorithm

2.6 Prediction algorithms, neural networks assets

Time series analysis and forecasting has been developed to a useful instrument in numerous applications in environmental engineering and other scientific areas in order to understand the evolving of environmental parameters, like solar radiation, temperature, wind potential, humidity, etc., over time. Atmospheric time series data demonstrate often a seasonal behavior yet not indubitable deterministic. As mentioned in Par. 2.5 understanding the nature and the degree of probable climate changes is of importance to engineers and policy makers as it gives them a chance to be prepared for better mitigation and adaptation measures. Time series analysis of climatic data is the key for the analysis and for the long term forecasting of the environmental parameters affecting the urban climate. Although any individual extreme climate event cannot be attributed

unequivocally to climate change, the probability of high temperature events will increase if there is an underlying trend of rising mean temperature. In fact, according to data from the reinsurance industry, the number of climate related disasters has increased significantly the 1970's. [34]

Various types of time series data either it is business - economic or atmospheric and environmental data are characterized by a strong, but not necessarily deterministic, seasonal behavior. The seasonal pattern may arise simply because observations at the same time point of the year are dynamically related across the years.

The probability density function gives the probability of specific temperature data to occur. It does not give any indication of how the temperature will vary in the future based on how it varied in the past. It does not give any information about the 'memory' of the time series temperature variables or the degree of their dependence. The function that gives us the abovementioned information is called autocorrelation function. This function results by multiplying each value of the time series with values of the same time series shifted in a number of places (lags) from the first value. The results added up to a value for each lag and normalized by dividing by the variance. The autocorrelation coefficient r of a time series $y_1, y_2 \ldots y_n$, for lag k is given by the formula:

$$r_k = \frac{\sum_{i=1}^{n-k}(y_{k+1} - \overline{y})(y_i - \overline{y})}{\sum_{i=1}^{n}(y_i - \overline{y})^2} \qquad (1)$$

When analyzing the dynamics of climatic variables, these are frequently considered to be a realization of stochastic processes associated with deterministic components for trend and seasonality. Time series models, such as the auto-regressive (AR) model, are tools for modelling the stochastic processes.

These models taken into account the dependence of chronologically ordered observations. It is based in an analysis which was developed by G.P. Box and M. Jenkins (1970) who introduced univariate models for time series which simply made systematic use of the information included in the observed values of time series. This offered an easy way to predict the future development of this variable. Today, the procedure is known as Box-Jenkins Analysis and is widely applied.[35]

A first order autoregressive process, an AR(1) process, can be written as an inhomogeneous stochastic first order difference equation,

$$x_t = \delta + a x_{t-1} + u_t$$

The justification for automatic ARMA modeling is the following:

- the method for building an ARMA model is somewhat complex and requires a deep knowledge of the method;
- consequently, building an ARMA model is often a difficult task for the user, requiring training in statistical analysis, a good knowledge of the field of application, and the availability of an easy to use but versatile specialized computer program;

- the number of series to be analyzed is often large. It is important to note, that nowadays, the most used commercial tools for the time-series forecasting (Stat graphics, SPSS, etc.) required intervention of an human expert for the definition of the ARMA model.

Traditional time series methods relied on the concept of probabilistic statistics, though lately, the idea of neural networks has also been integrated into time series forecasting. Following effort to overcome the disadvantages of the linear methods, while at the same time the development and expansion of artificial intelligence have resulted in the development of nonlinear modeling. In this kind of nonlinear modeling approach belong the Neural networks which are able to provide a fairly accurate universal approximation to any function. For that reason they can be trained to forecast the potential future values of a dependent variable. While parameters of other nonlinear models need to be determined, neural networks are in many cases preferable because there is no need of a previous declaration of the models is for the process under consideration. It is important to note that in the literature of time series forecasting with artificial neural networks (ANN), the ARMA model is used as a benchmark to test the effectiveness of the proposed methodology. [36] A basic tenet of the ARMA modeling approach is the assumption of linearity among the variables. However, there are many time series events for which the assumption of linearity may not hold. Clearly, ARMA models cannot be effectively used to capture and explain nonlinear relationships. When ARMA models are applied to processes that are nonlinear, forecasting errors often increase greatly as the forecasting horizon becomes longer. [37]

An Artificial Neural Network (ANN) is an information processing paradigm that is inspired by the way biological nervous systems, such as the brain, process information. The key element of this paradigm is the novel structure of the information processing system. It is composed of a large number of highly interconnected processing elements (neurons) working in unison to solve specific problems. ANNs, like people, learn by example. An ANN is configured for a specific application, such as pattern recognition or data classification, through a learning process. Learning in biological systems involves adjustments to the synaptic connections that exist between the neurons. This is true for ANNs as well. The first artificial neuron was produced in 1943 by the neurophysiologist Warren McCulloch and the logician Walter Pits. But the technology available at that time did not allow them to do too much. The neural networks re applied in simulation techniques or to explain problems requiring human perceptive approach. The central processing component of a neural network is a neuron, which can process a local memory and can carry out localized information. Each neuron computes a weighted sum of the inputs it receives and adding it with a bias (b) to form the net input (x). The bias is included in the neurons to allow the activation function to be offset from zero,

$$x = w_{1,1} \cdot p_1 + w_{1,2} \cdot p_2 + ... + w_{1,j} \cdot p_j = b$$

The net input (x) is then passed to the subsequent layer through a non-linear sigmoid function to form its own output

$$y_j = \frac{1}{1 + e^{-x}}$$

Afterward, the output y_j was compared with the target output t_j using an error function of the form

$$\delta_\kappa = (t_j - y_j) y_j (1 - y_j)$$

For the neuron in the hidden layer, the error term is given by the following equation:

$$\delta_j = y_j (1 - y_j) \sum \delta_\kappa w_k$$

where δ_κ is the error term of the output layer, and w_κ is the weight between the hidden layer and output layer. The error can also be propagated backward from the output layer to the input layer to update the weight of each connection as follows [39]:

$$w_{ij}(t+1) = w_{ij}(t) + \eta \delta_j y_j + a(w_{ij}(t) - w_{ij}(t-1))$$

A neural network consists of an input layer, an output layer and one or more intervening layers also referred to as hidden layers. The hidden layers capture the nonlinear relationship among the time series variables. Each layer consists of multiple neurons that are connected to neurons in adjacent layers. Since these networks contain many interacting nonlinear neurons in multiple layers, the networks can capture relatively complex phenomena.

The training of a neural network is achieved by assessing the features and characteristics of the time series using the historical data. The model parameters as the connection weights w_{ti} and node biases b are adjusted iteratively by a process of minimizing the forecast errors. For each training iteration, an input vector, randomly selected from the training set, is submitted to the input layer of the network being trained. The output of each processing unit (or neuron) was propagated forward through each layer of the network, using the equation

$$NET_t = \sum_{i=1}^{N} w_{ti} x_i + b_t$$

Where NET_t is an output of unit t

w_{ti} is the weight on connection from the i_{th} to the t_{th} unit

x_i is an input data from unit i (input node) to t

b_t denotes a bias on the t_{th} unit; and

N is the total number of input units. A bias or activation threshold of a proper magnitude can affect output activation in the same manner as imposing a limit on the network mapping function.
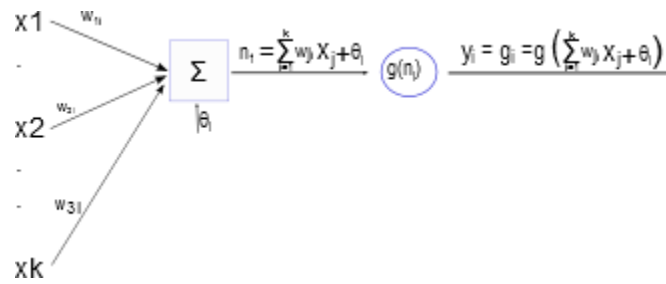
Figure 8. Single node in an ANN network

The procedures for developing the neural network model are as follows [40]:

(a) Normalize the learning set;

(b) Decide the architecture and parameters: i.e., learning rate, momentum, and architecture. The selection of transfer functions performed by artificial neurons has been so far little explored ways to improve performance of neural networks in complex problems. The simplest approach is to test several networks with different transfer functions and select the best one. [41]

There are no criteria in deciding the parameters except on a trial-and-error basis;

(c) Initialize all weights randomly;

(d) Training, where the stopping criterion is either the number of iterations reached or

when the total sum of squares of error is lower than a pre-determined value;

(e) Choose the network with the minimum error;

(f) Forecast future outcome.[38]
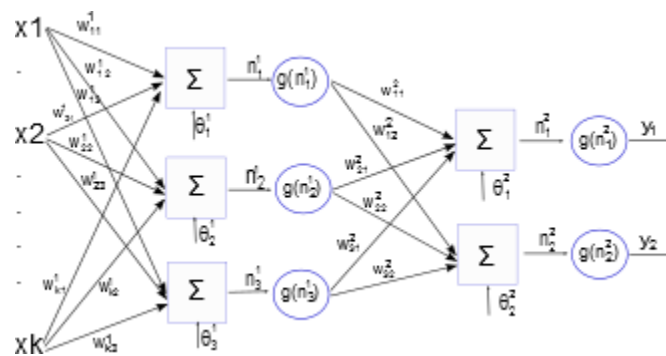
Figure 9. A multilayer perceptron network with one hidden layer. Here the same activation function g is used in both layers. The superscript of n, θ , or w refers to the layer, first or second

During the development of the prediction techniques, it was found that ARIMA models can be linked with neural networks to improve the accuracy of the forecasting. Maia et al. have used auto regressive moving average models (ARMA) with neural network and Maia et al. present models for interval valued time series forecasting based on AR, ARIMA and Artificial Neural Networks. [42] the hybrid model using ARIMA to model the linear

component of the series and artificial neural networks to capture the nonlinearity aspects achieved the best average performance concerning the error measures considered.[43]

Autoregressive integrated moving average (ARIMA) is one of the popular linear models in time series forecasting during the past three decades. Recent research activities in forecasting with artificial neural networks (ANNs) suggest that ANNs can be a promising alternative to the traditional linear methods. ARIMA models and ANNs are often compared with mixed conclusions in terms of the superiority in forecasting performance. [44] Many of the hybrid ARIMA–ANN models which exist in the literature apply an ARIMA model to given time series data, consider the error between the original and the ARIMA-predicted data as a nonlinear component, and model it using an ANN in different ways. Though these models give predictions with higher accuracy than the individual models, there is scope for further improvement in the accuracy if the nature of the given time series is taken into account before applying the models. [45]

3. Calculation Methodology

3.1 40 years' time series data

According to the fourth IPCC report for climate change in 2007 [20], the Mediterranean Basin will be among the areas to be most adversely affected in terms of a rise in temperature, a decrease in overall water balance and a higher frequency of extreme climatic events. The findings of the analysis of the fifth report in 2013, indicated that the mean annual CDD appear maxima in the southeastern Aegean Sea, while minima are found in northwestern Greece [21].

Furthermore, WMO's provisional statement on the Status of the Global Climate in 2014 indicated that the global average air temperature over land and sea surface for January to October was about 0.57° Centigrade (1.03 Fahrenheit) above the average of 14.00°C (57.2 °F) for the 1961-1990 reference period, and 0.09°C (0.16 °F) above the average for the past ten years (2004-2013). [46]

In order to initiate the development of the prediction methodology, hourly environmental parameters covering the forty year period 1970–2010 from one meteorological Station of the Hellenic National Meteorological Service (HNMS) in Heraklion-Crete was used. E 25° 18' 15"   N 35° 17' 55" [47]. The accuracy of their temperature measurement devices (thermometers) and their relative humidity measurement devices is 0.2^o C and 1% respectively.

As a first outline, Heraklion has a Subtropical-Mediterranean climate. Summers are warm to hot and dry with clear skies. Dry hot days are often relieved by seasonal breezes. Winters are very mild with moderate rain. Measurements from the aforementioned meteorological station have already been used in previous studies regarding the climate change and the UHI in Mediterranean areas. J. Kapsomenakis et.all (2013) [22] used the data of the Heraklion station together with other measurement points in Greece, in order to understand the impact of air temperature and relative humidity trends on the energy consumption of buildings. P.T. Nastos et.all (2009) to find out the spatial and temporal variability of the dry and wet spells in Greece, during the period 1958–2007.

3.2 Statistical analysis of existing data

In Figure 10-Figure 20, the temperature data used in our study are presented.
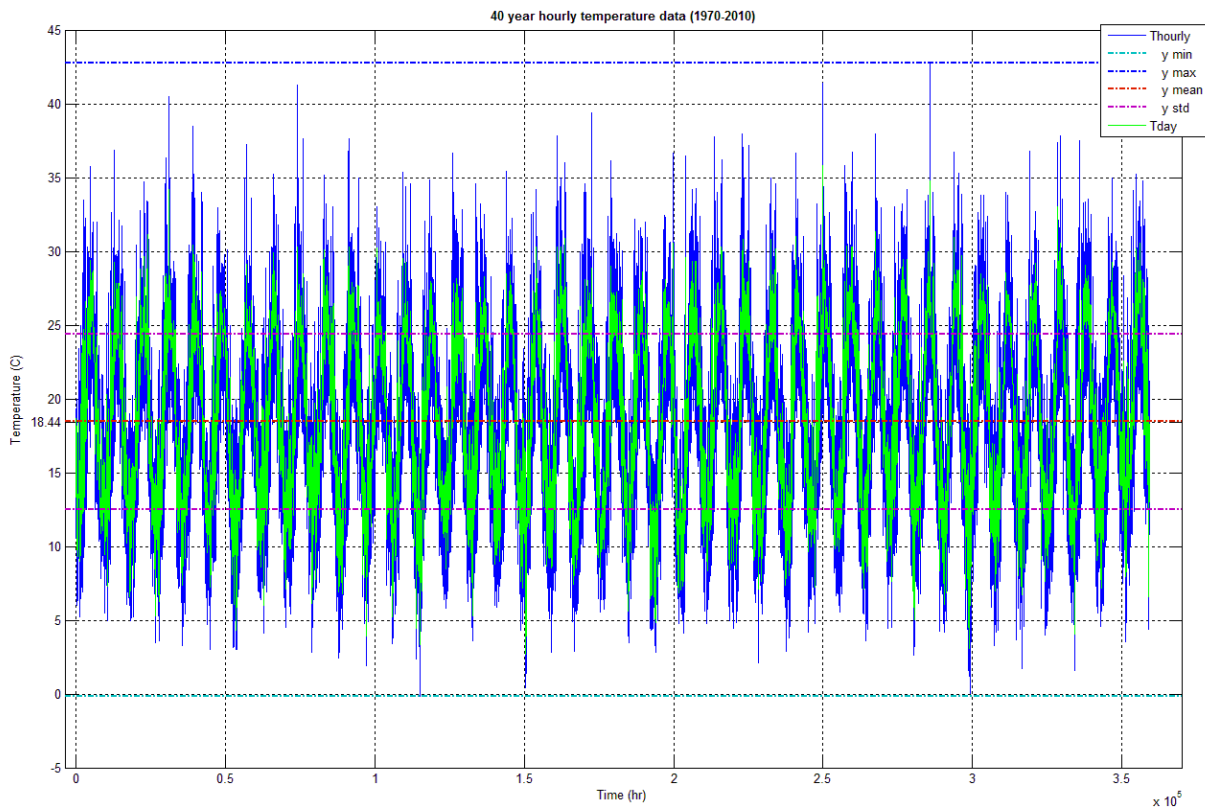
Figure 10. Hourly temperature data from the reference station in Heraklion-Crete, for the period 1970 – 2010. The green line corresponds to the mean daily temperature.
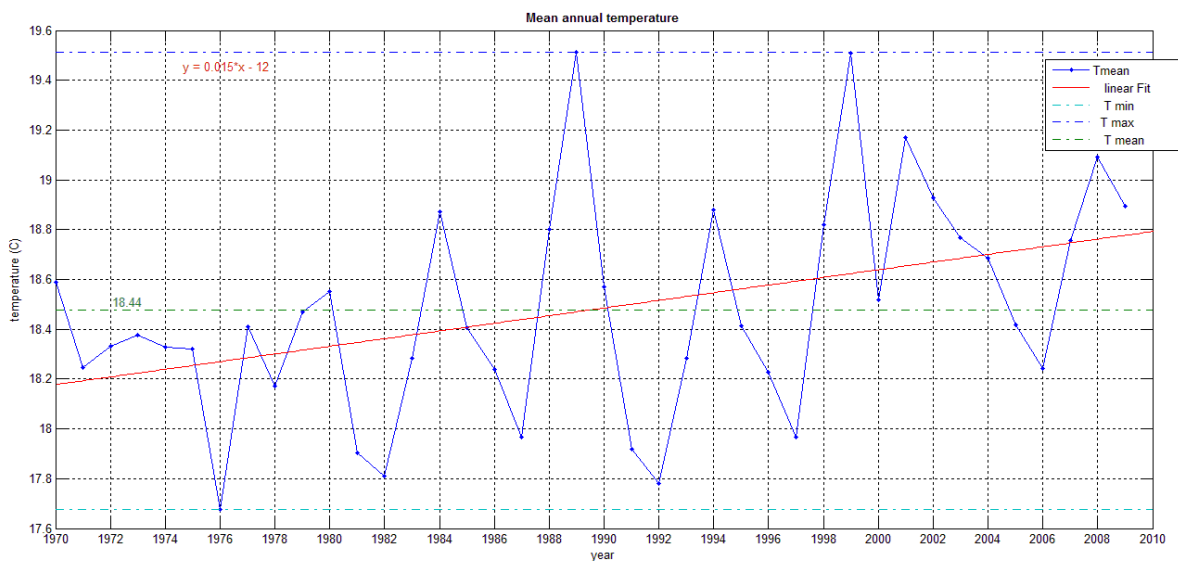

Figure 11. Mean annual temperature with the linear trend representation for the reference period 1970-2009.
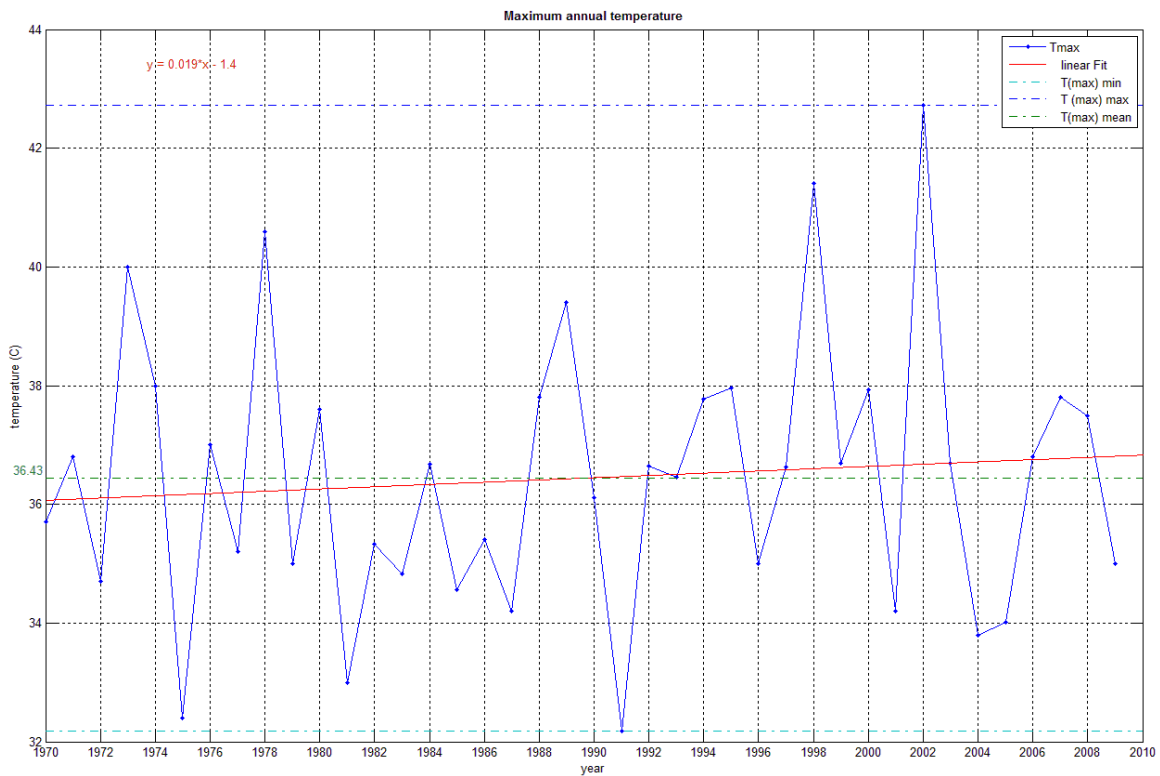
Figure 12. Maximum annual temperature with the linear trend representation for the reference period 1970-2009.
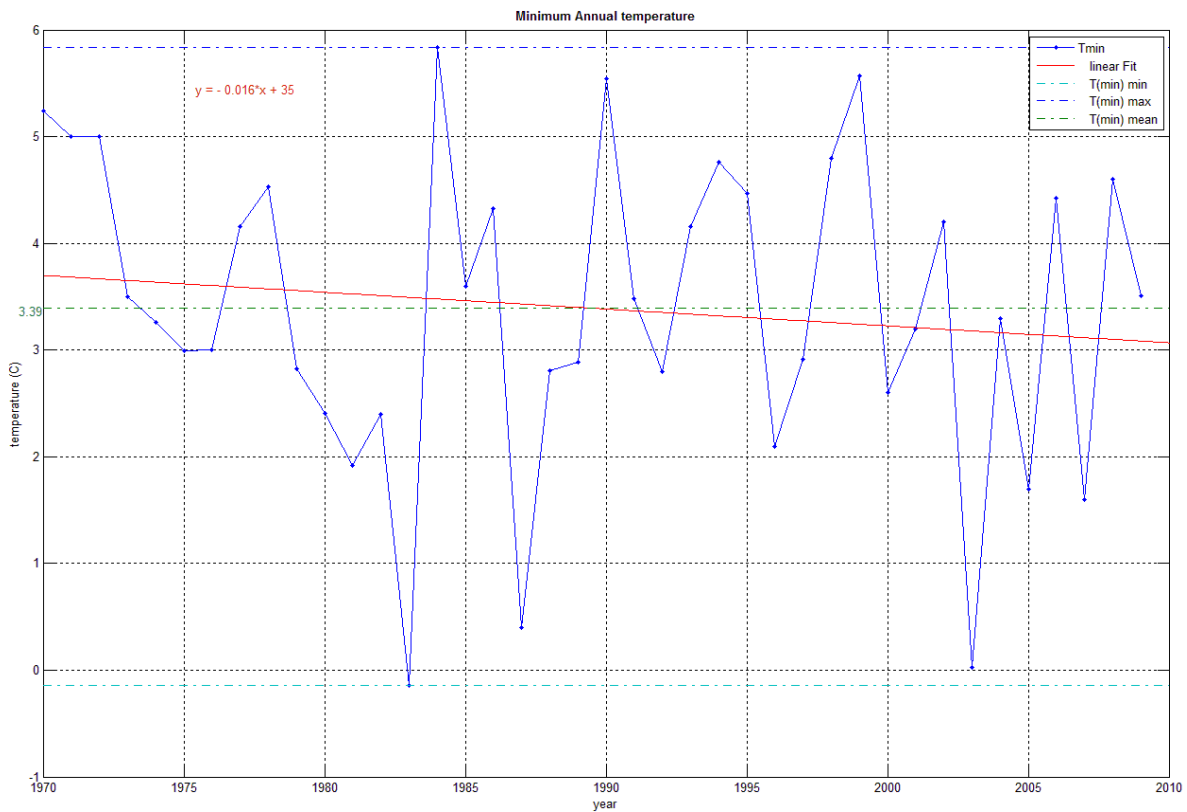
Figure 13. Minimum annual temperature with the linear trend representation for the reference period 1970-2009.
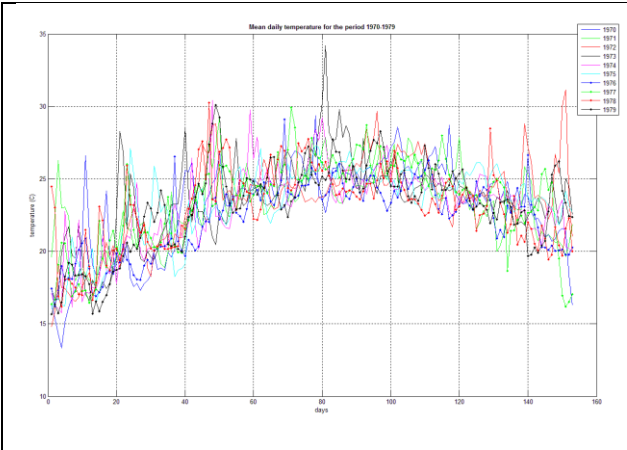
Figure 14. Mean daily temperature data for the summer period (May to September) decade 1970-1979
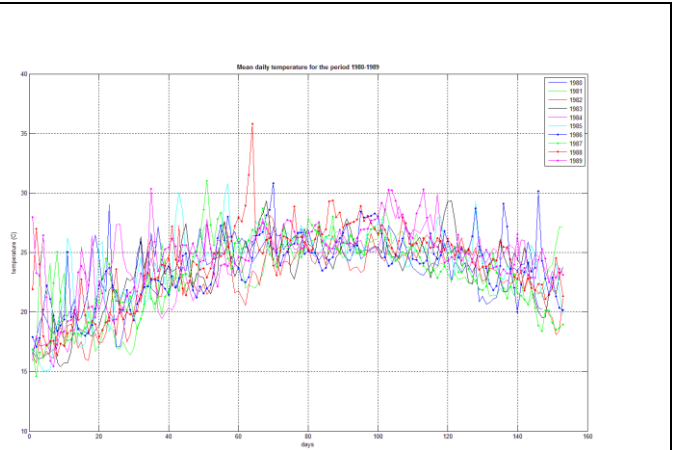
Figure 15. Mean daily temperature data for the summer period (May to September) decade 1980-1989
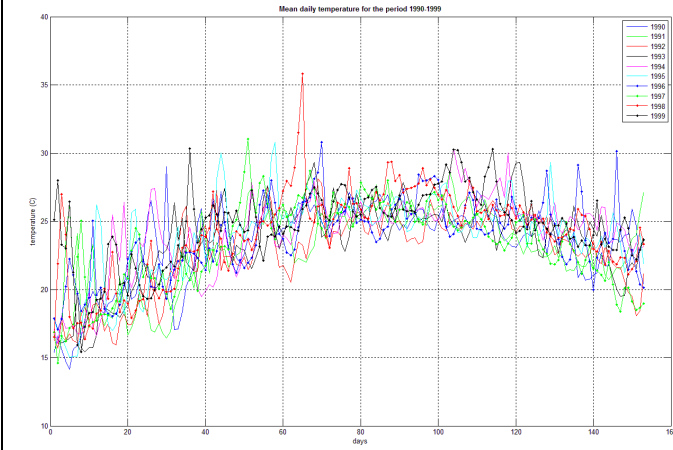
Figure 16. Mean daily temperature data for the summer period (May to September) decade 1990-1999
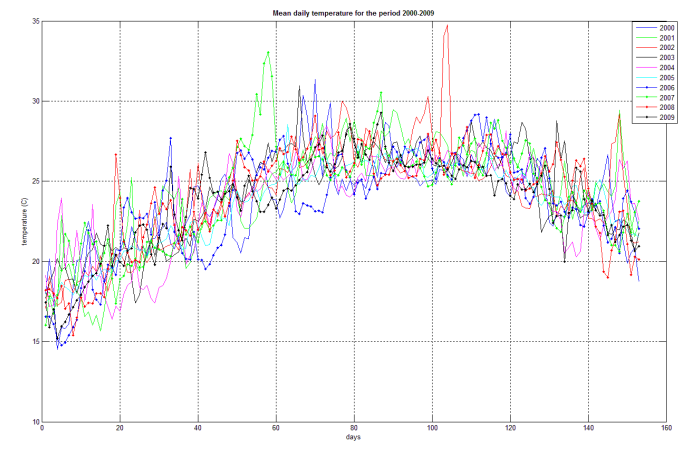
Figure 17. Mean daily temperature data for the summer period (May to September) decade 2000-2009

27
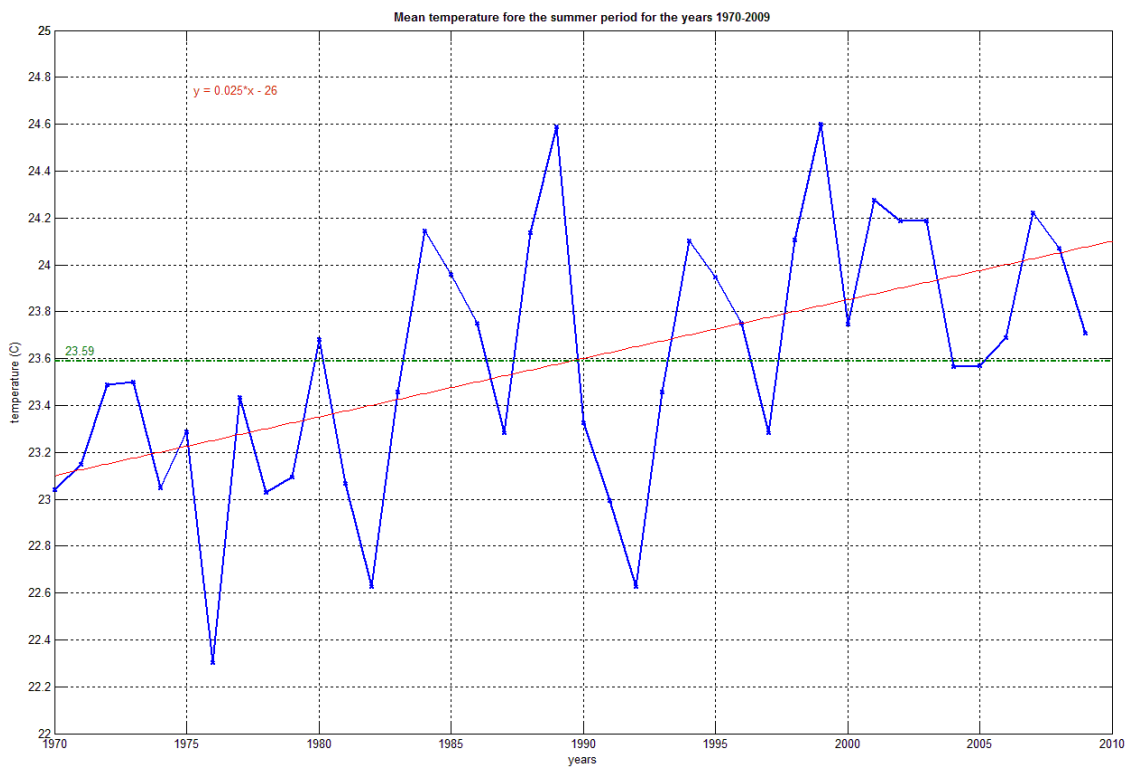
Figure 18. Mean temperature data for the whole summer periods (May to September) years 1970-2009
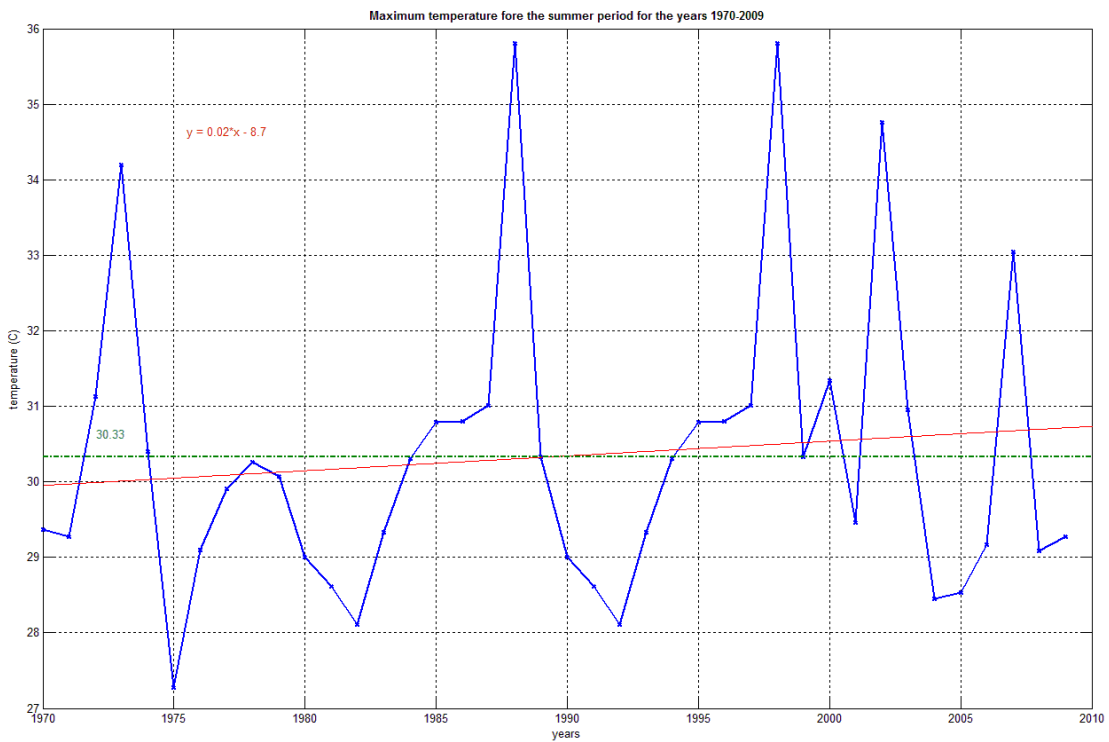
Figure 19. Maximum temperature data for the whole summer periods (May to September) years 1970-2009
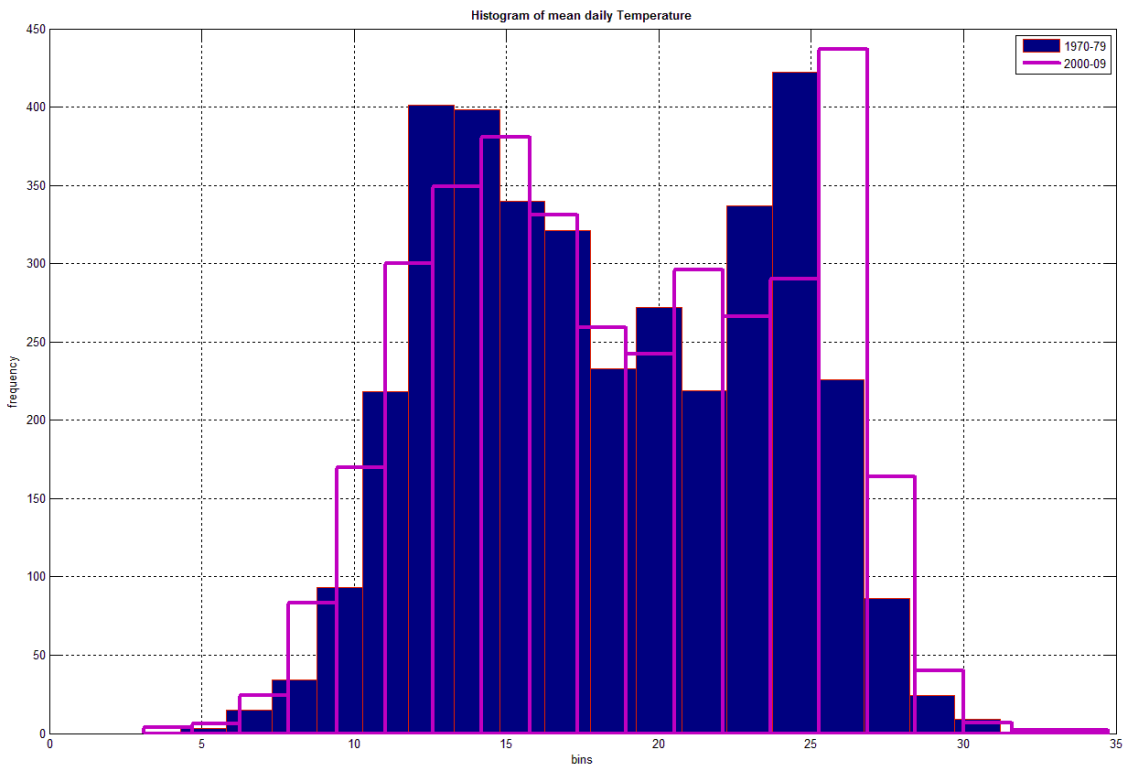
Figure 20. Histogram of daily mean temperature for the periods 1970-79 and 2000-09

A small increase in maximum temperature especially in the summer months can be seen. While the trend lines in daily maxima and minima are somewhat weak, the frequency distribution of air temperatures show interesting patterns of change: lower temperatures shifted downwards in the histogram chart (less frequent) and an increase in the frequency of higher temperatures. Figure 20 shows the frequencies for the first and the last decades of the data series, 1970-1979 and 2000-2009.

3.3 Simulating the temperature data

As stated in Par. 3.6, starting the temperature data simulation and prediction, an ARMA model is used as a benchmark and baseline methodology. The temperature series present a strong yearly seasonality which resembles a sinusoid function. The first though on simulating the temperature data is to compose the temperature values adding to a sinusoid function the daily deviations from the function values. As a result, the temperature series is modeled as a sum of two components, a deterministic non-linear function that explains the seasonal or expected temperature for a given hour in a given year and a stochastic component that explains deviations of actual temperature from average values. The deterministic or expected temperature component is modeled with a sum of sines model, motivated by the physical nature of temperature and periodicities observed in the data (Figure 21).
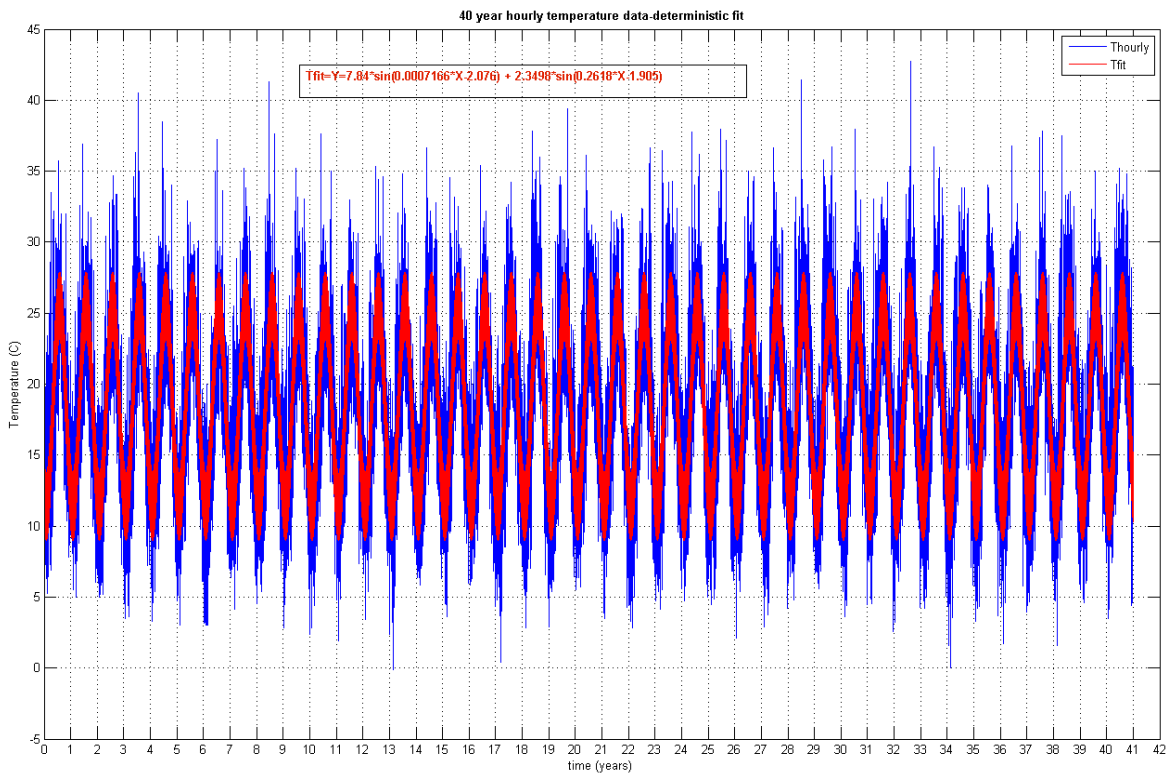
Figure 21. Deterministic fit of the air temperature data for the forty years period.

The daily min max and mean values are calculated from one-hour time step available data. The autocorrelation coefficients of the daily mean temperature data are shown in Figure 22. As we can see, there is an upper and lower peak which approximately corresponds to winter and summer periods. One upper peak to the next

corresponds to one year period. The autocorrelation coefficient indicates good prediction ability in terms of mean daily temperature data.
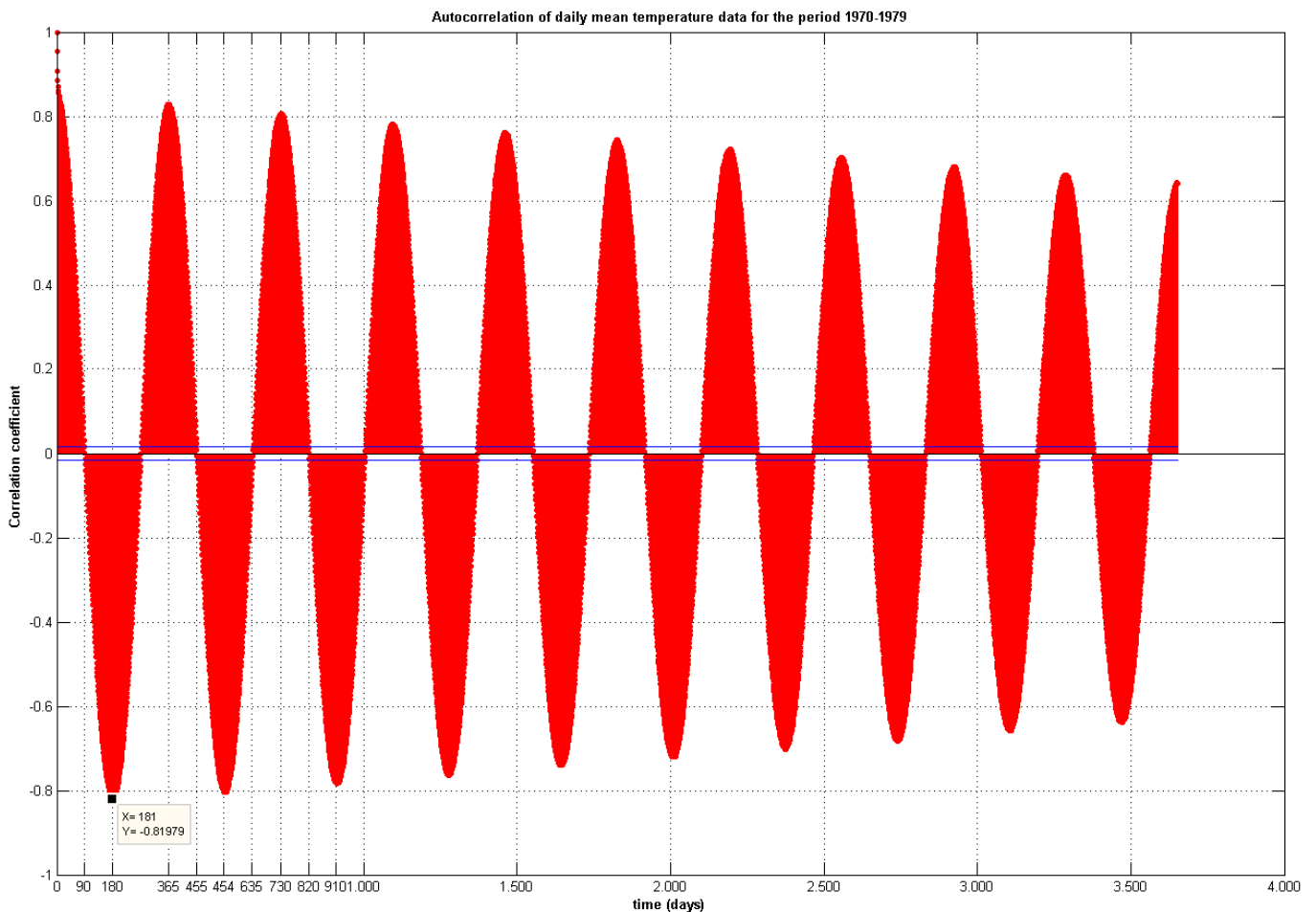
Figure 22. Autocorrelation coefficients of daily mean air temperature data time serie for the reference station of Heraklion. Each lag corresponds to one day.

The results for ten year prediction are shown in Table 5, with help of Matlabs temperature simulation model. This result can be considered as reference basis for our further prediction techniques. As observed, the seasonal autoregressive model can produce adequate mean Temperature data, while it indicates weakness in simulating the maximum temperature values. In Figure 23, an excess in maximum temperature peaks is indicated which exceeds the actual high temperatures of our evaluation data.

Table 5. Main statistical values of actual and simulated temperature data for the period 2000-2009

	Tmean	Tmax	Tmin	Tvar	MSE	R squared
Actual Temperature (max)	21.82	42.73	5.45	33.41	-	-
Simulated Temperature (max)	21.54	46.96	4.35	34.82	15.6	0.79
Actual Temperature (min)	15.36	28.6	0.03	30.15	-	-
Simulated Temperature (min)	15.00	31.50	0.81	30.12	10.74	0.82
Actual Temperature (mean)	18.75	34.75	3.1	31.56	-	-
Simulated Temperature (mean)	18.61	32.28	4.41	31.1	9.16	0.85
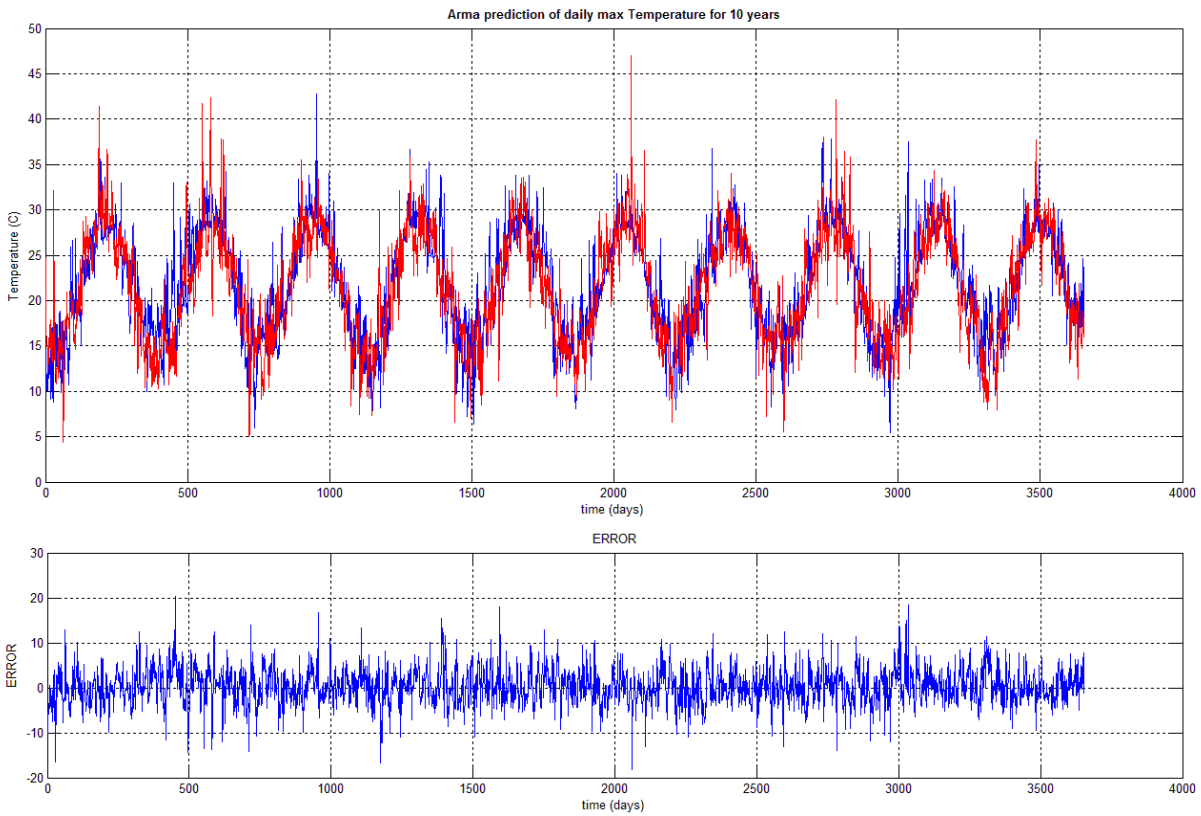
Figure 23. Predicted (red line) and actual (blue line) daily max temperature data for the reference station of Heraklion, year 2000-2009 (MSE = 15.6)
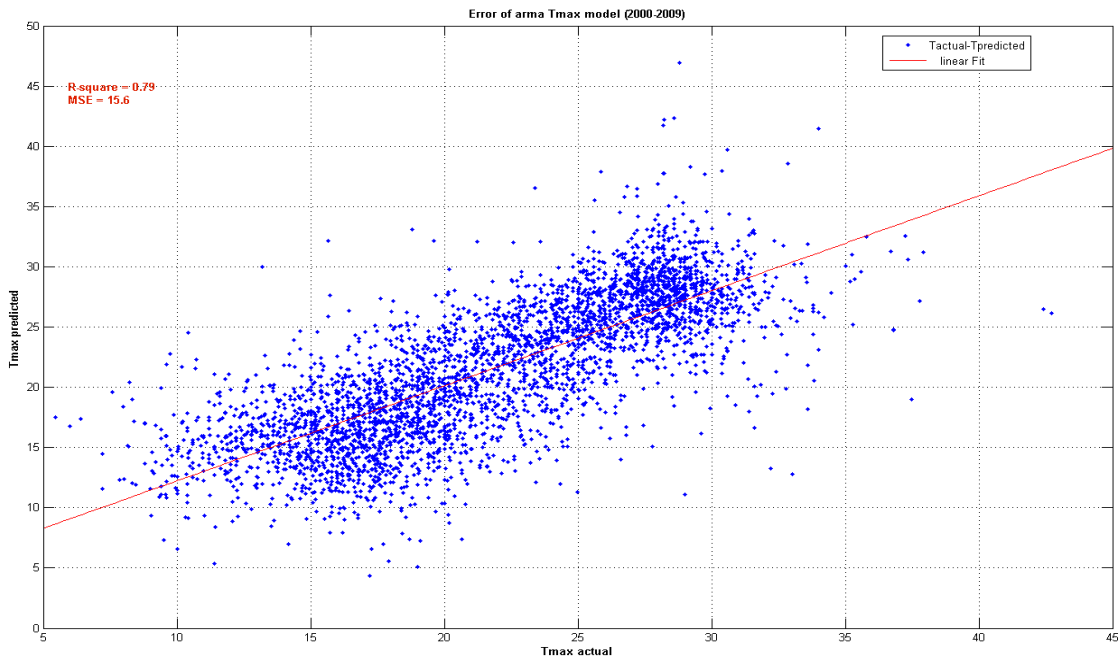
Figure 24. Actual daily max temperature versus predicted
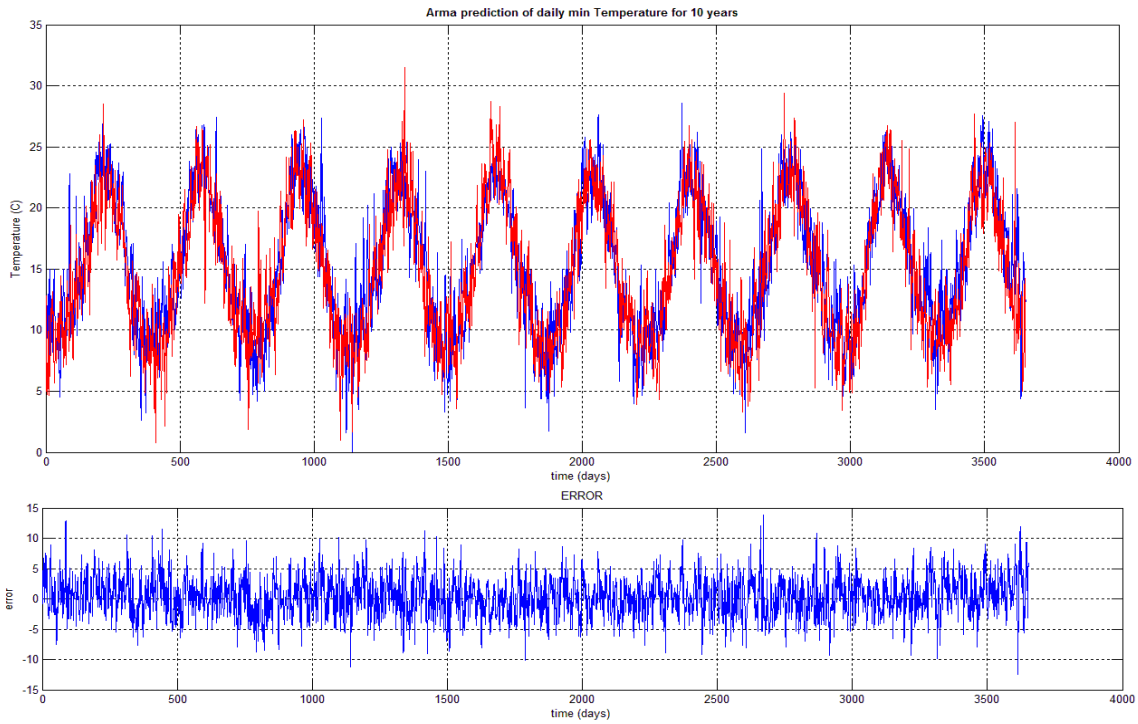
Figure 25. Predicted (red line) and actual (blue line) daily min temperature data for the reference station of Heraklion, year 2000-2009 (MSE = 10.74)
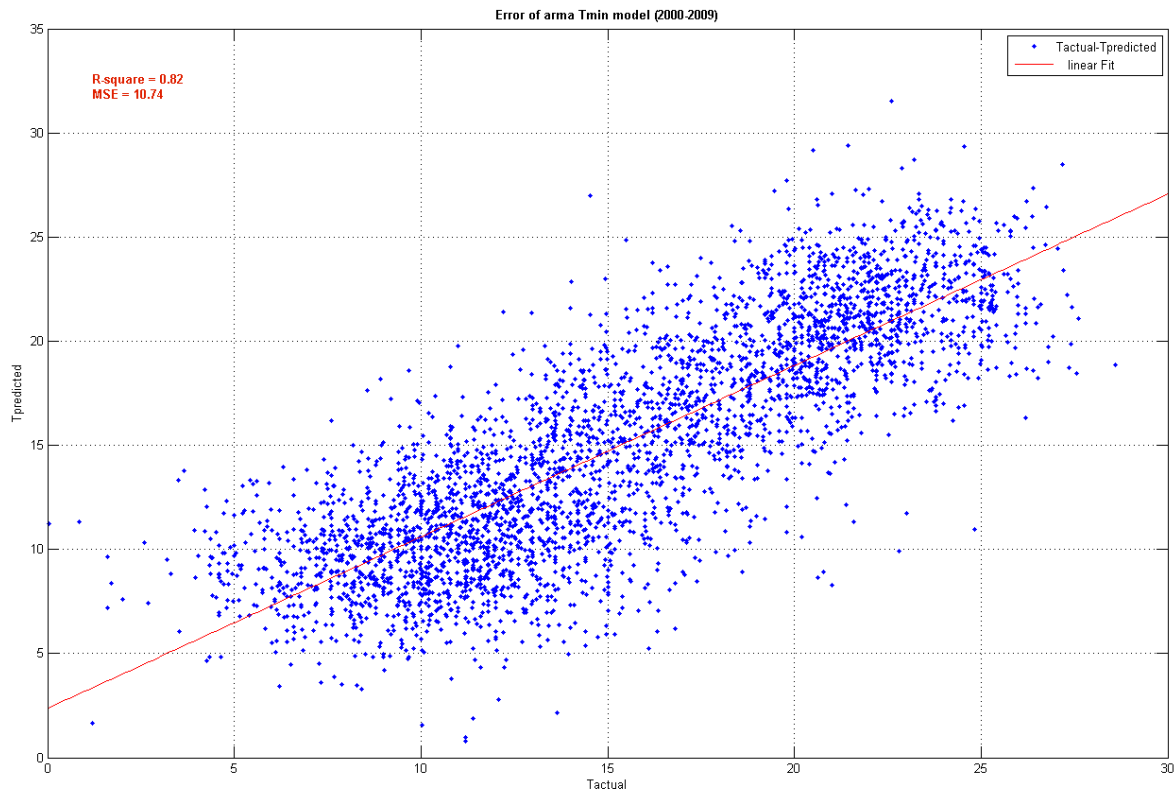
**Figure 26. Actual daily min temperature versus predicted**
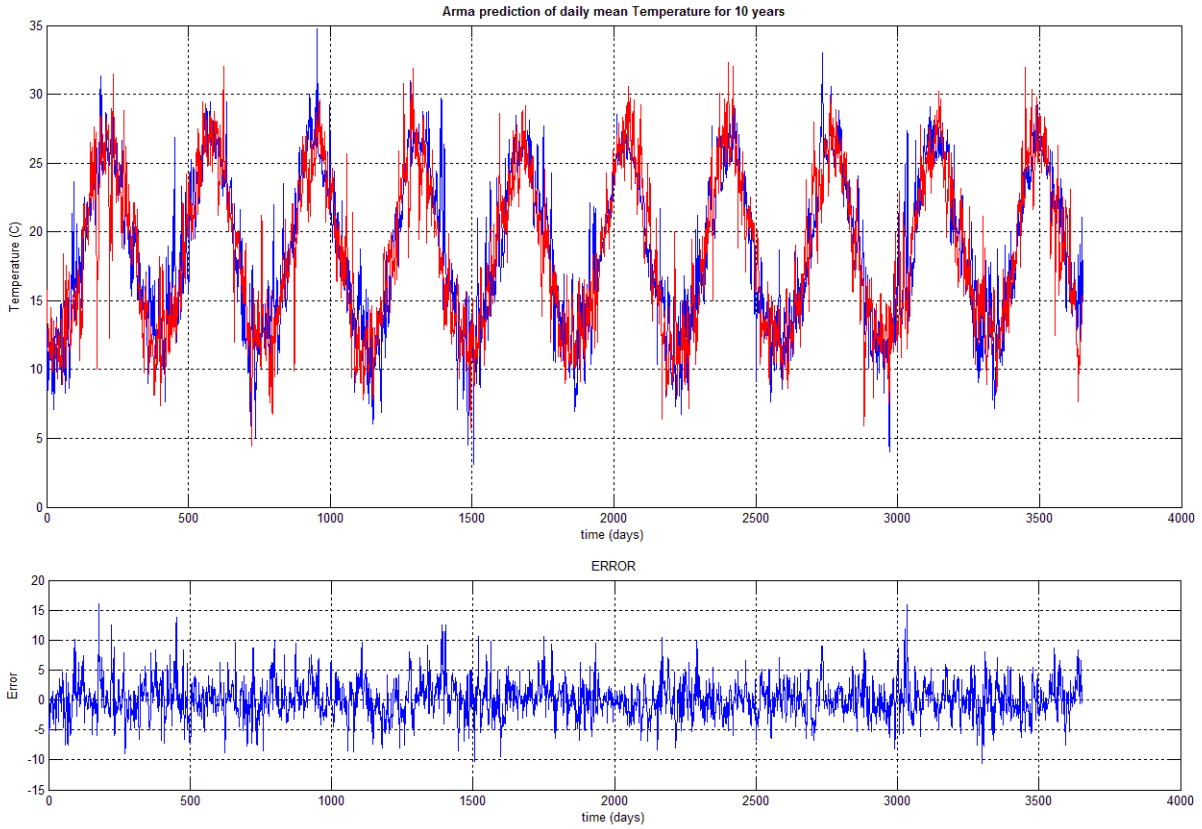
Figure 27. Predicted (red line) and actual (blue line) daily mean temperature data for the reference station of Heraklion, year 2000-2009 (MSE = 9.16)
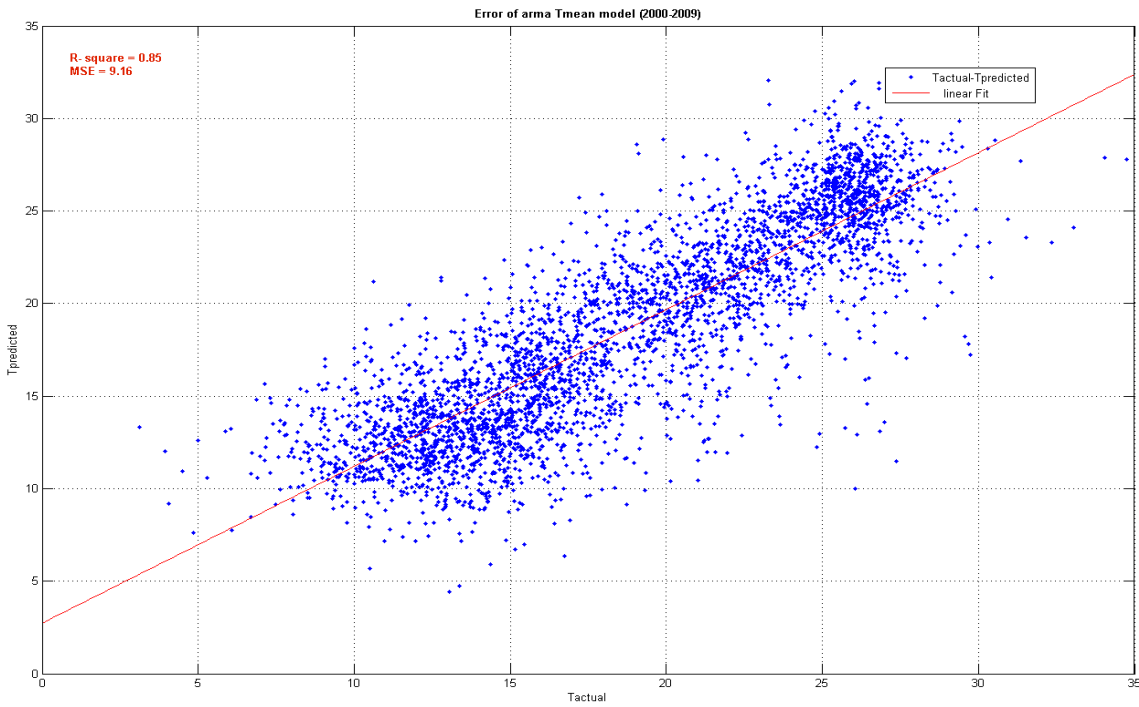
Figure 28. Actual daily max temperature versus predicted

Finally the Cooling Degree Days are calculated for the actual and predicted maximum Temperature data considering as reference temperature 26ºC. The maximum temperature values are chosen because of the difficulty to predict the highest temperatures.
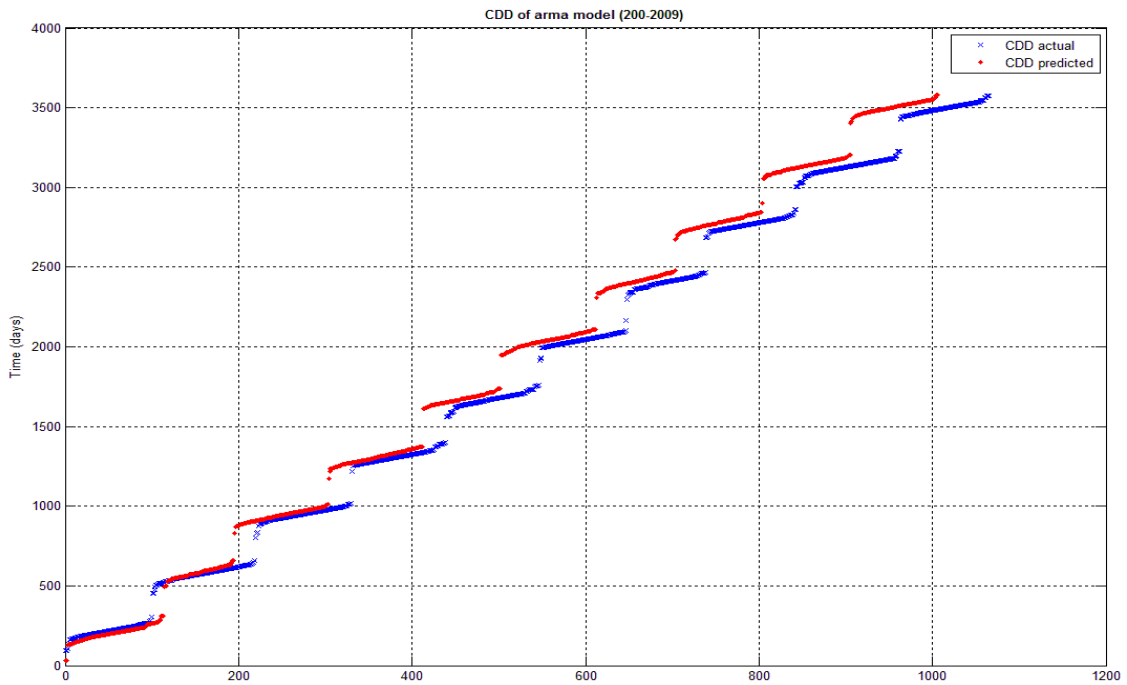
Figure 29. CDD of max daily temperatures for arma predicted (red, CDD=1065) and actual (blue, CDD = 1006) data.
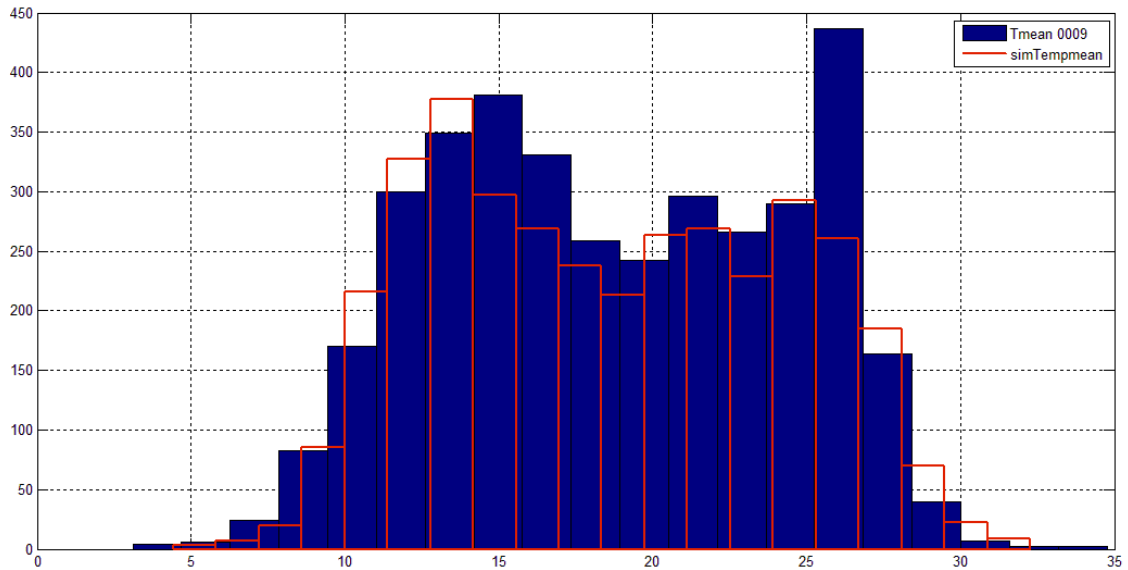
Figure 30. Histogram of actual (blue) and simulated (red) mean temperature for the years 2000-2009.

3.4 Forecasting the temperature data with ANN

Several studies have already been made for the meteorological data forecasting, using techniques as ARMA models and neural networks. Most of these studies refer to short term predictions.

The common parameters in designing a neural network are:

→ Selection of the neural network type (i.e. feed forward back propagation algorithm)

→ Selection of input parameters - external parameters (i.e. temperature, day, hour)

→ Selection of the activation function (i.e. the 1 / (1 + e ^ (-x))

→ Selection of the hidden levels

→ Selection of the training function

→ Development of the model in Matlab

In order to evaluate if and which type of a neural network model can predict with accuracy air temperature data for long terms, the available time series are divided into testing periods.

Data of the four available decades are selected, more specific our input data include the normalized intervals of the following series:

1.   Year

2.   Month

3.   Days

4.   Minimum Daily Temperature (C)

5.   Mean Daily Temperature

6.   Maximum Daily Temperature

We first proceed with a 10 year training period for three decades 1970 – 1979, 1980 – 1989, 1990 – 1999, and use the last decade 2000-2009 for the evaluation of our results.

Secondly we try a 5-year training period increasing the training assets and using the last five years 2004-2009 for the evaluation of our results.

Finally we also trained the neural network using one single training period of 15 years daily data.

Regarding the neural network type, we choose the feed forward network (FF) and the nonlinear autoregressive network with exogenous inputs (NARX). For each different neural network architecture the optimal, hidden layers and number of neurons are investigated. It was observed that by increasing the number of hidden layers, the results did not correspond to the evaluation temperature data. In contrast, the predicted data resulting from multilayer networks, tended to converge in the mean temperature. One possible explanation is that NNs with more hidden layers are extremely hard to train, while in our long term prediction case, there exist limited training sets. For that reason, a single layer network has been used in each of the cases. Regarding the training functions, there are two types evaluated, the common Levenberg-Marquardt "trainlm" and the BFGS quasi-Newton (trainbfg) "trainbfg" function. Apart from the above mentioned network types the elman and cascade network were used without proving any significant differences from the feed forward network.

Feed Forward ANN

We first begin with creating a feed forward network using the Levenberg-Marquardt algorithm in a single layer (Figure 31). Feed-Forward NN is an artificial neural network where input layer consists of the inputs of the neural and connected to an output layer composed of neurons (computational nodes). In this network, the information moves in only one direction, forward, from the input nodes, through the hidden nodes (if any) and to the output nodes. The main results and statistical values of our prediction and validation mean maximum and minimum temperature data, are depicted in Table 6.
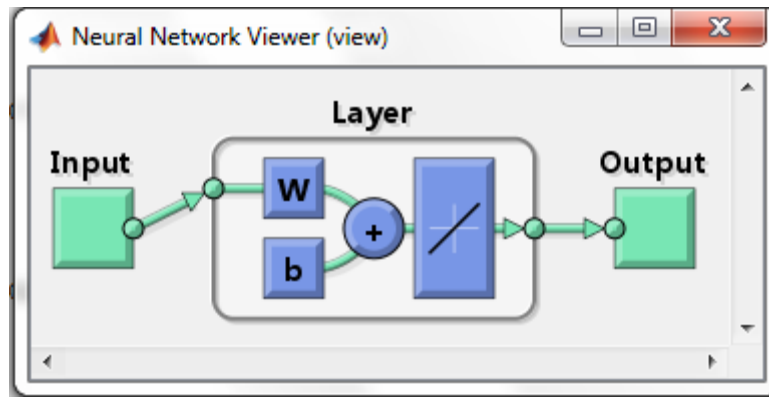
Figure 31. Feed Forward single layer network

Table 6. Main statistical values of actual and simulated temperature data for the period 2000-2009

trainlm	Tmean	Tmax	Tmin	Tvar	SME	R squared
Actual Temperature (max)	21.82	42.73	5.45	33.41	-	-
Simulated Temperature (max)	21.31	38.00	7.79	32.15	12.7655	0.79
Actual Temperature (min)	15.36	28.6	0.03	30.15	-	-
Simulated Temperature (min)	15.14	27.49	4.33	28.75	8.6230	0.82
Actual Temperature (mean)	18.75	34.75	3.1	31.56	-	-
Simulated Temperature (mean)	18.43	33.94	6.2	31.6	9.0303	0.86
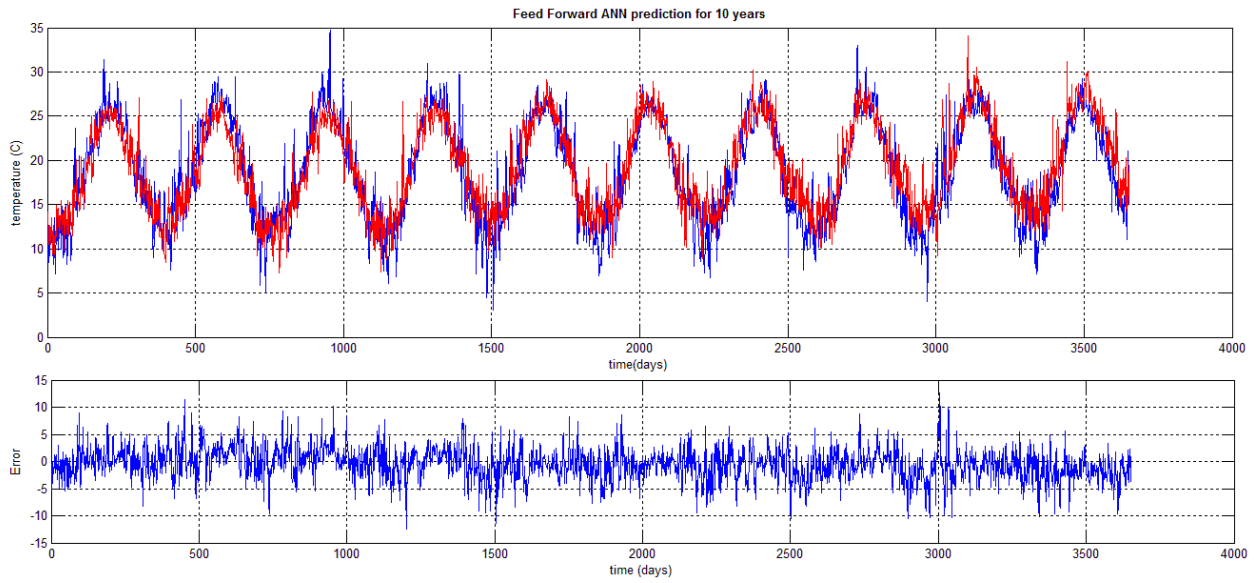
Figure 32. Predicted (red line) and actual (blue line) of the daily mean temperature data for the reference station of Heraklion, year 2000-2009 (MSE = 9.03)
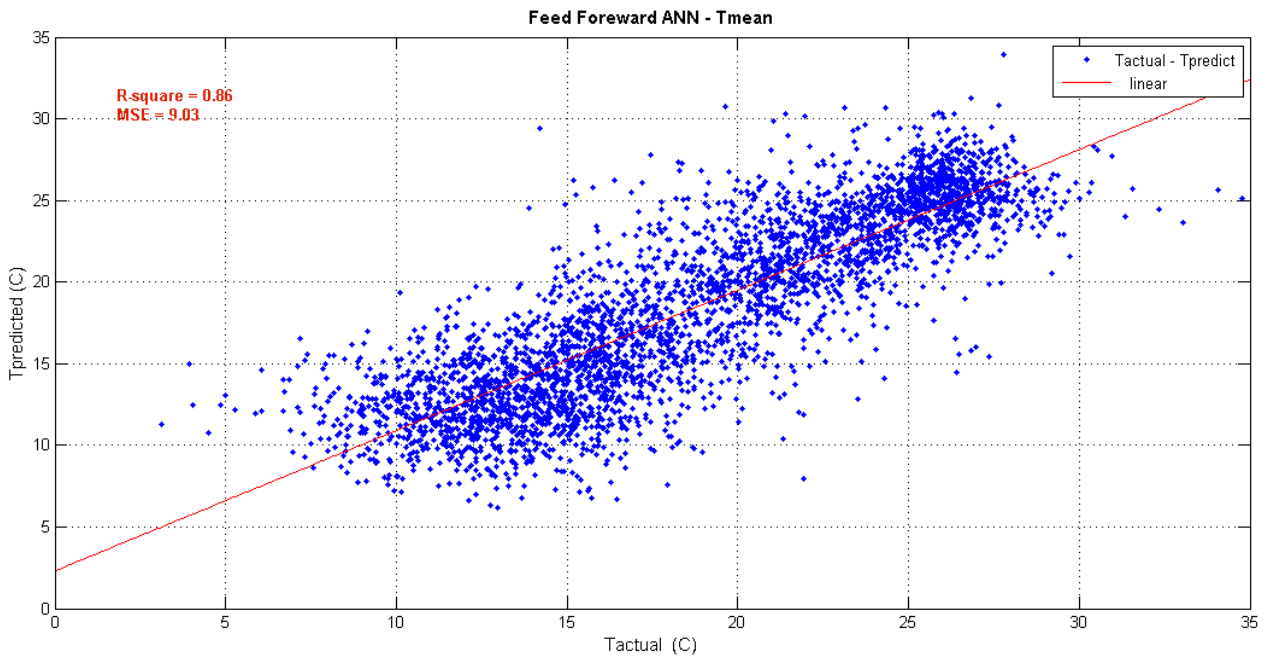

**Figure 33. Actual daily mean temperature versus predicted**
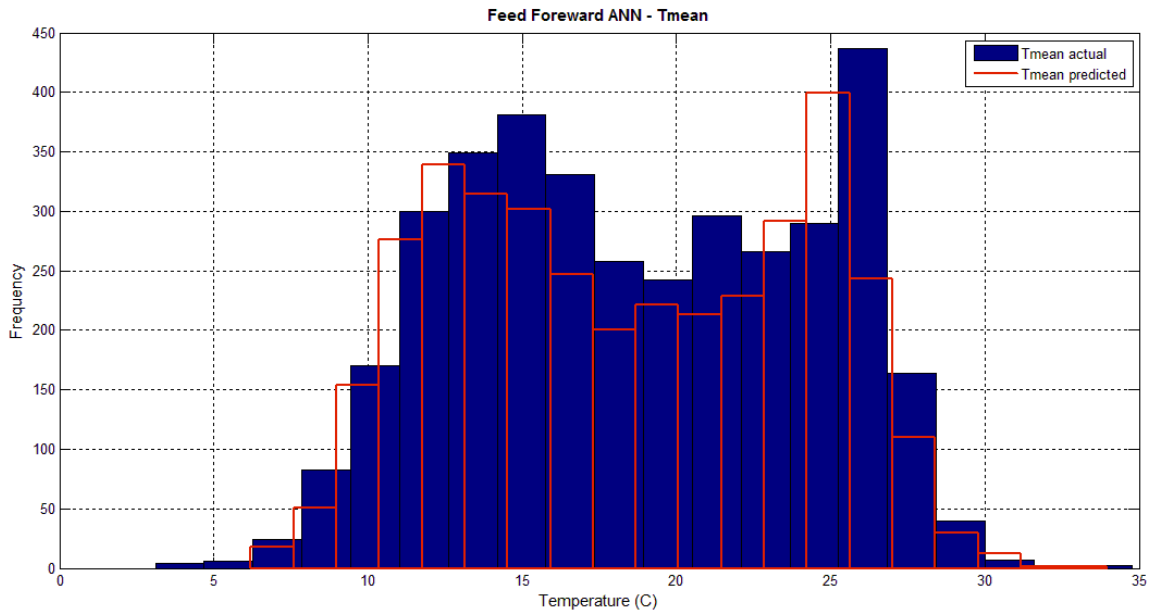
**Figure 34. Histogram of actual (blue) and simulated (red) mean temperature for the years 2000-2009.**
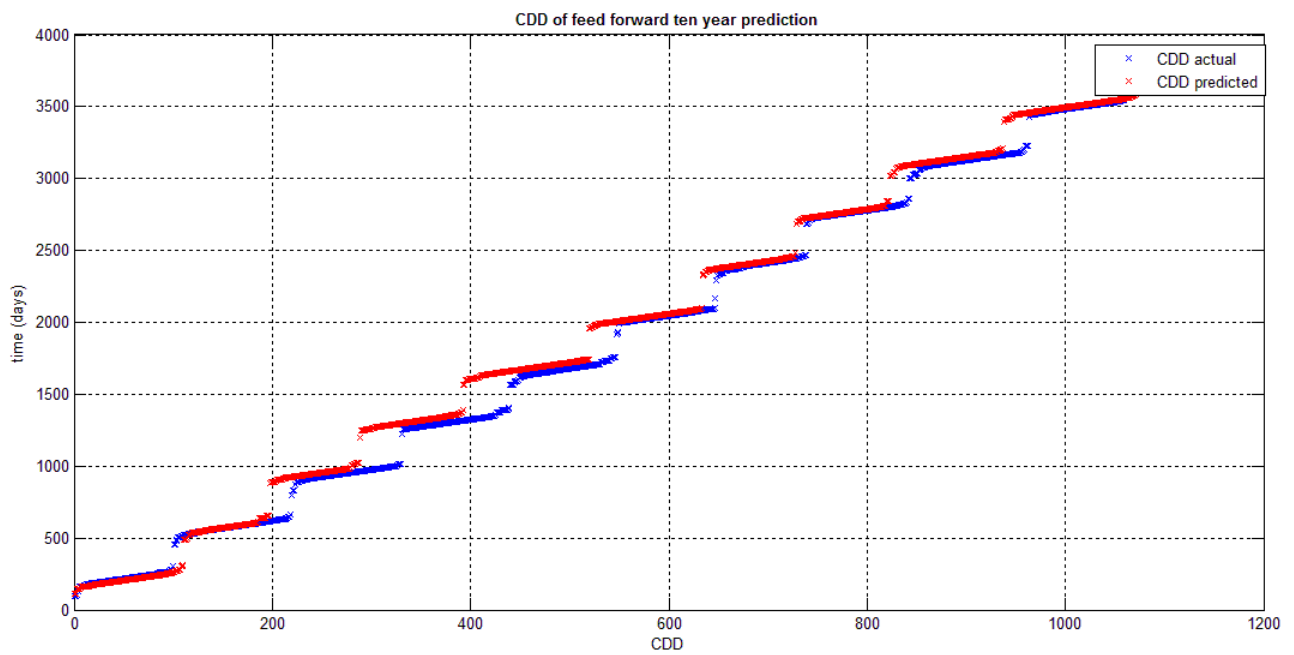
Figure 35. CDD of max daily temperatures for feed forward predicted (red, CDD=1065) and actual (blue, CDD = 996) data.
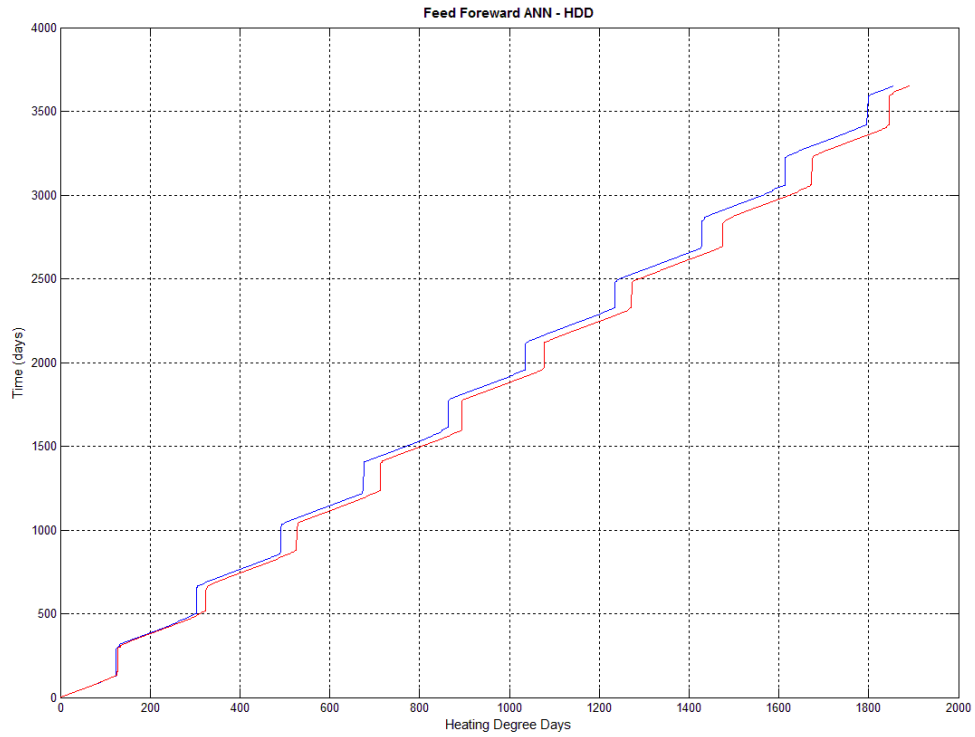
Figure 36. HDD of max daily temperatures for feed forward predicted-red and actual - blue data.
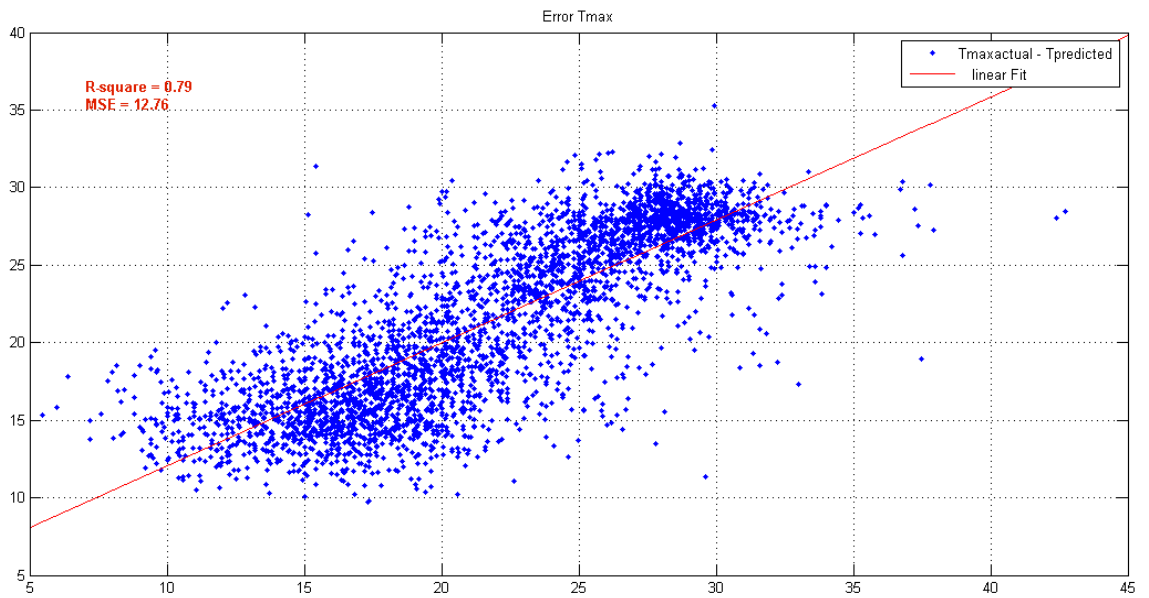

**Figure 37. Actual daily max temperature versus predicted**
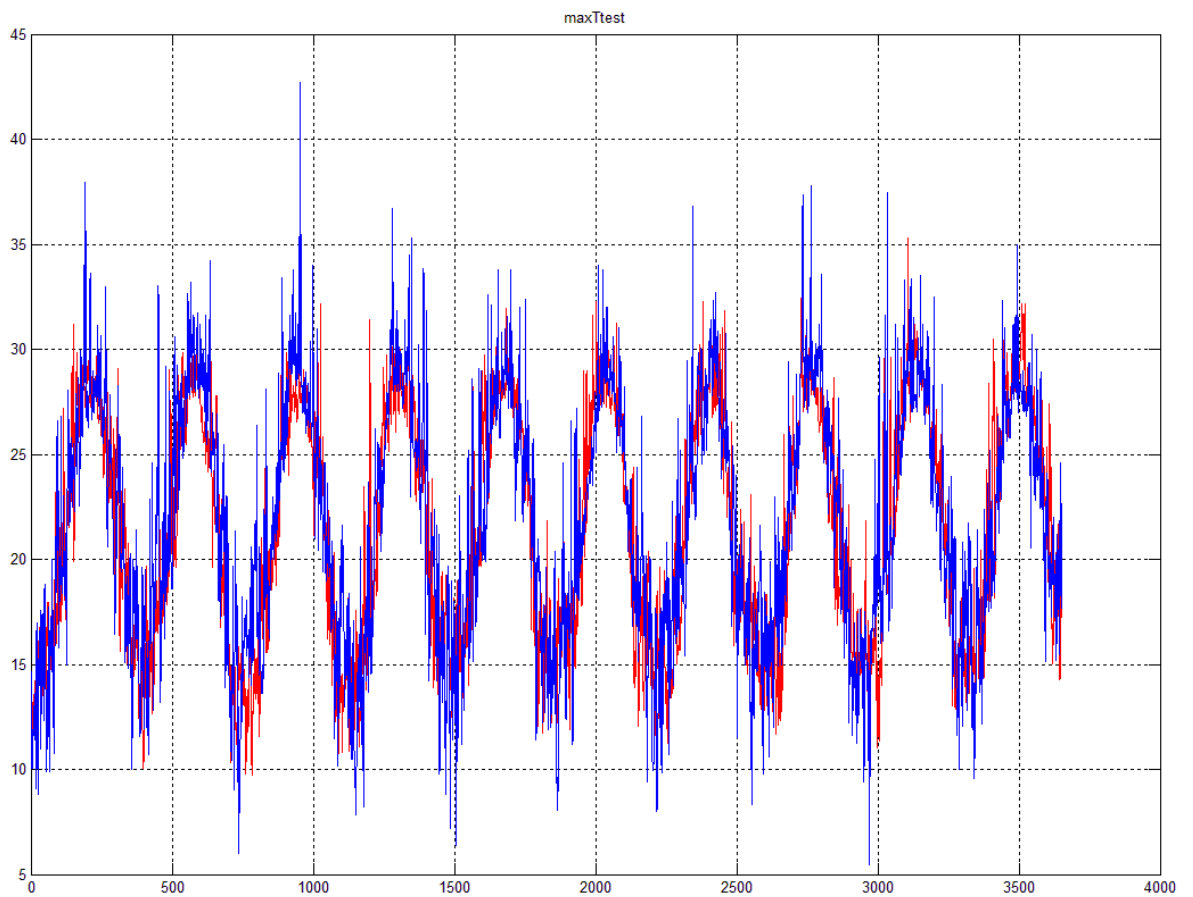
Figure 38. Predicted (red line) and actual (blue line) of the daily max temperature data for the reference station of Heraklion, year 2000-2009 (MSE = 12.76)
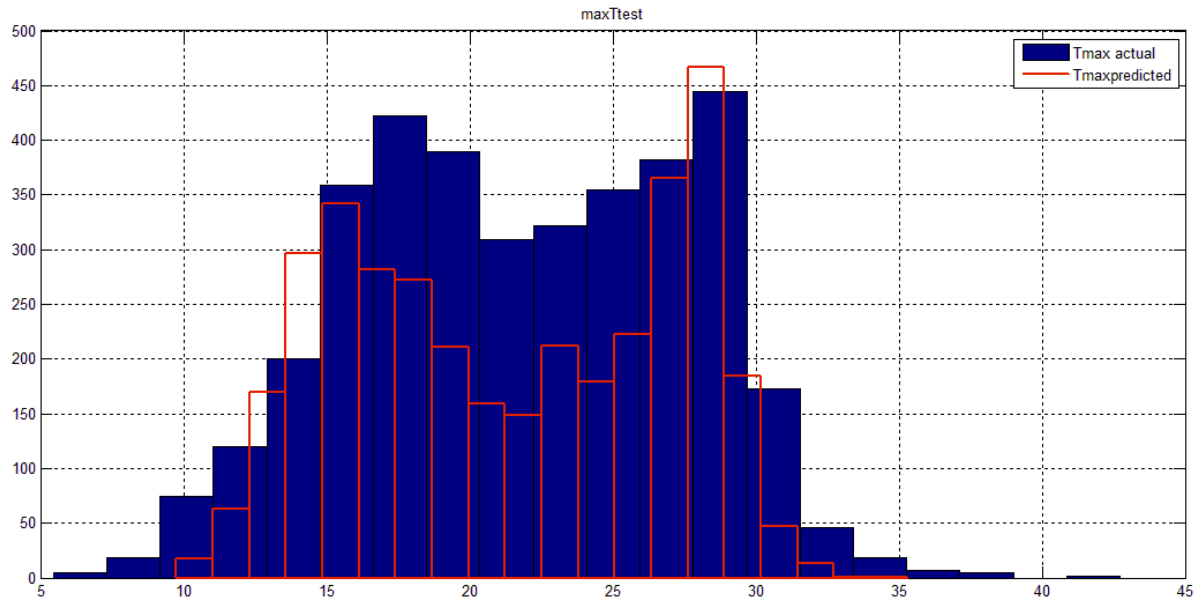
Figure 39. Histogram of actual (blue) and simulated (red) max temperature for the years 2000-2009.

Following the 10 year prediction periods and the results presented in Figure 32 to Figure 39, we assume that the feed forward neural network predicts adequately the mean values of our temperature data, with an r-squared error 0.86 and MSE 9.03. Considering the long term prediction of 10 years ahead, the predicted mean temperature values follow the frequency distribution in the histogram (Figure 34). The cooling degree days, i.e the amount of temperature data exceeding the 26°C, is 6,48% lower than the actual CDD of the period 2000-2009. Regarding the maximum temperature data prediction, we assume an underestimation of the model, with r-square error 0.79 and MSE 12.76 (Figure 37, Figure 38). The maximum predicted temperature reaches the 38°C, while the actual maximum temperature of the decade 2000-2009 is 42.73^{o}C. This can be explained observing Figure 12. Maximum annual temperature with the linear trend representation for the reference period 1970-2009. The training sets of our feed forward neural network do not contain as high maximum temperature information as it appears in the decade 2000-2009 and the value of 42.73 does not exist in the previous years. Not being trained, the neural model is unable to predict higher temperatures, while it seems to move around the mean maximum temperature of the decades 1970-2000, i.e. 36.43^{o}C.

Following our first feed forward network model, and after assessing further training functions in a single layer network without any significant deviations from the trainlm prediction, we proceed with increasing the training periods, with 5 year training sets, 1970-1974, 1975-1979,..,1995-1999. Then the network is being used for a ten year prediction and evaluated in the prediction of air temperature data for the decade 2000-2009.

We create again a feed forward network using the Levenberg-Marquardt algorithm in a single layer with the training function 'trainlm'. The main results and statistical values of our prediction and validation mean maximum and minimum temperature data, are depicted in Table 7.

Table 7. Main statistical values of actual and simulated temperature data for the period 2000-2009

| trainlm	Tmean	Tmax	Tmin	Tvar	SME	R squared
Actual Temperature (max)	21.82	42.73	5.45	33.41	-	-
Simulated Temperature (max)	22.26	37.29	10.12	24.75	11.56	0.70
Actual Temperature (min)	15.36	28.6	0.03	30.15	-	-
Simulated Temperature (min)	15.75	29.26	4.44	23.00	8.63	0.74
Actual Temperature (mean)	18.75	34.75	3.1	31.56	-	-
Simulated Temperature (mean)	19.25	34.06	7.23	25.23	8.47	0.77
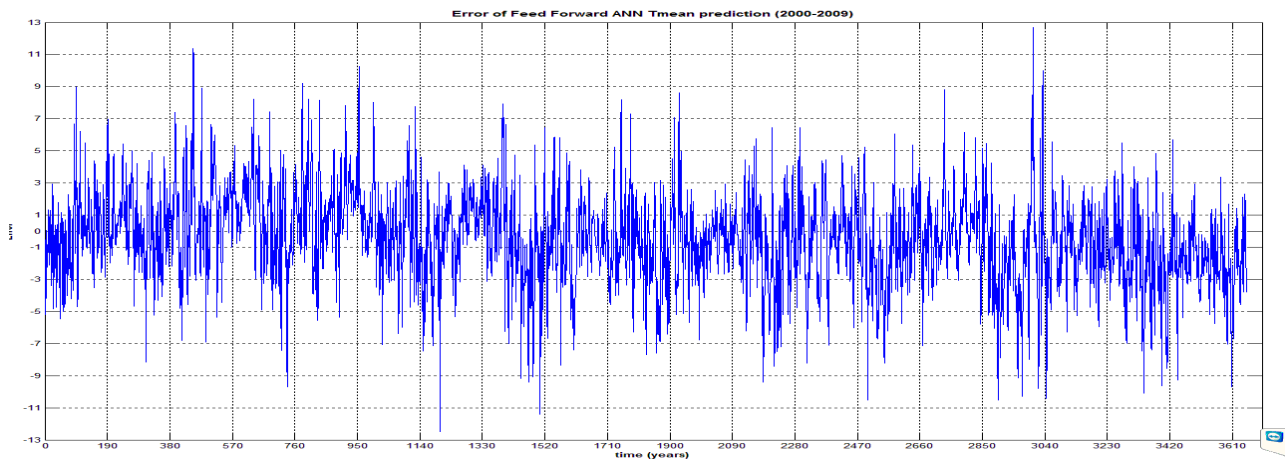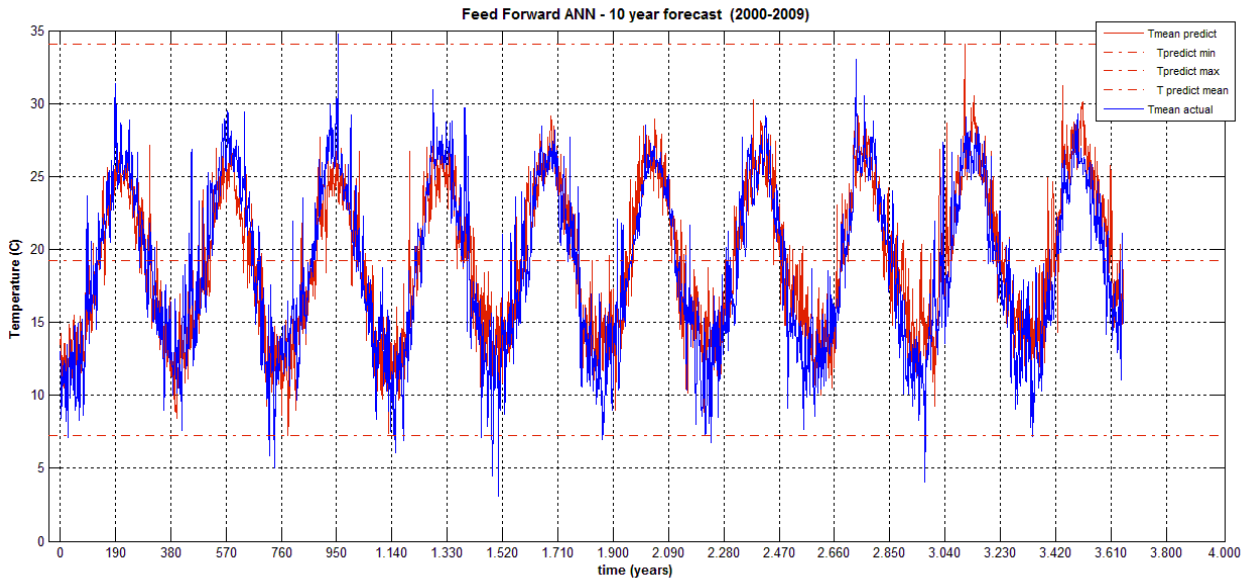
Figure 40. Predicted (red line) and actual (blue line) of the daily mean temperature data for the reference station of Heraklion, year 2000-2009 (MSE = 8.47)
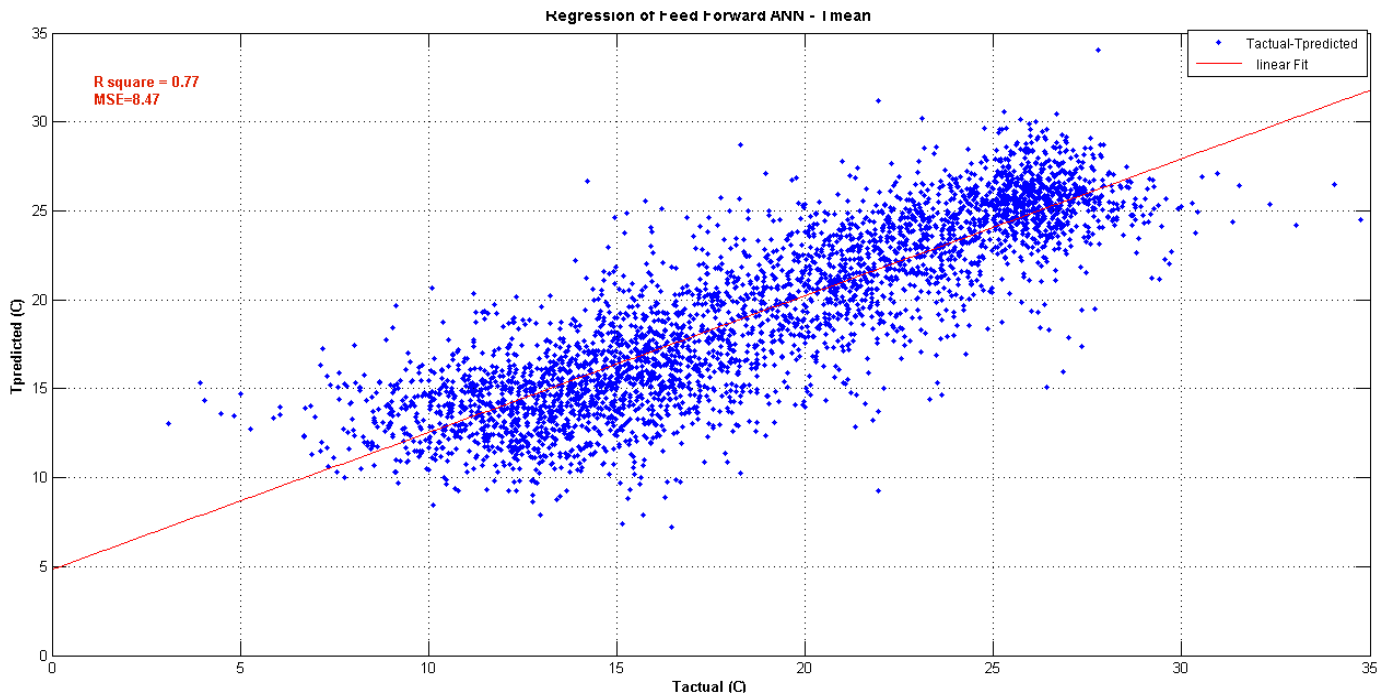
**Figure 41. Actual daily mean temperature versus predicted.**
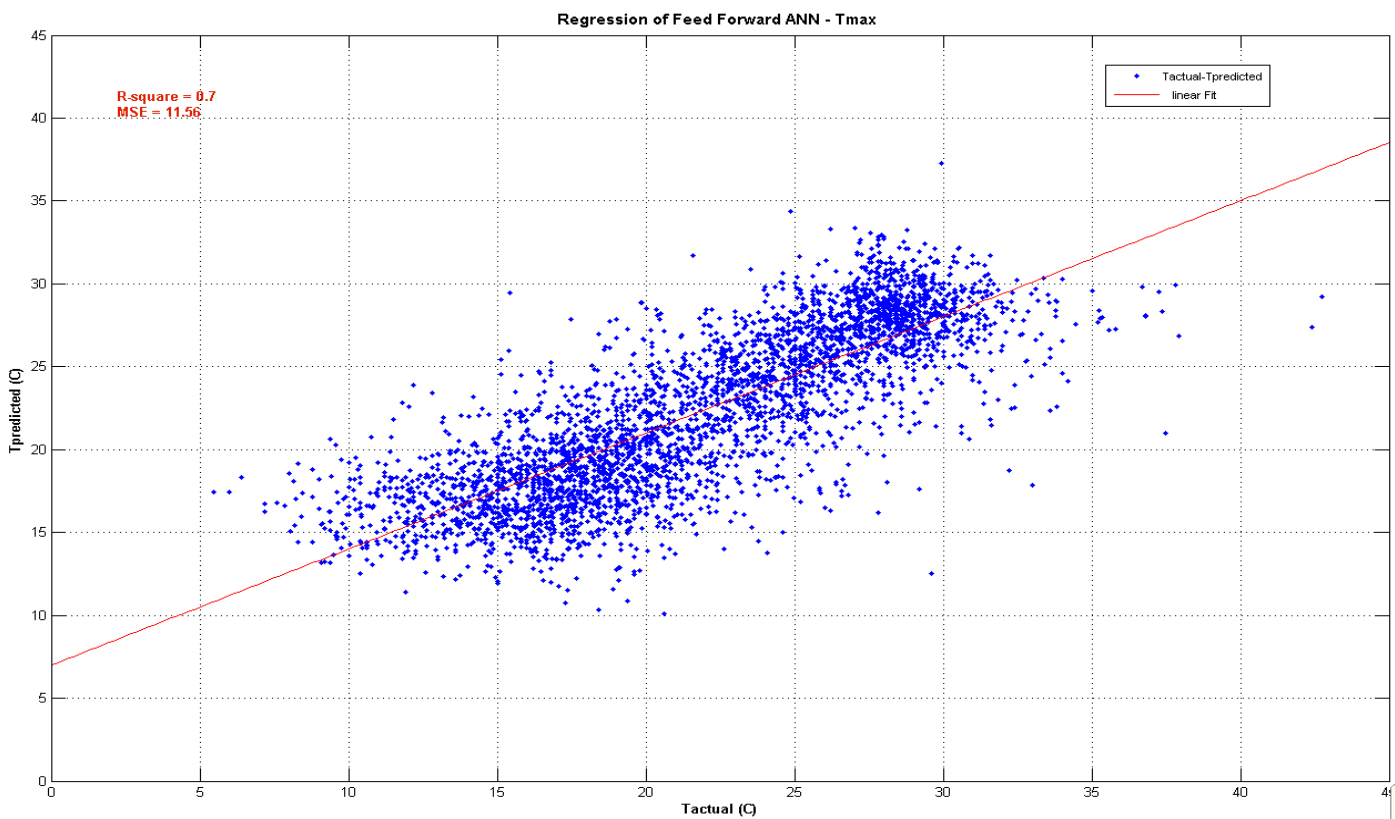
**Figure 42. Actual daily maximum temperature versus predicted.**
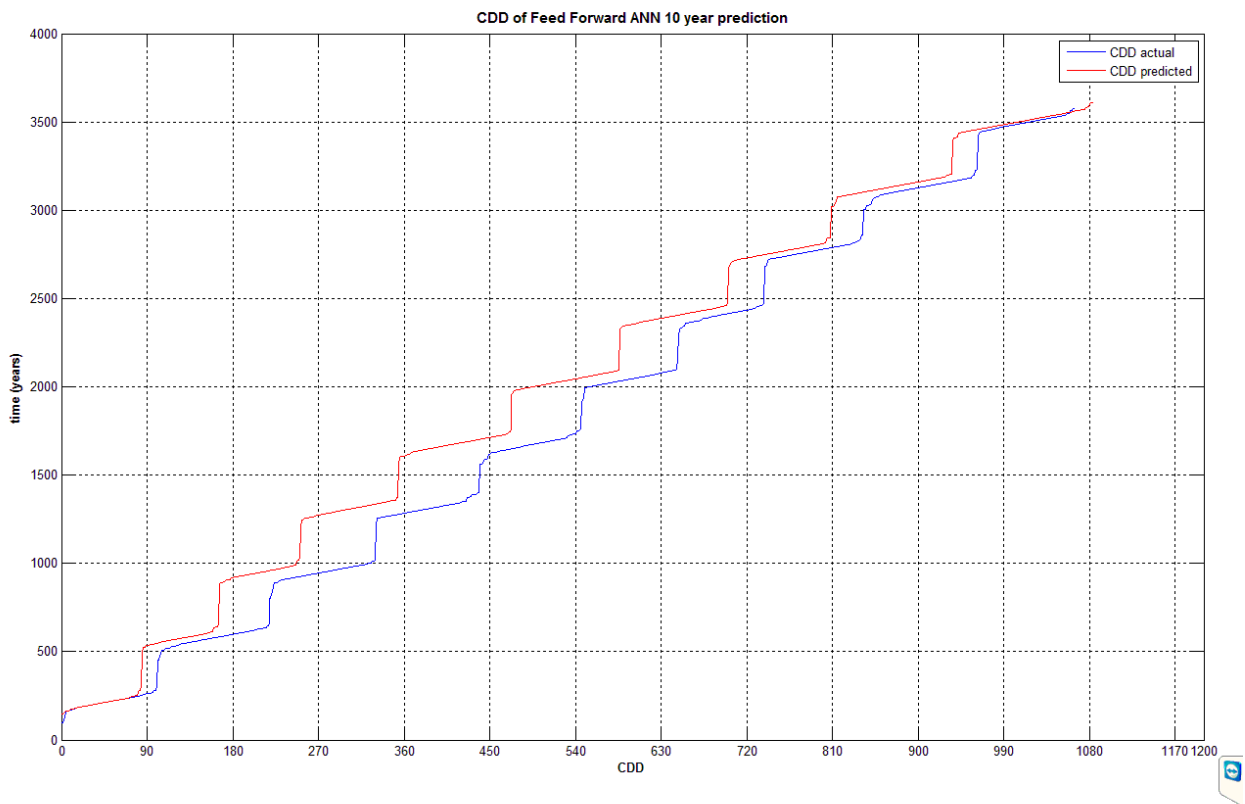
Figure 43. CDD of max daily temperatures for feed forward predicted (red, CDD=1065) and actual (blue, CDD = 1084) data.

Following the 10 year prediction periods and the results presented in Figure 40 to Figure 43 we assume that the feed forward neural network with the 5-year training sets predicts the mean values of our temperature data, with an r-squared error 0.77 and MSE 8.47, similar to the firstly developed model with 10-year training periods. The cooling degree days, are predicted with a better accuracy, exceeding the actual CDD only by 1,78% for the period 2000-2009. Regarding the maximum temperature data prediction, the model underestimates again the actual maximum values, with r-square error 0.70 and MSE 11.56 (Figure 37, Figure 38). The maximum predicted temperature reaches the 37.29°C, while the actual maximum temperature of the decade 2000-2009 is 42.73°C. The explanation remains the same, namely the lack in such high temperature in our training sets.

The same feed forward network is being evaluated in the prediction of air temperature data for the five year period 2004-2009, as shown in Table 8.

Table 8. Main statistical values of actual and simulated temperature data for the period 2004-2009

| trainlm	Tmean	Tmax	Tmin	Tvar	MSE	R squared
Actual Temperature (max)	21.79	37.8	5.45	31.63	-	-
Simulated Temperature (max)	21.05	32.26	5.67	24.38	11.48	0.78
Actual Temperature (min)	15.13	28.6	1.60	29.90	-	-
Simulated Temperature (min)	14.56	24.52	-0.54	22.86	8.57	0.74
Actual Temperature (mean)	18.68	34.75	4.04	30.61	-	-
Simulated Temperature (mean)	17.91	29.13	1.97	25.47	8.61	0.71
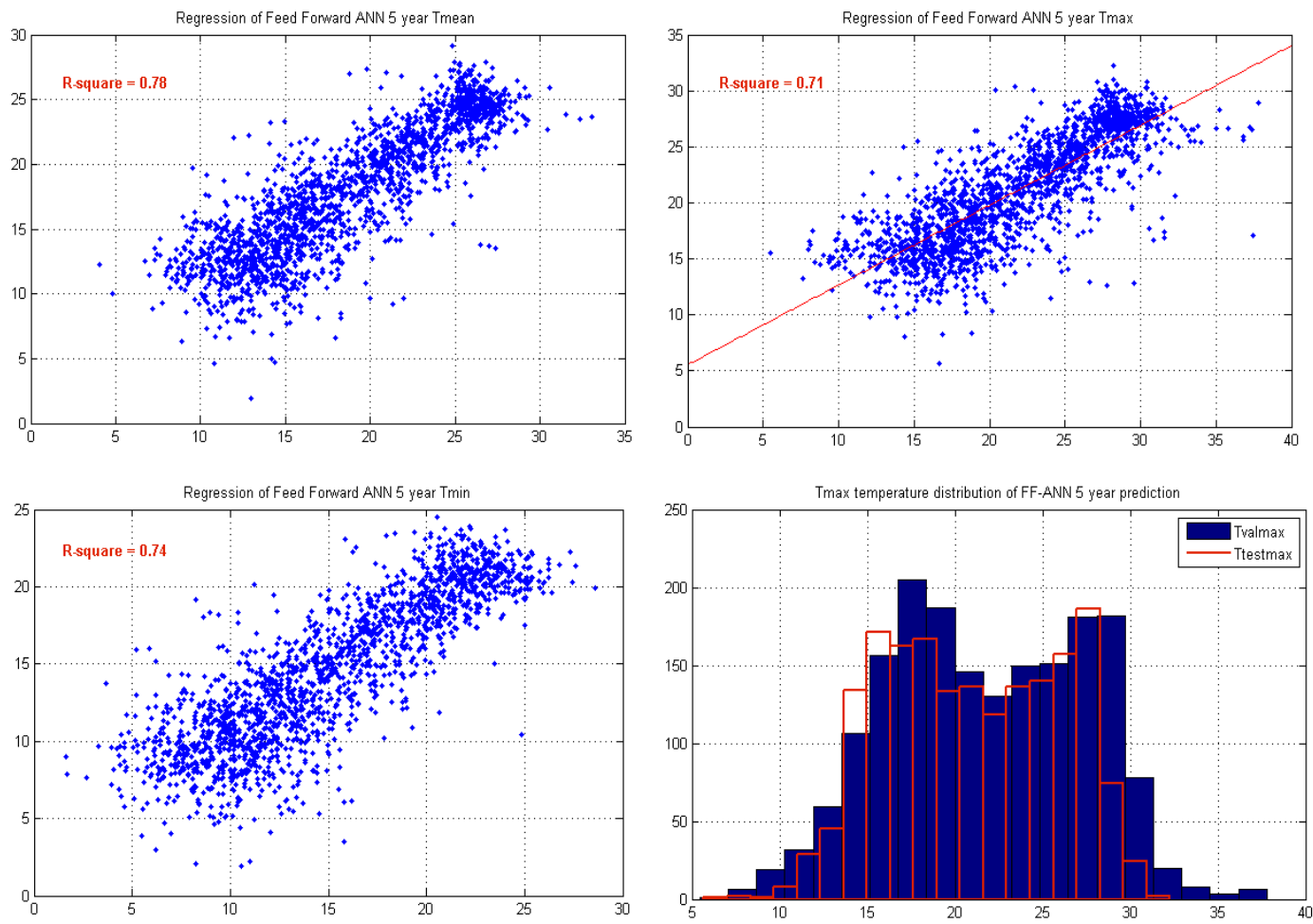
Figure 44. Actual daily mean-maximum and minimum temperature versus predicted temperature & frequency distribution of the maximum temperature.
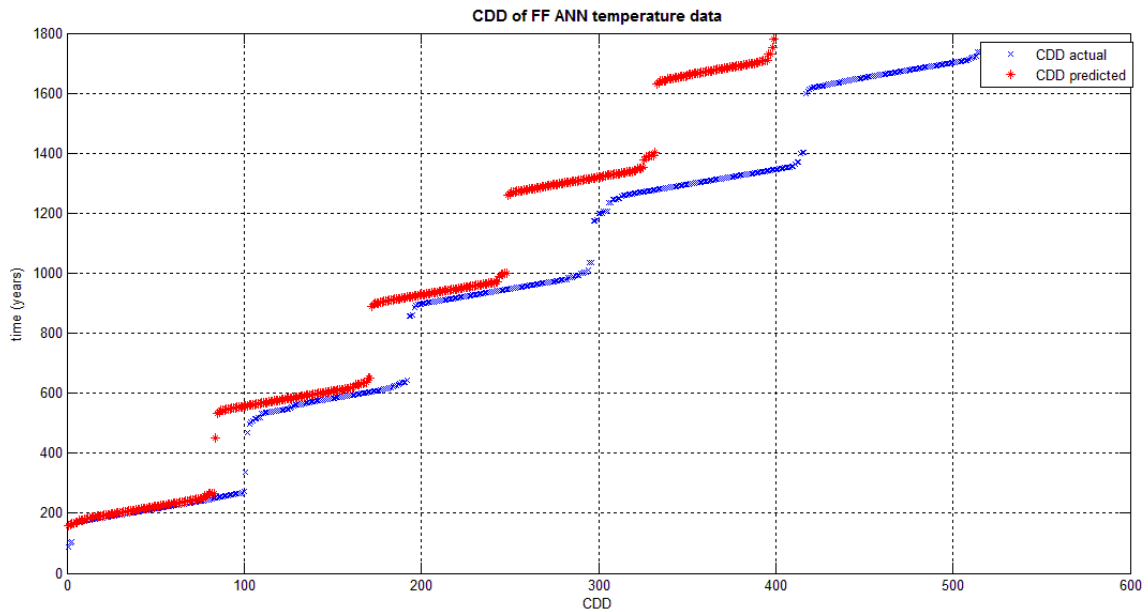
Figure 45. CDD of max daily temperatures for feed forward predicted (red, CDD=737) and actual (blue, CDD = 519) data.

Following the 5 year prediction periods and the results presented in Figure 43, Figure 45 we assume that the feed forward neural network with the 5-year training sets predicts the mean values of our temperature data less sufficiently with an r-squared error 0.78 and MSE 8.61. The cooling degree days, are predicted less accurate, exceeding the actual CDD by 42% for the period 2004-2009. Regarding the maximum temperature data prediction, the model underestimates again the actual maximum values, with r-square error 0.71 and MSE 11.48.The maximum predicted temperature reaches the 32.26oC, while the actual maximum temperature of the 5-year period 2005-2009 is 37.8oC.

NARX ANN

Subsequently we create a nonlinear autoregressive network with exogenous inputs. The specific feature of such neural networks respect to static feed-forward networks, such as back propagation (BP) ANN or cascade-forward ANN is their capability to learn dynamic or time series relationships. In particular, in dynamic ANNs, the output depends not only on the current input but on the current and previous inputs, outputs or states of the network, as well. The NARX network, differently from the focused networks, is a recurrent dynamic network, with feedback connections enclosing several layers of the network. The NARX model is based on the linear ARX model, it is well suited to model nonlinear dynamic systems and is commonly used in time-series modeling thanks to its adaptive learning process also with small scale meteorological data, collected, for example in less than one year. [49]
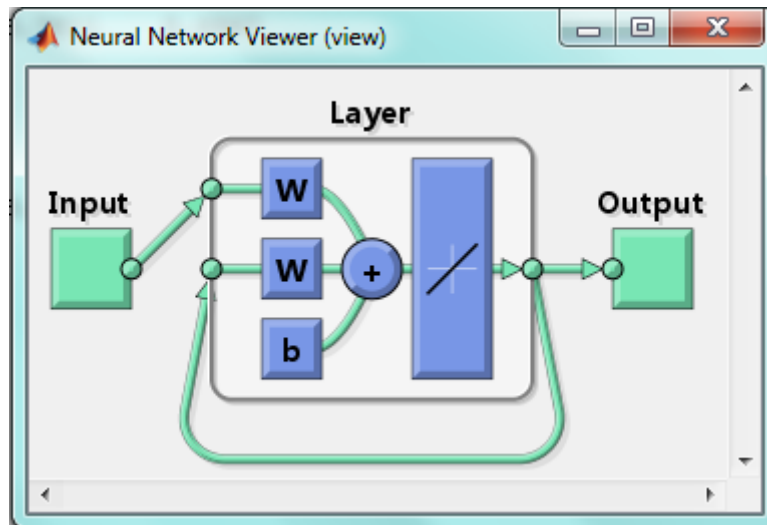
Figure 46. Nonlinear autoregressive single layer network

Table 9. Main statistical values of actual and simulated temperature data for the period 2005-2009

| trainlm	Tmean	Tmax	Tmin	Tvar	SME	R squared
Actual Temperature (max)	21.79	37.8	5.45	31.63	-	-
Simulated Temperature (max)	21.50	32.40	5.91	24.13	10.81	0.78
Actual Temperature (min)	15.13	28.6	1.60	29.90	-	-
Simulated Temperature (min)	14.51	24.54	-0.57	22.39	8.59	0.74
Actual Temperature (mean)	18.68	34.75	4.04	30.61	-	-
Simulated Temperature (mean)	18.10	29.27	2.08	25.18	8.23	0.71
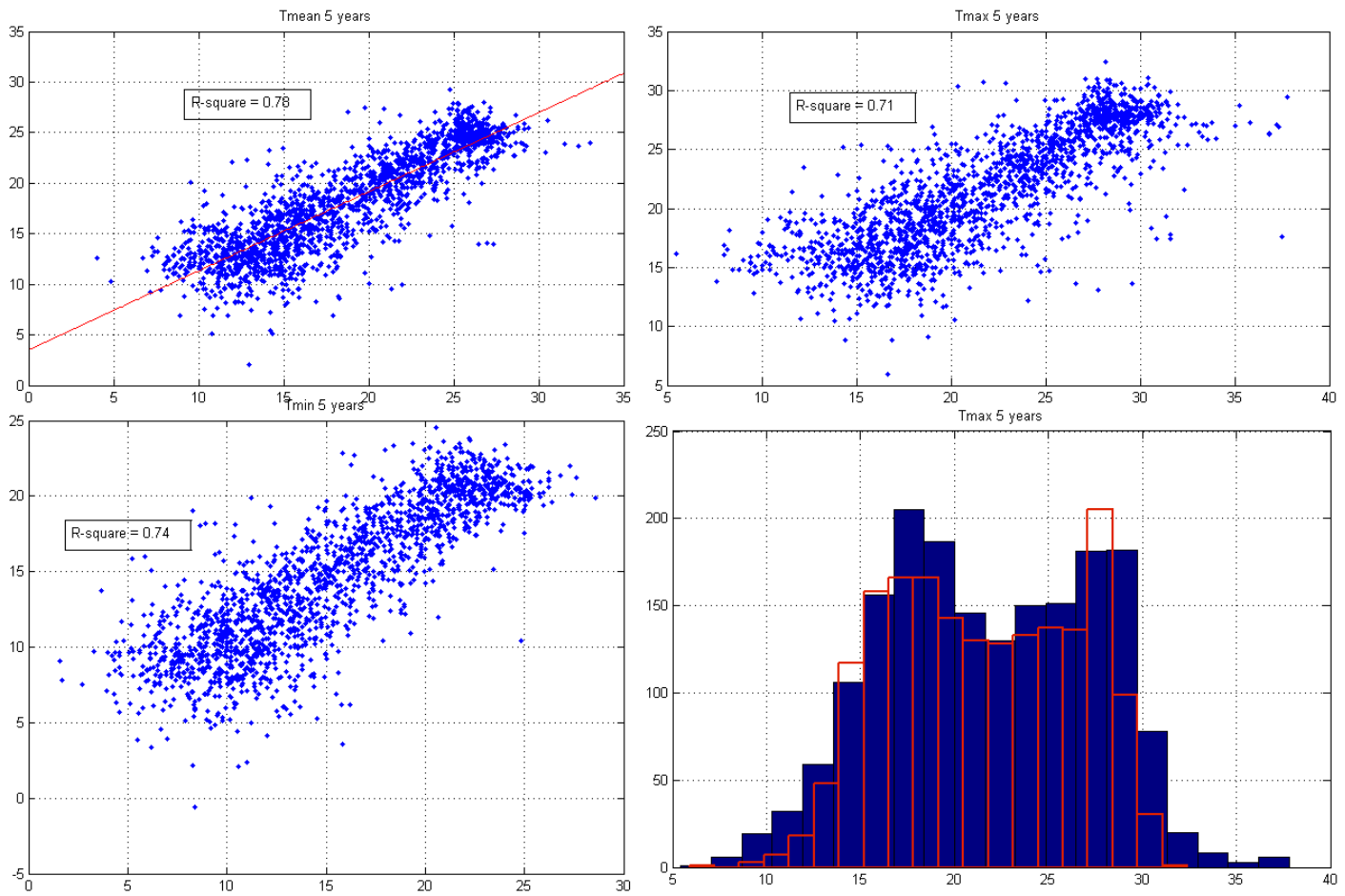
Figure 47. Actual daily mean-maximum and minimum temperature versus predicted temperature & frequency distribution of the maximum temperature.
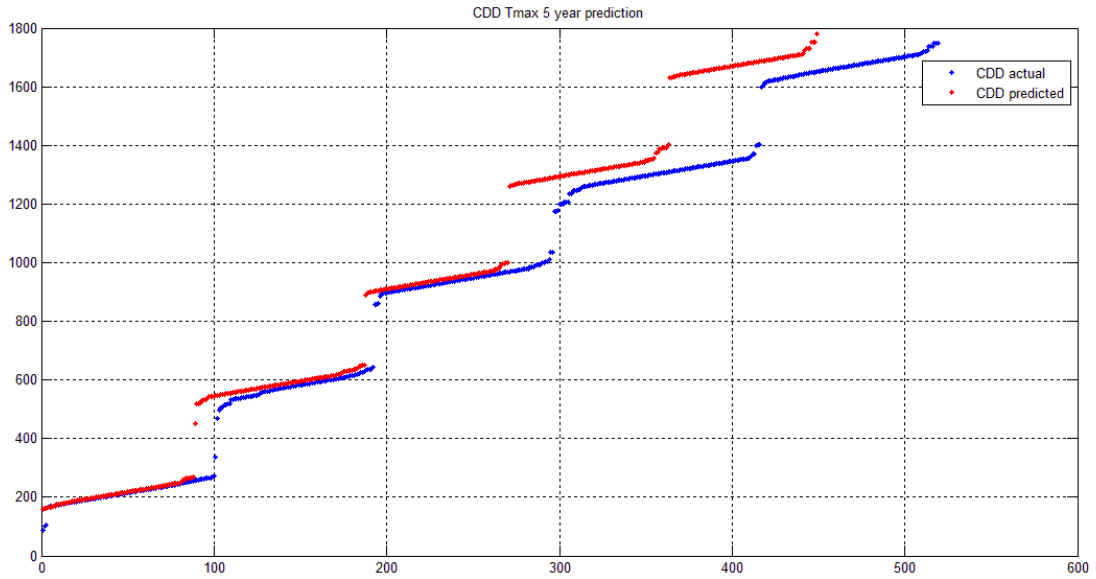
Figure 48. CDD of max daily temperatures for feed forward predicted (red, CDD=449) and actual (blue, CDD = 519) data.

Following the 5 year prediction periods and the results presented in Figure 47, Figure 48 we assume that the NARX neural network with the 5-year training sets predicts the mean values of our temperature data with an r-squared error 0.71 and MSE 8.23, which is slightly under the feed forward network. The cooling degree days, are predicted more accurate, extending underneath the actual CDD by 13.49% for the period 2004-2009. Regarding the maximum temperature data prediction, the model underestimates again the actual maximum values, with r-square error 0.70 and MSE 10. 81. The maximum predicted temperature reaches the 32.40 ºC, while the actual maximum temperature of the 5-year period 2005-2009 is 37.8 ºC.

After the better results of the NARX net, considering the better maximum temperature predictions as well the frequency distribution, we decide to explore another training function, namely the BFGS quasi-Newton back propagation "trainbfg". The new NARX network is being evaluated in the prediction of air temperature data for the same five year period 2004-2009, as shown in Table 10.

Table 10. Main statistical values of actual and simulated temperature data for the period 2004-2009

trainbfg	Tmean	Tmax	Tmin	Tvar	SME	R squared
Actual Temperature (max)	21.79	37.8	5.45	31.63	-	-
Simulated Temperature	22.14	34.17	5.78	26.99	7.98	0.8

|					
(max)					
Actual Temperature (min)	15.13	28.6	1.60	29.90	-	-
Simulated Temperature (min)	15.58	26.54	1.08	23.15	10.9	0.74
Actual Temperature (mean)	18.68	34.75	4.04	30.61	-	-
Simulated Temperature (mean)	19.18	31.07	3.54	26.14	8.2	0.71
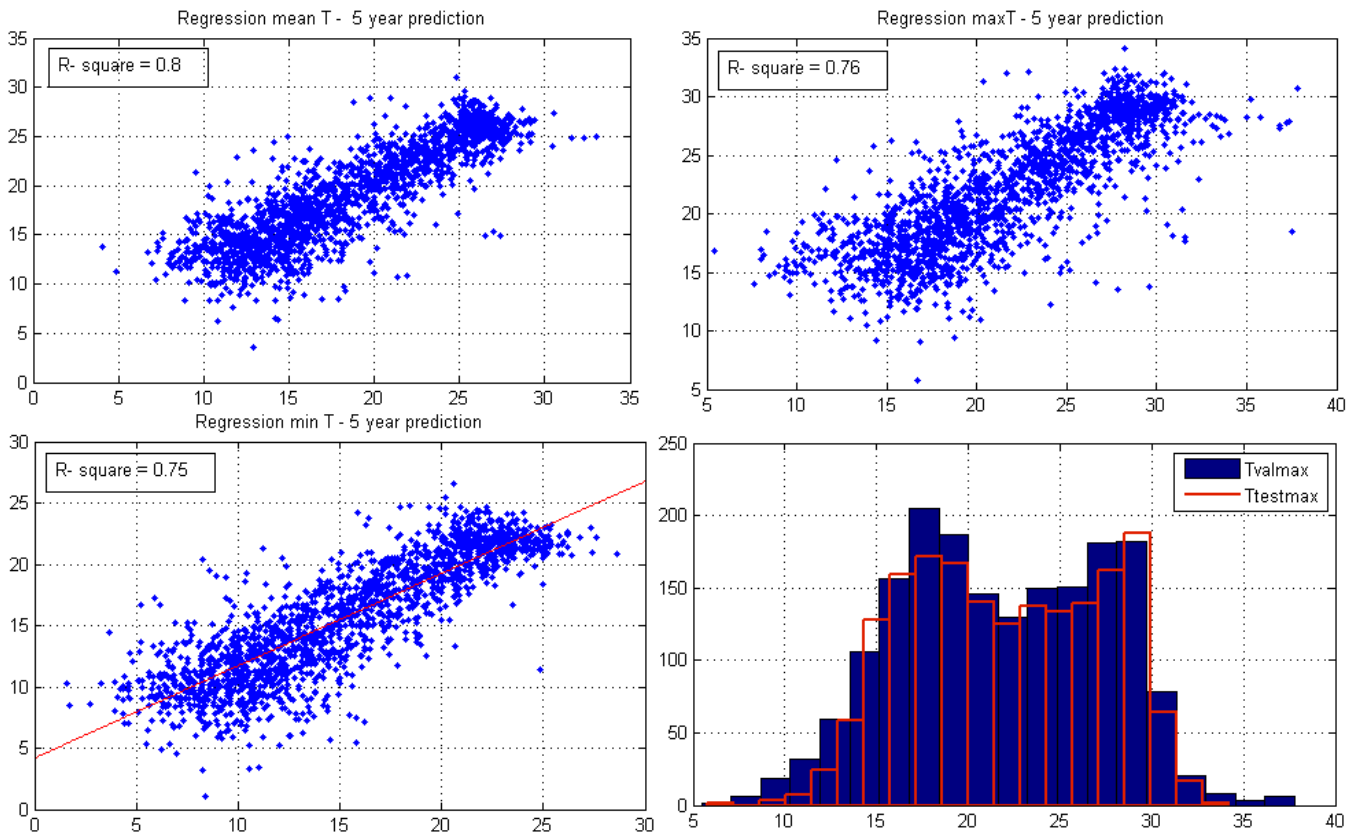
Figure 49. Actual daily mean-maximum and minimum temperature versus predicted temperature & frequency distribution of the maximum temperature.
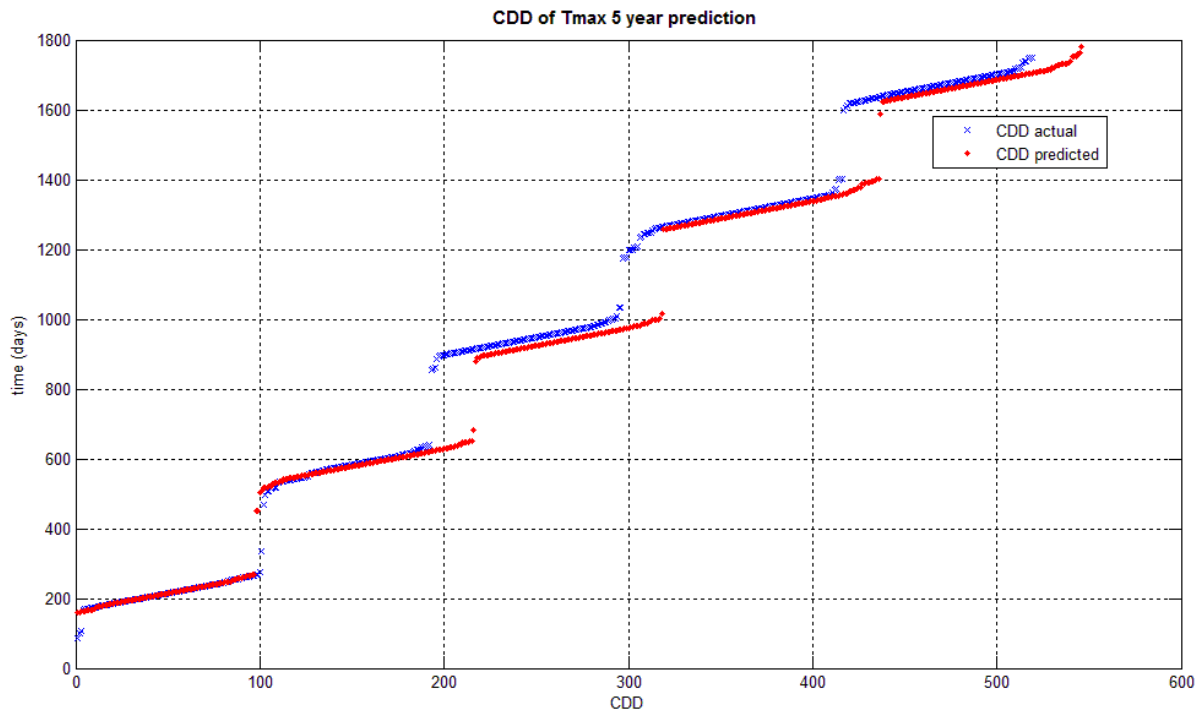
Figure 50. CDD of max daily temperatures for feed forward predicted (red, CDD=546) and actual (blue, CDD = 519) data.

Following the 5 year prediction periods and the results presented in Figure 49, Figure 50, we assume that the NARX neural network with the 5-year training sets and the BFGS quasi-Newton backpropagation training function predicts the mean values of our temperature data with an r-squared error 0.71 and MSE 8.2, similar to the previous NARX network. The cooling degree days, are predicted more accurate, exceeding the actual CDD by 5.2 % for the period 2004-2009. Regarding the maximum temperature data prediction, the model underestimates again the actual maximum values, with r-square error 0.80 and the MSE has significant decreased to 7.98. The maximum predicted temperature reaches the 34.70 °C, while the actual maximum temperature of the 5-year period 2005-2009 is 37.8 °C. Furthermore, the frequency distribution (histogram) of the maximum temperature corresponds better to the actual temperature data.

After several trials including also elman and cascade networks, it was decided to proceed our long term temperature prediction using the NARX network with BFGS quasi-Newton back propagation. As a result, we used the 5-year training periods for the forecast of the years 2010-2014, as shown in Figure 51.
We used the trained neural network, in order to predict the mean maximum and minimum daily temperature for the decade 2010-2014.
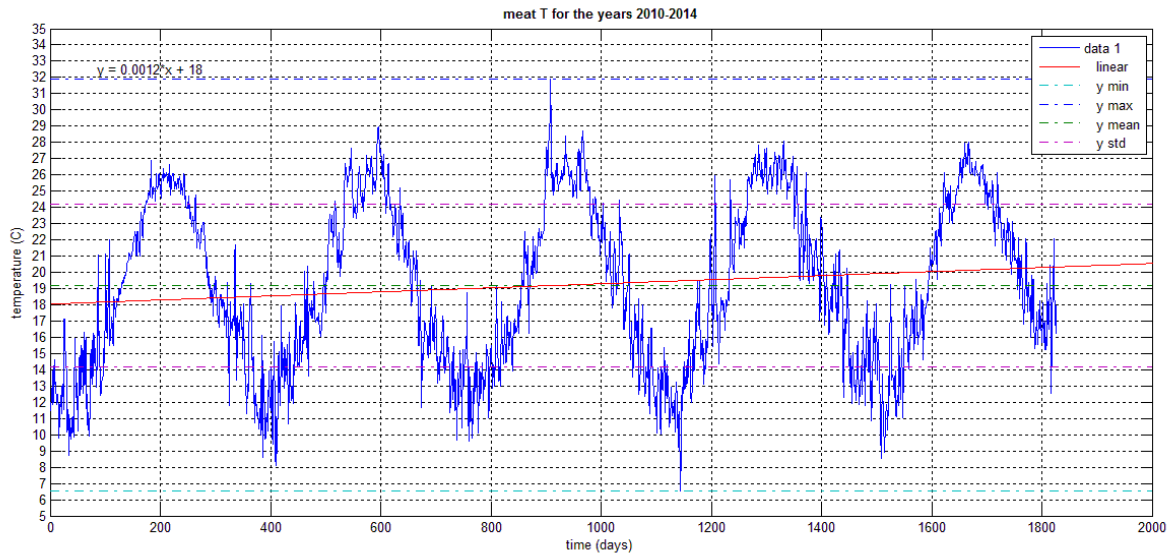
Figure 51. Five year prediction of mean-minimum and maximum daily temperature data using NARX net.

Continuing, we use the predicted data set as an input, in order to extend the forecasting period till 2019, Figure 52.
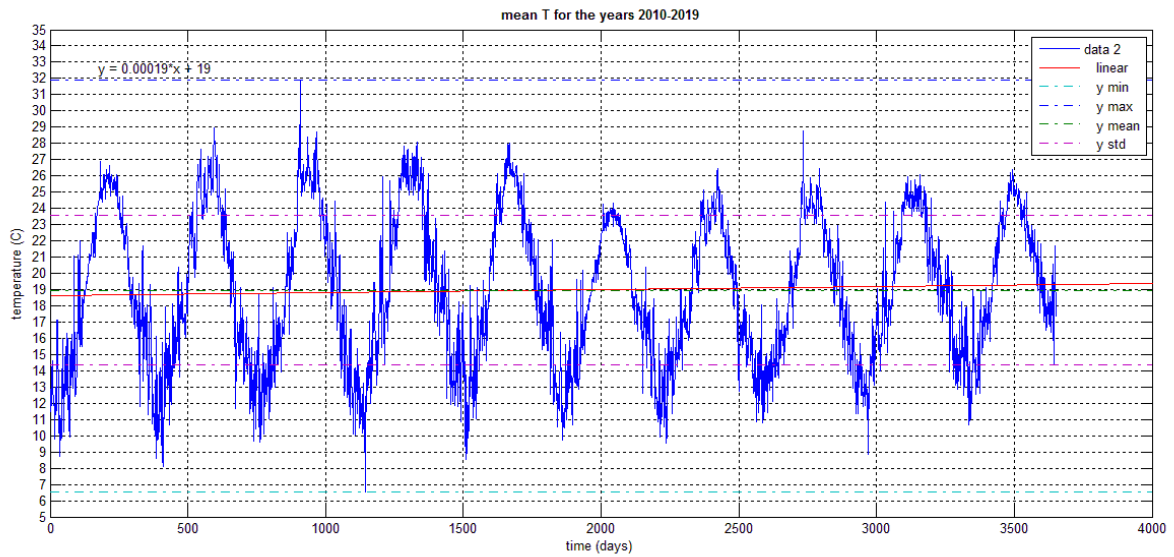

Figure 52. Ten year prediction of mean-minimum and maximum daily temperature data using NARX net.
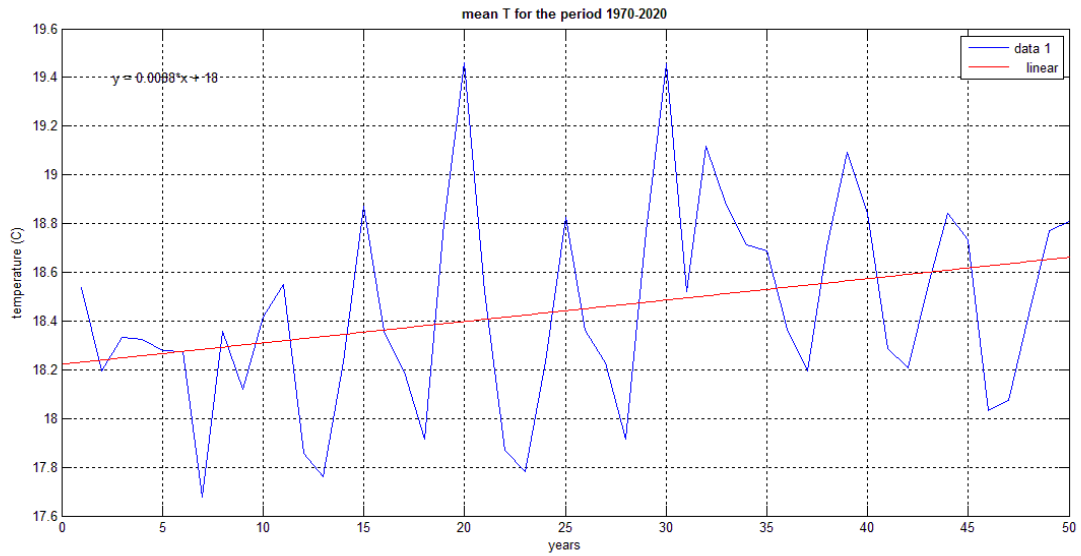
Figure 53. Mean annual temperature with the linear trend representation for the reference & predicted period 1970-2019.

We proceed with a training period of 15 years. It was considered that the trend lines of the collected temperature data would be better trailed if the training set would include a longer period of the time series with a more representative inclination.

Then the network is being evaluated in the prediction of air temperature data for the decade 2000-2009. We first begin with creating the feed forward network using the Levenberg-Marquardt algorithm.
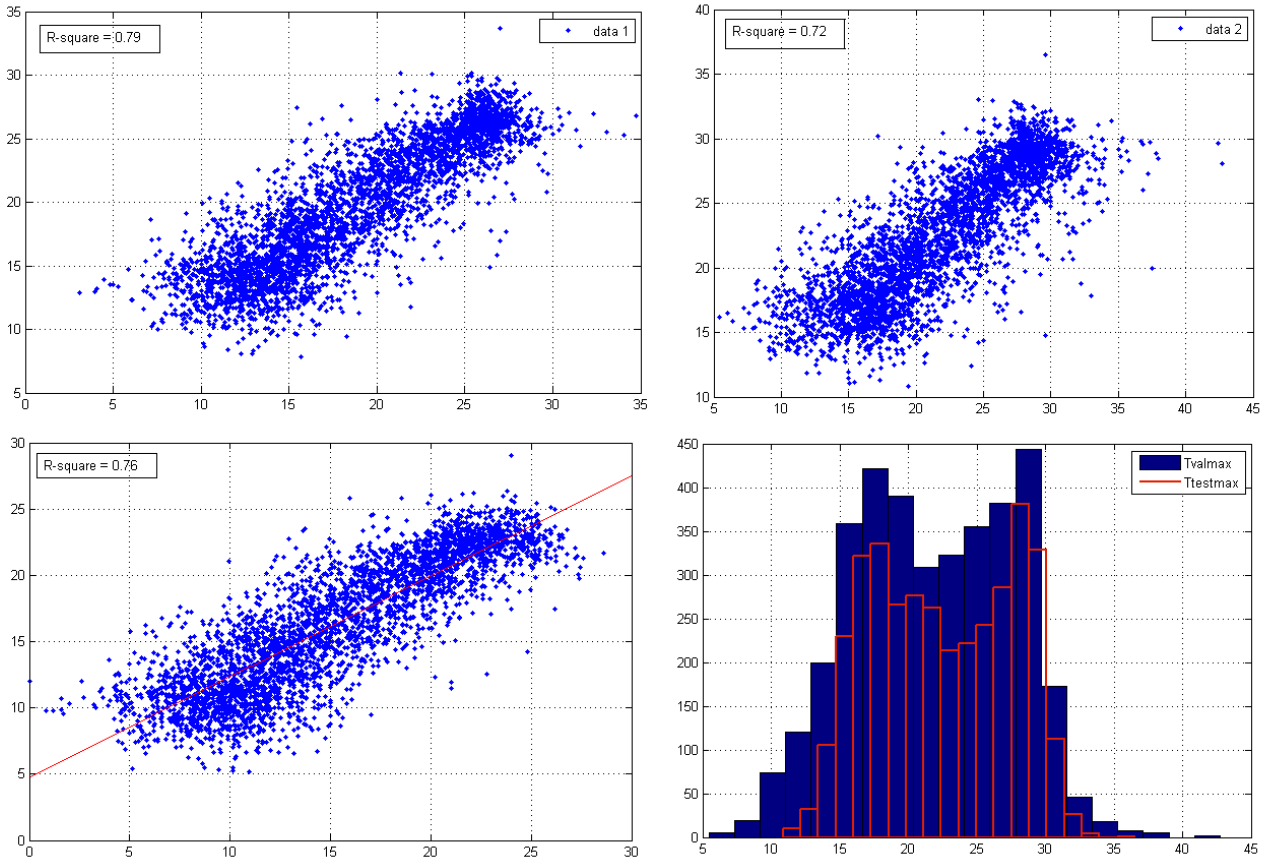
Figure 54. Actual daily mean-maximum and minimum temperature versus predicted temperature & frequency distribution of the maximum temperature.
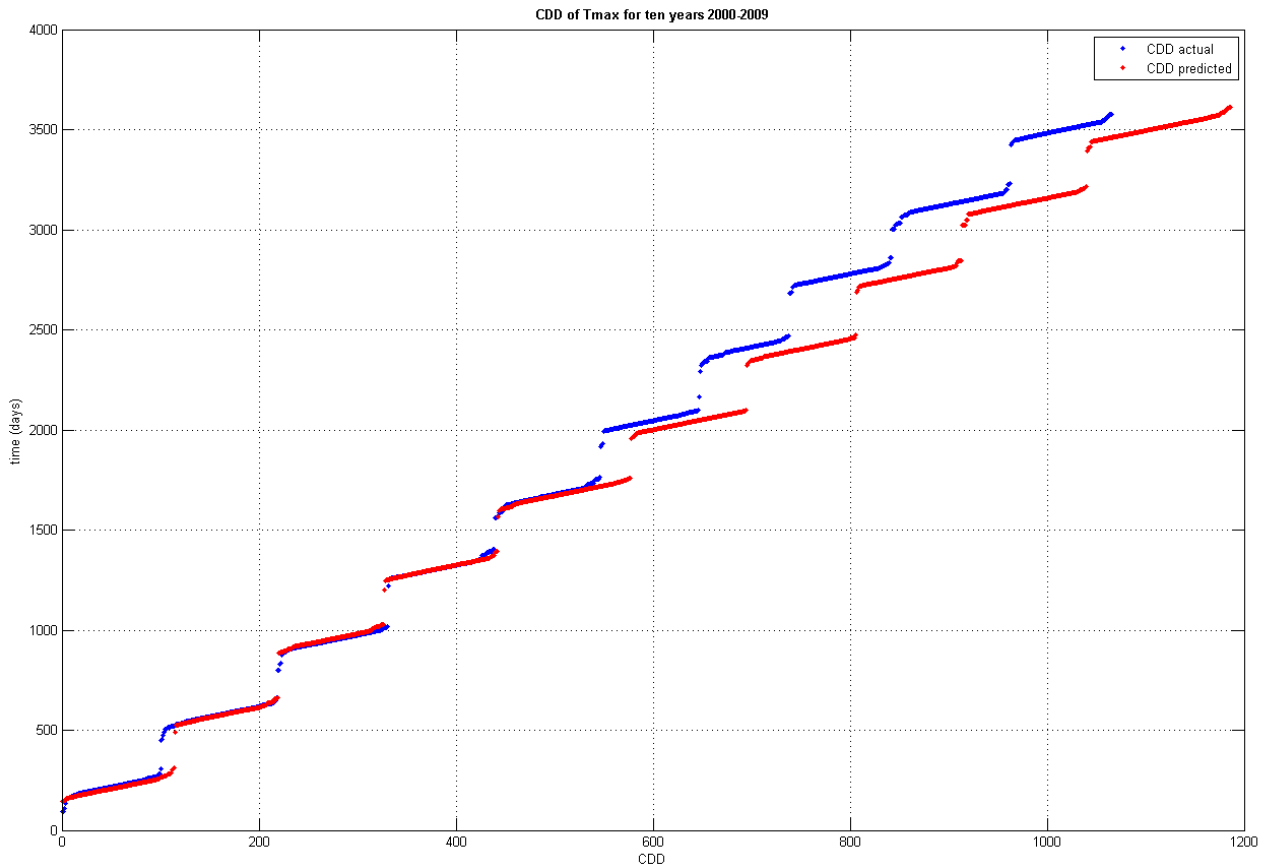
Figure 55. CDD of max daily temperatures for feed forward predicted (red, CDD=1186) and actual (blue, CDD = 1065) data.

Table 11 Main statistical values of actual and simulated temperature data for the period 2000-2009

trainlm	Tmean	Tmax	Tmin	Tvar	SME	R squared
Actual Temperature (max)	21.82	42.73	5.45	33.41	-	-
Simulated Temperature (max)	22.5577	36.5061	10.8649	25.2829	11.1920	0.72
Actual Temperature (min)	15.36	28.6	0.03	30.15	-	-
Simulated Temperature	16.3164	29.0563	5.1495	23.6981	9.2196	0.76

	(min)					
Actual Temperature (mean)	18.75	34.75	3.1	31.56	-	-
Simulated Temperature (mean)	19.6813	33.6781	7.8674	26.0031	8.5347	0.79

Following the 10 year prediction periods and the results presented in Figure 54 to Figure 55 we assume that the feed forward neural network with one training set of fifteen years, predicts less adequately the mean values of our temperature data, with an r-squared error 0.79 and MSE 8.53. The cooling degree days, i.e the amount of temperature data exceeding the 26°C, exceeds the actual data by 11.36% for the period 2000-2009. Regarding the maximum temperature data prediction, we assume again an underestimation of the model, with r-square error 0.72 and MSE 11.19. The maximum predicted temperature reaches the 36.5^{o}C (lower than the one resulting from the ten year training sets in Figure 35) , while the actual maximum temperature of the decade 2000-2009 is 42.73^{o}C.

For the NARX network trained with a fifteen yearlong daily temperature data set, the results are neither improving the networks performance.
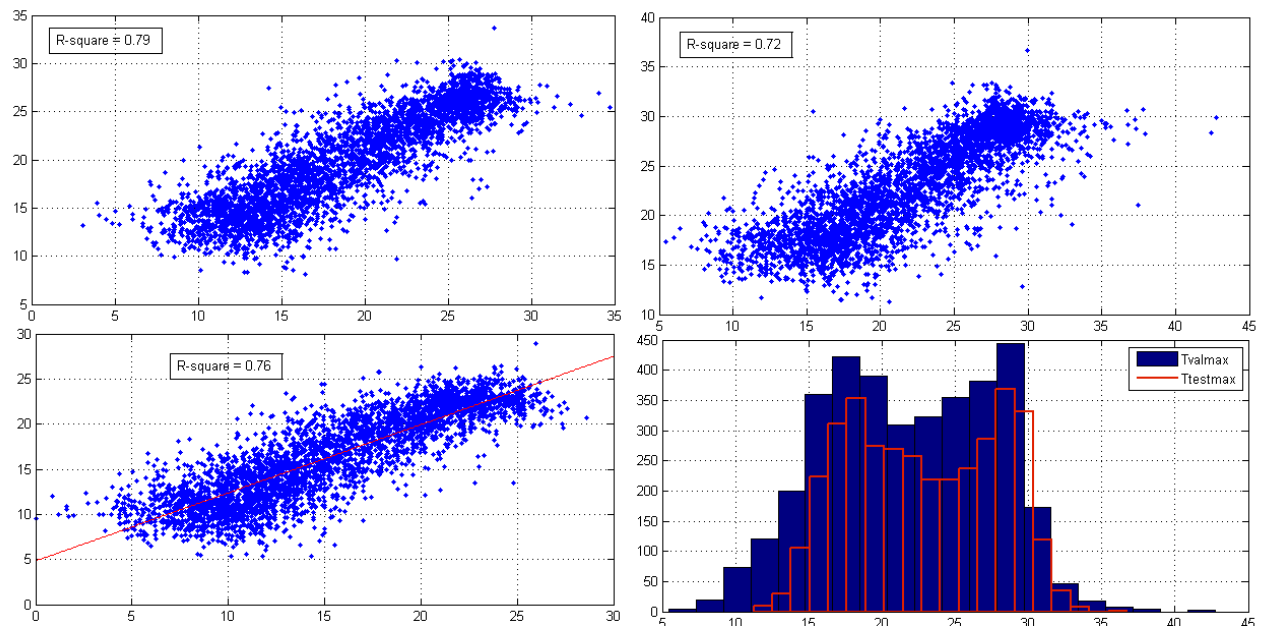
Figure 56. Actual daily mean-maximum and minimum temperature versus predicted temperature & frequency distribution of the maximum temperature.

**Table 12. Main statistical values of actual and simulated temperature data for the period 2000-2009**

| trainbfg	Tmean	Tmax	Tmin	Tvar	SME	R squared
Actual Temperature (max)	21.82	42.73	5.45	33.41	-	-
Simulated Temperature (max)	22.8869	36.7102	11.2441	25.2441	11.8942	0.79
Actual Temperature (min)	15.36	28.6	0.03	30.15	-	-
Simulated Temperature (min)	16.3451	28.8955	5.3169	23.5420	9.2688	0.72
Actual Temperature (mean)	18.75	34.75	3.1	31.56	-	-
Simulated	19.8355	33.6306	8.1288	25.7914	8.8916	0.76
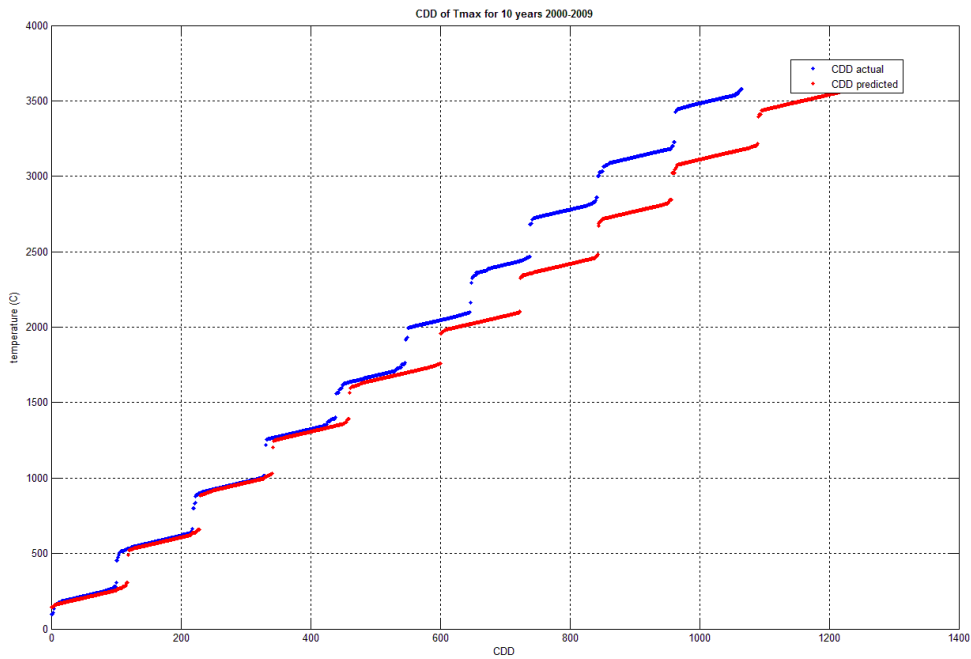
Figure 57. CDD of max daily temperatures for feed forward predicted (red, CDD=1243) and actual (blue, CDD = 1065) data.

Using the "trainbfg" function, the results are depicted in Figure 56 and Figure 57. As shown in Table 12, the statistical values of the predicted mean maximum and minimum temperature data, do not differ significant from the feed forward network, while the cooling degree days are overestimated by 17.71%.

HYBRID ARMA ANN

Considering the error between the original and the ARIMA-predicted data as a nonlinear component, we create an extra input interval for the feed forward ANN. The results of a ten year prediction for the years 2000-2009 in conjunction to our validation data set, are depicted in Figure 58 to Figure 60, and in Table 13.
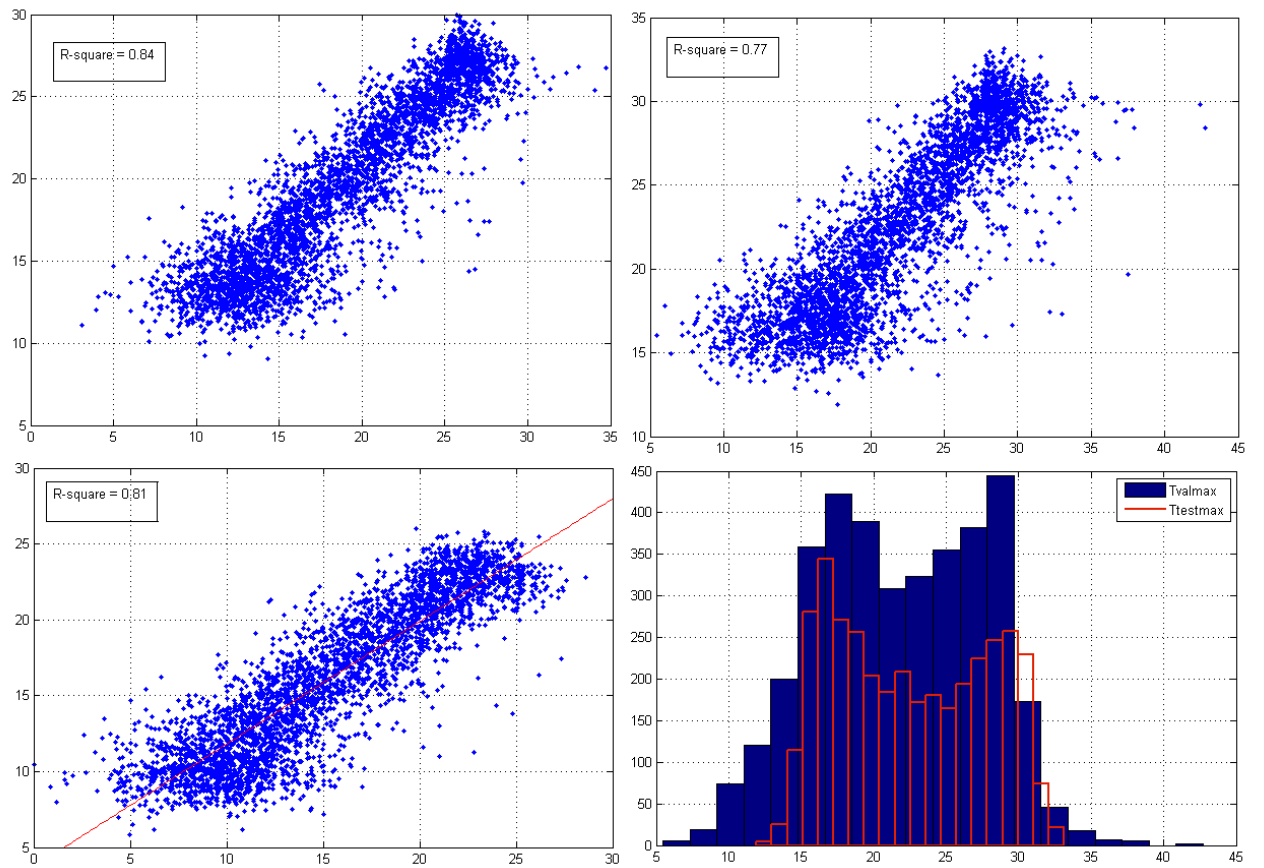
**Figure 58. Actual daily mean-maximum and minimum temperature versus predicted temperature & frequency distribution of the maximum temperature.**
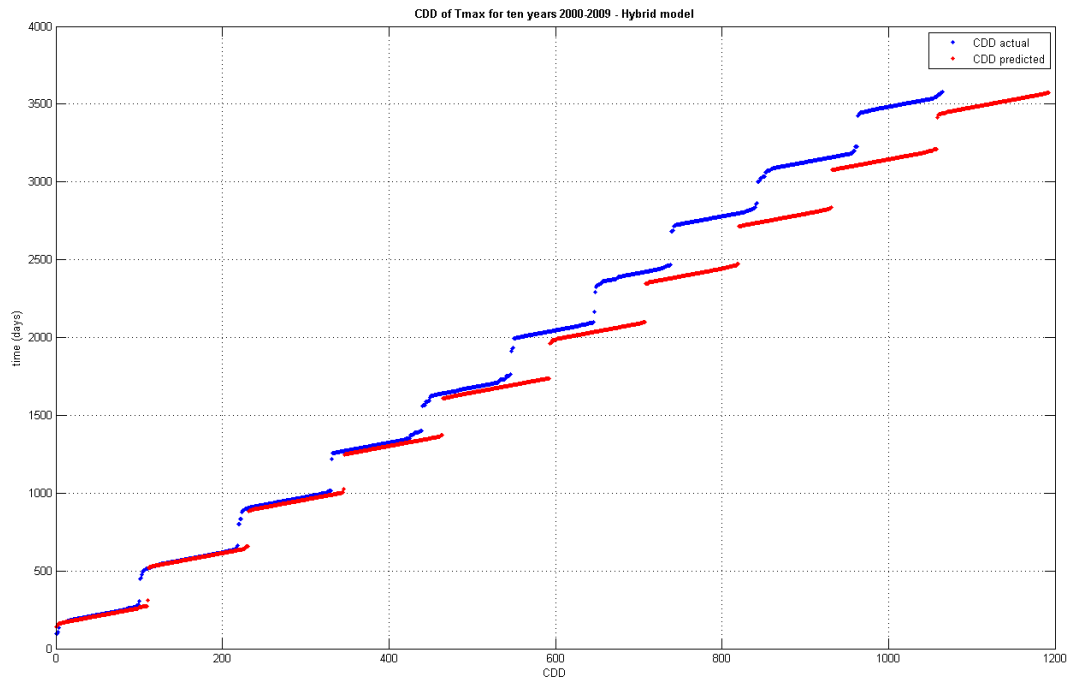
Figure 59. CDD of max daily temperatures for feed forward predicted (red, CDD=1192) and actual (blue, CDD = 1065) data.
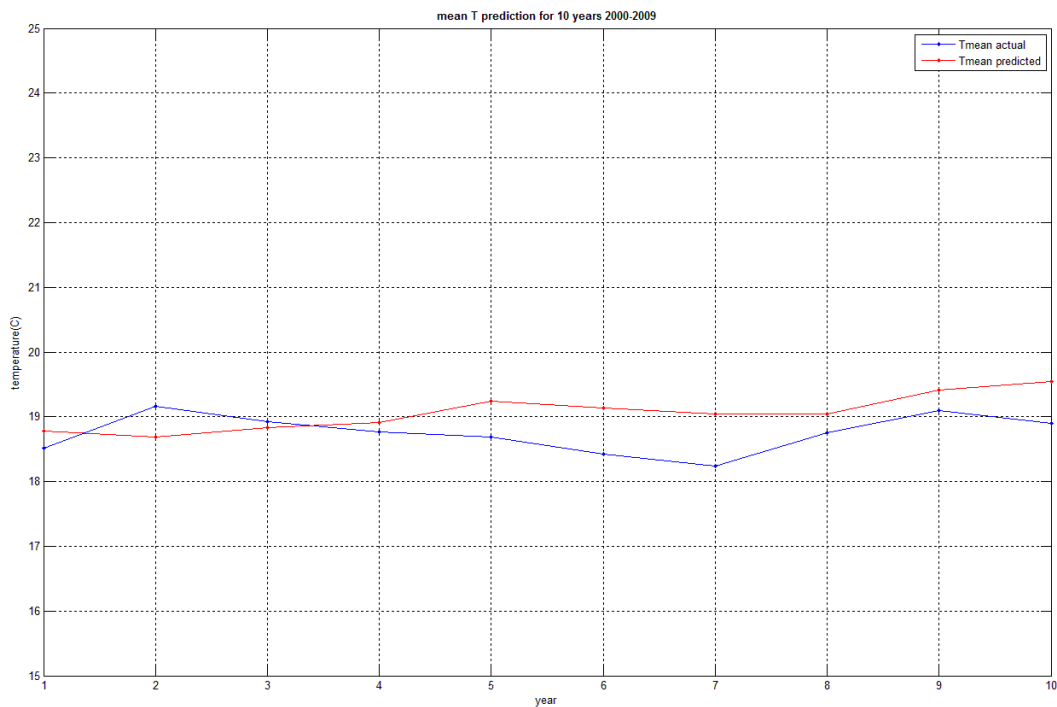

Figure 60. Annual mean temperature of the actual temperature data (blue) and the hybrid ANN (red) prediction.

Table 13. Main statistical values of actual and simulated temperature data for the period 2000-2009

trainlm	Tmean	Tmax	Tmin	Tvar	SME	R squared
Actual Temperature (max)	21.82	42.73	5.45	33.41	-	-
Simulated Temperature (max)	22.5890	33.1330	11.9204	27.0084	9.5702	0.77
Actual Temperature (min)	15.36	28.6	0.03	30.15	-	-
Simulated Temperature (min)	16.0477	26.0144	5.8069	24.9872	7.0095	0.8
Actual Temperature (mean)	18.75	34.75	3.1	31.56	-	-
Simulated Temperature (mean)	19.5359	29.9741	9.0694	27.5467	6.4517	0.84

After the 10 year prediction periods using the hybrid ARMA-ANN model and the results presented in Figure 58 to Figure 60 we assume that the Hybrid ARMA-feed forward neural network, predicts the mean values of our temperature data with an r-squared error 0.84 and MSE 6.45. The cooling degree days, i.e the amount of temperature data exceeding the 26°C, exceeds the actual data by 11.9% for the period 2000-2009. Regarding the maximum temperature data prediction, this model does not reach higher temperature, with r-square error 0.77 and MSE 9.57. The maximum predicted temperature reaches the 33.13°C (lower than the one resulting from the ten year training sets in Figure 35) , while the actual maximum temperature of the decade 2000-2009 is 42.73°C. Unlike the simple ANN models, we assume in Figure 58 that the histogram of the predicted temperatures deviates from the actual temperature distribution.

After the observation of the test predictions for the decade 2000-2009, we decide to proceed with the ten year ahead temperature predictions for the decade 2010-2019, using as input the last decade of our reference temperature data 2000-2009.

First we begin with the feed forward network as it was developed and trained with ten year temperature data sets (Figure 32 to Figure 39). The predicted data are juxtaposed with the temperatures of the decade 2000-2009 in order to have an icon of the difference, the increase or decrease. The main statistical values of the long term ten year prediction for the years 2010 to 2019 are shown in Table 14.

Table 14. Main statistical values of actual and simulated temperature data for the period 2010-2019

trainlm	Tmean	Tmax	Tmin	Tvar	SME	R squared
2000-2009 Temperature (max)	21.82	42.73	5.45	33.41	-	-
2010-2019 Temperature (max)	24.0776	36.7828	7.7073	26.4038		
2000-2009 Temperature (min)	15.36	28.6	0.03	30.15	-	-
2010-2019 Temperature (min)	17.0918	28.7122	1.6540	24.0103		
2000-2009 Temperature (mean)	18.75	34.75	3.1	31.56	-	-
2010-2019 Temperature (mean)	20.8617	33.5417	4.4356	26.7168		
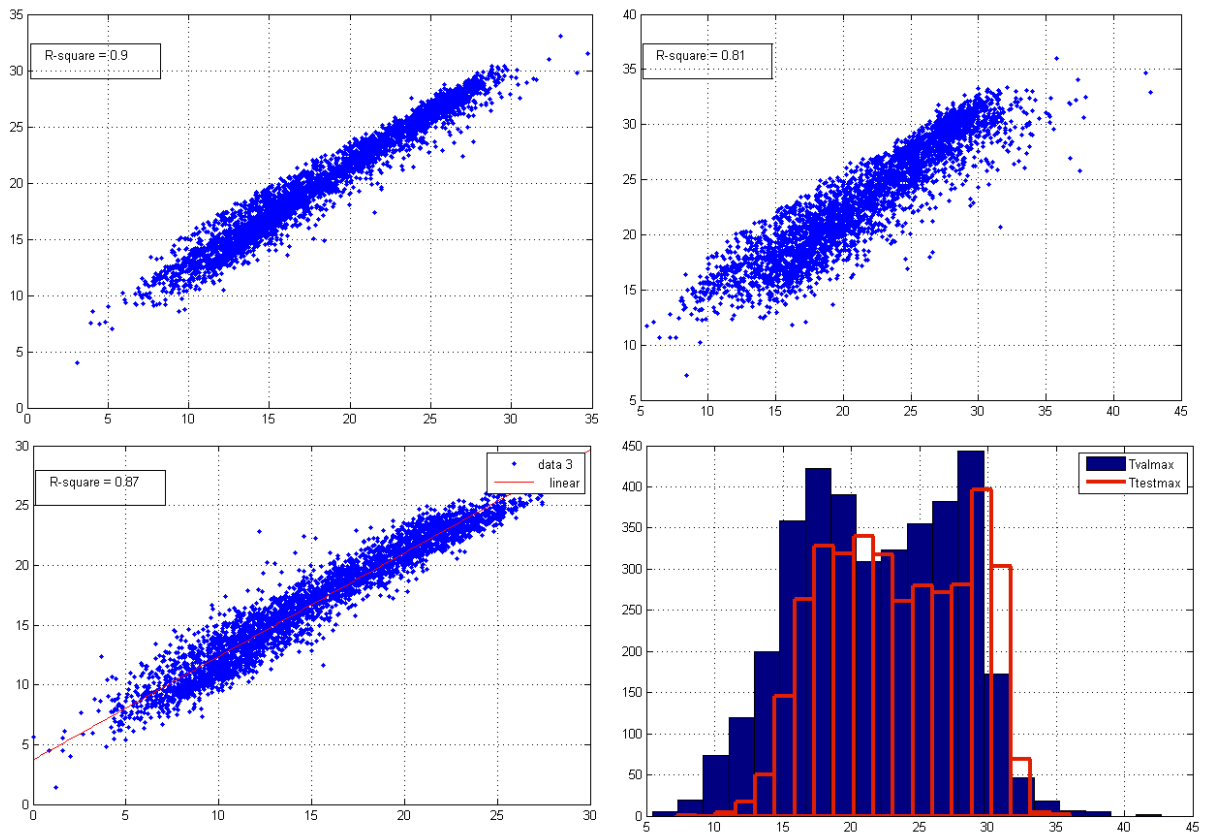
**Figure 61. Daily mean-maximum and minimum temperature of the years 2000-2009 versus 2010-2020 predicted temperature & frequency distribution of the maximum temperature.**
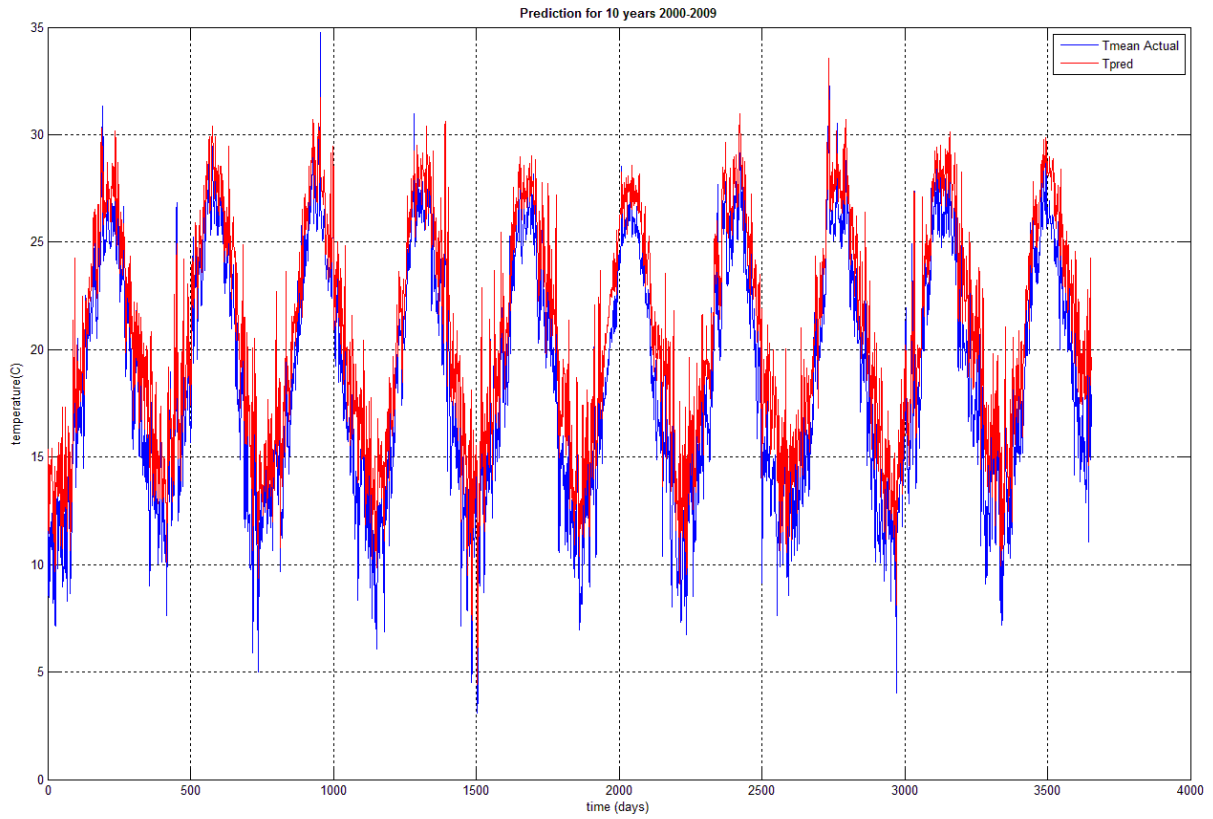
Figure 62. Temperature data of the decade 2000-2009 and predicted temperature data of 2010-2019
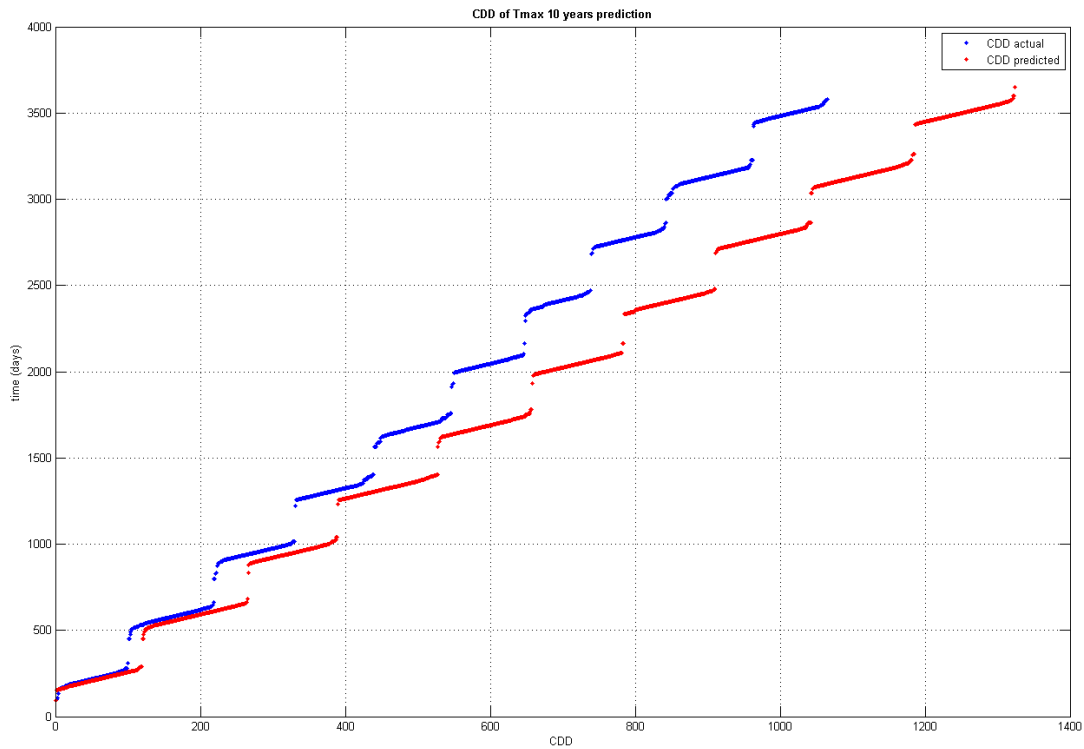

Figure 63. CDD of max daily temperatures for feed forward predicted (red, CDD=1324) and 2000-2009 (blue, CDD = 1065) data.
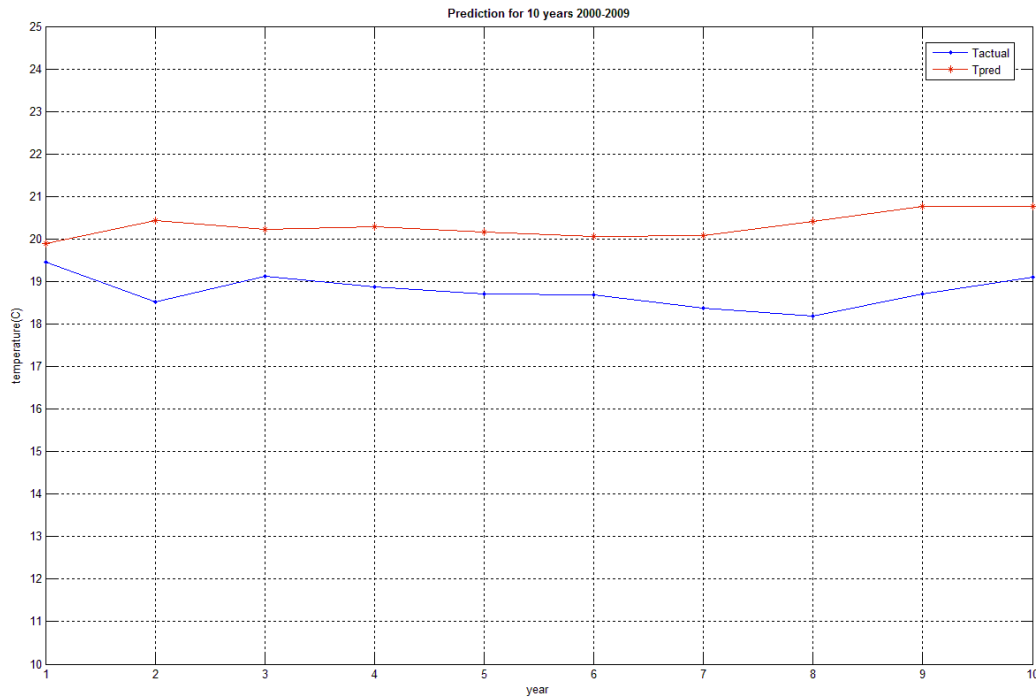
Figure 64. Mean yearly temperature data of the actual data for the years 2000-2009 and the prediction (red line) for the decade 2010-2019.

As it can be seen in Table 14, the mean temperature of the next decade 2010-2019 raises to 20.86, from 18.75, 2.11 degrees higher than the previous decade. This can also be seen in the mean maximum temperature, were it also increases from 21.82 to 24.0776, while the maximum temperature reaches the 36.78 ᵒC. The cooling degree days are increased in relation to the last decade, i.e, 24.32%. We assume that the model perceives the temperature increase according to the last 40 years data, projecting higher mean temperatures for the future, as it is also seen in the histogram in Figure 61.

We proceed with the NARX network as it was developed and trained with ten yearlong temperature data sets. The predicted data are juxtaposed with the temperatures of the decade 2000-2009 in order to have an icon of the difference, the increase or decrease. The main statistical values of the long term ten year prediction for the years 2010 to 2019, are shown in Table 15.

Table 15. Main statistical values of actual and simulated temperature data for the period 2010-2019

<u>trainbfg</u>	Tmean	Tmax	Tmin	Tvar	SME	R squared
2000-2009 Temperature	21.82	42.73	5.45	33.41	-	-

71

(max)					
2010-2019 Temperature (max)	22.8869	36.7102	11.2441	25.7011	
2000-2009 Temperature (min)	15.36	28.6	0.03	30.15	-	-
2010-2019 Temperature (min)	16.3451	28.8955	5.3169	23.9735	
2000-2009 Temperature (mean)	18.75	34.75	3.1	31.56	-	-
2010-2019 Temperature (mean)	19.8355	33.6306	8.1288	26.3040	
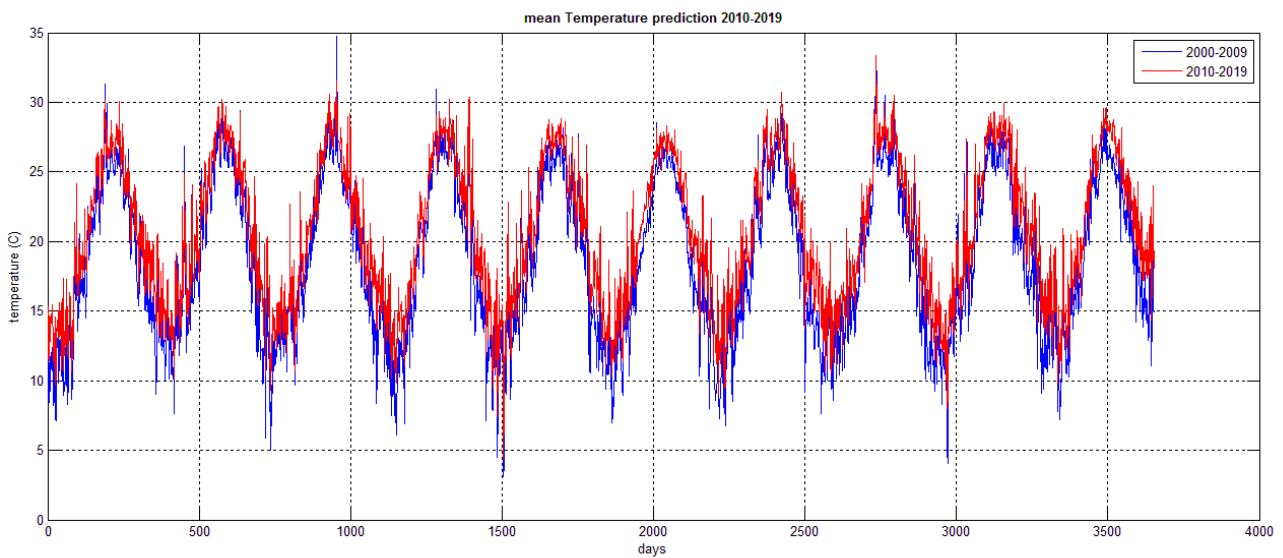
Figure 65. Temperature data of the decade 2000-2009 and predicted temperature data of 2010-2019
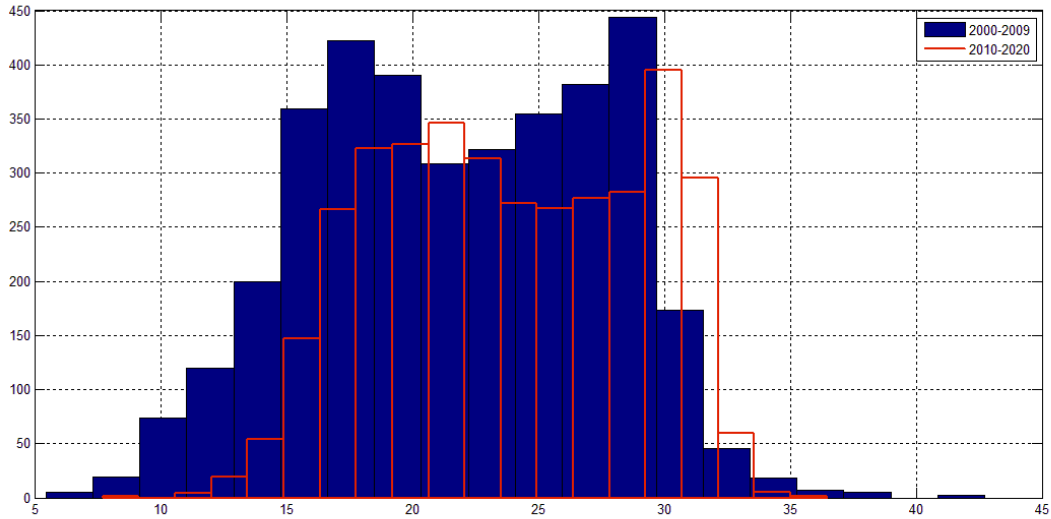
Figure 66. Actual daily maximum temperature versus predicted temperature frequency distribution.
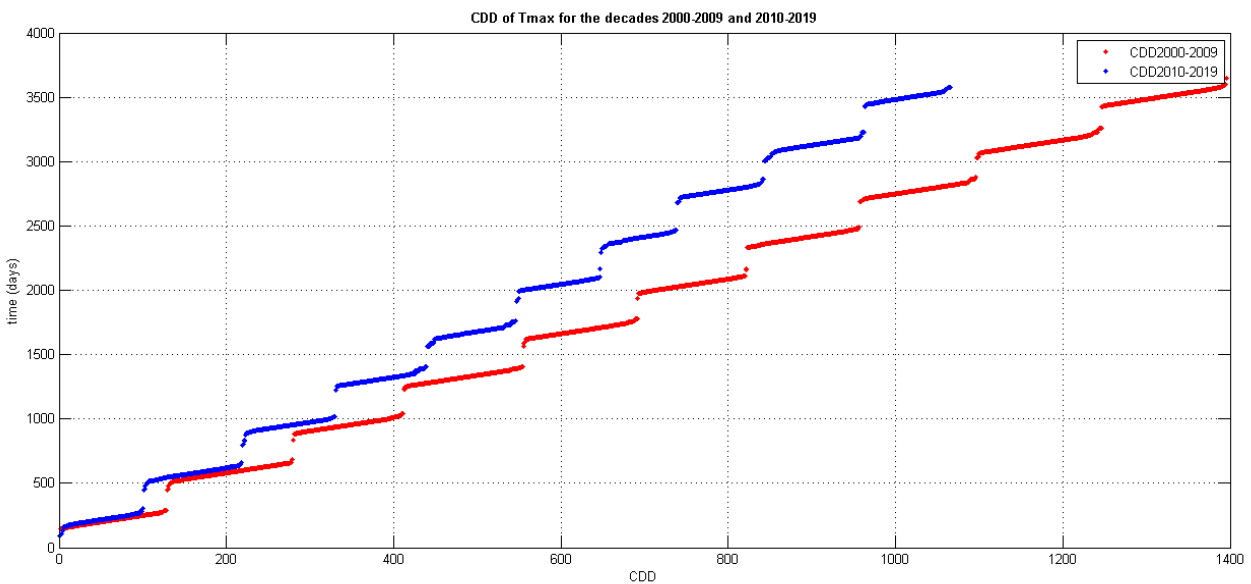
Figure 67. CDD of max daily temperatures for NARX NET predicted (red, CDD=1243) and actual (blue, CDD = 1065) data.

As it can be seen in Table 15, the mean temperature of the next decade 2010-2019 raises to 19.83, from 18.75, 1.08 degrees higher than the previous decade. This represents a more rational increase compared to the feed forward network results, although it is still a high temperature increase. Furthermore, the mean maximum temperature, also increases from 21.82 to 22.88, while the maximum temperature reaches the 36.71 °C. The cooling degree days are increased in relation to the last decade, i.e., 16.71%. We assume that the model

perceives the temperature increase according to the last 40 years data, projecting higher mean temperatures for the future, as it is also seen in the right shift of the maximum temperatures in the histogram in Figure 66.

Finally we use the developed hybrid model for the ten year prediction. The main statistical values of the long term ten year prediction for the years 2010 to 2019 are shown in Table 16.

Table 16. Main statistical values of actual and simulated temperature data for the period 2010-2019

| trainlm	Tmean	Tmax	Tmin	Tvar	SME	R squared
2000-2009 Temperature (max)	21.82	42.73	5.45	33.41	-	-
2010-2019 Temperature (max)	23.3481	33.9470	11.5955	26.4204		
2000-2009 Temperature (min)	15.36	28.6	0.03	30.15	-	-
2010-2019 Temperature (min)	16.5475	26.0695	5.5617	24.6607		
2000-2009 Temperature (mean)	18.75	34.75	3.1	31.56	-	-
2010-2019 Temperature (mean)	20.1765	30.5872	8.4889	27.0664		
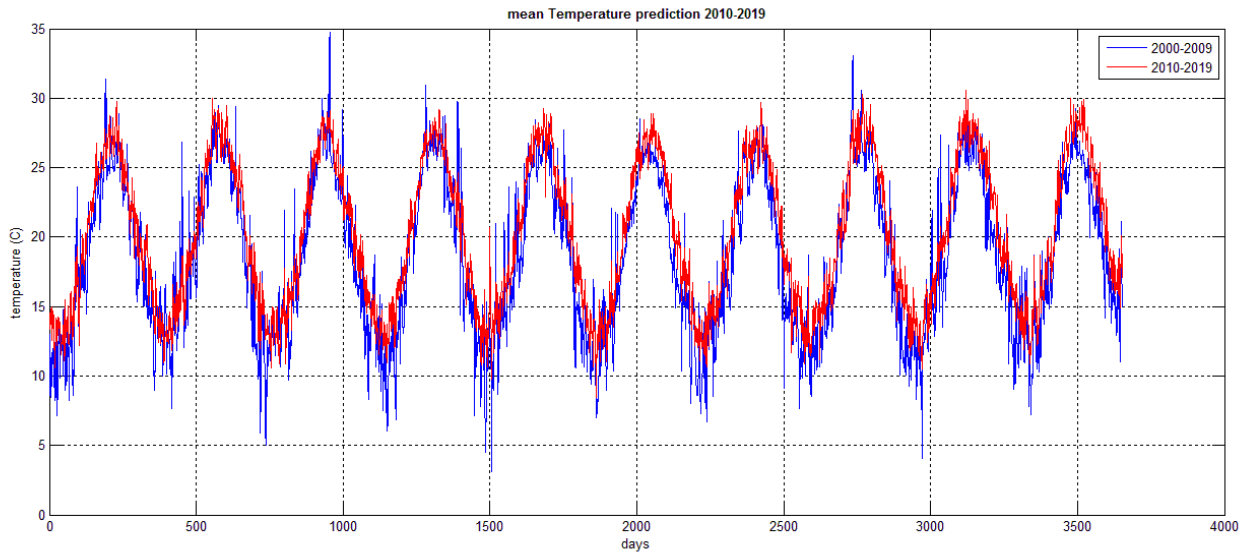
Figure 68. Temperature data of the decade 2000-2009 and predicted temperature data of 2010-2019
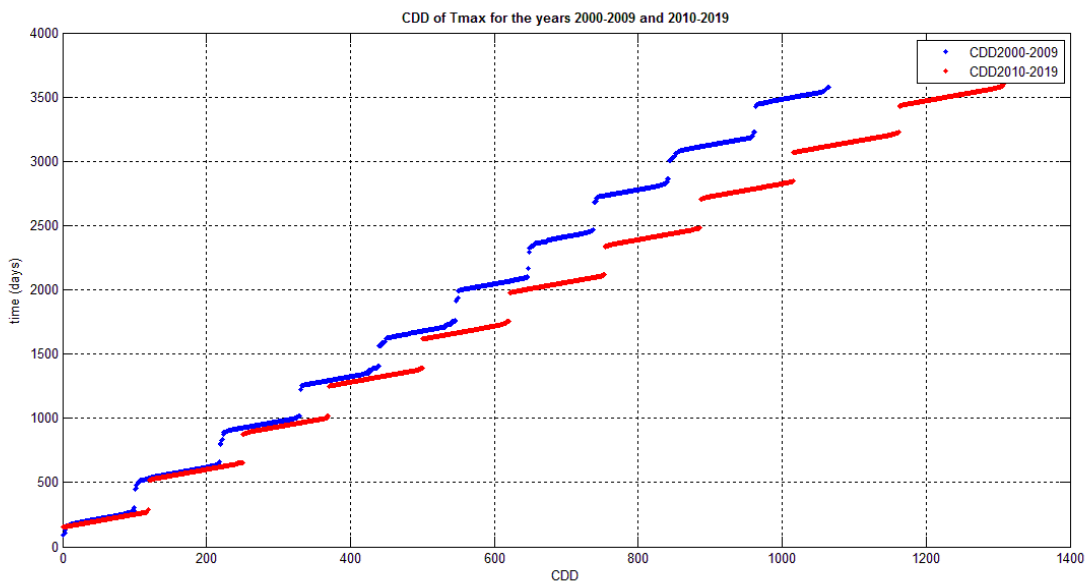
Figure 69. CDD of max daily temperatures for feed forward predicted (red, CDD=1307) and actual (blue, CDD = 1065) data.
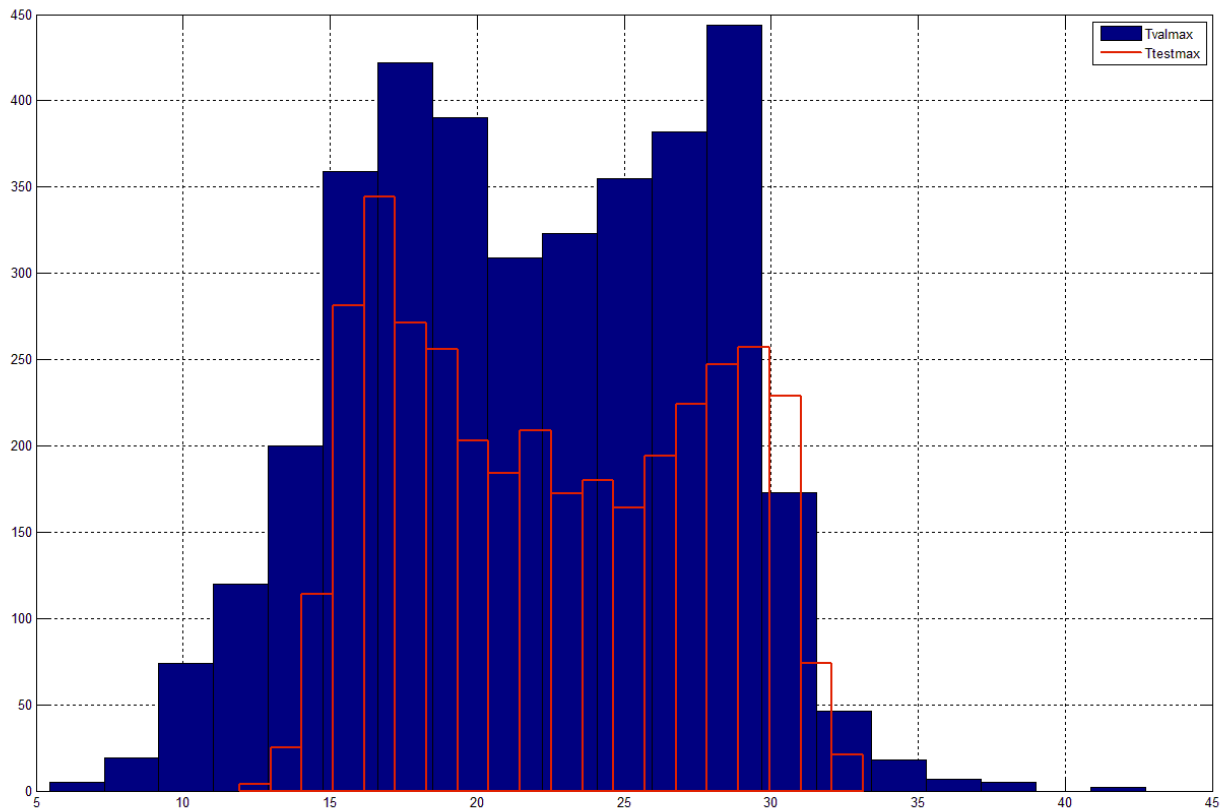
Figure 70. Actual daily mean-maximum and minimum temperature versus predicted temperature & frequency distribution of the maximum temperature.

As it can be seen in Table 16, the mean temperature of the next decade 2010-2019 raises to 20.17, from 18.75, 1.42 degrees higher than the previous decade. The mean maximum temperature also increases from 21.82 to 23.34, while the maximum temperature reaches the 33.94 °C, which is not accepted as an accurate result. The cooling degree days are increased exceedingly in relation to the last decade, i.e., 22.72%. We assume that the model perceives in an inordinate degree the temperature increase according to the last 40 years data, projecting much higher mean temperatures for the future. The maximum temperatures do not track the histogram of the previous data in Figure 70Figure 66.

4. Application in a typical office building in Crete

The rapidly growing world energy use has already raised concerns over supply difficulties, exhaustion of energy resources and heavy environmental impacts (ozone layer depletion, global warming, climate change, etc.). The International Energy Agency has gathered frightening data on energy consumption trends. During the last two decades (1984– 2004) primary energy has grown by 49% and CO_2 emissions by 43%, with an average annual increase of 2% and 1.8% respectively. Current predictions show that this growing trend will continue. Energy use by nations with emerging economies (Southeast Asia, Middle East, South America and Africa) will grow at an average annual rate of 3.2% and will exceed by 2020 that for the developed countries (North America, Western Europe, Japan, Australia and New Zealand) at an average growing rate of 1.1%. The case of China is striking, taking only 20 years to double its energy consumption at an average growing rate of 3.7%. Interesting consequences can be obtained from the analysis of the trend of main world energy indicators between 1973 and 2004:

→ The rate of population growth is well below the GDP, resulting in a considerable rise of per capita personal income and global wealth,

→ primary energy consumption is growing at a higher rate than population, leading to the increase of its per capita value on 15.7% over the last 30 years,

→ CO2 emissions have grown at a lower rate than energy consumption showing a 5% increase during this period,

→ electrical energy consumption has drastically risen (over two and a half times) leading to a percentage increase in final energy consumption, 18% in 2004,

→ efficiency in exploiting energy resources, shown as the relation between final and primary energy, has declined by 7% points, especially due to soaring electrical consumption, and

→ final and primary energy intensities have dropped because of the higher rate of growth of the GDP over the energy consumption increasing ratio, resulting in an overall improvement of the global energy efficiency. [51]

Densely built urban areas in warmer climates may suffer from the urban heat island (UHI) effect, resulting in, among others, higher urban temperatures in the city centers than in the surrounding rural or suburban areas. The air temperature in the cities can be as much as 5 ^{o}C higher than these other areas. The UHI effect has multiple negative effects: increased energy use for cooling and related CO2 emissions, abated air quality, human discomfort, physical and psychological health risks, alter local weather patterns. Therefore, UHI has a

major impact on the quality of people's life, environment and infrastructure and can be mitigated by better built and operated buildings.[52]

A building affects its surrounding environment, and conversely its indoor environment is influenced by its surroundings. In order to obtain a more accurate prediction of the indoor thermal environment, it is necessary to consider the interactions between the indoor and outdoor thermal environments. [53]

Approaches for assessing energy use in buildings

Computer programs which are used to generate an energy performance prediction from calculations.

IES, TAS, Energy Plus, **ESPr**, eQuest etc.

There exists a dynamic three-way interaction between climate, people and buildings dictates our energy needs in buildings:

People

Energy use is influenced by
Climatic, social, economic and
Cultural context

Climate   **Buildings**
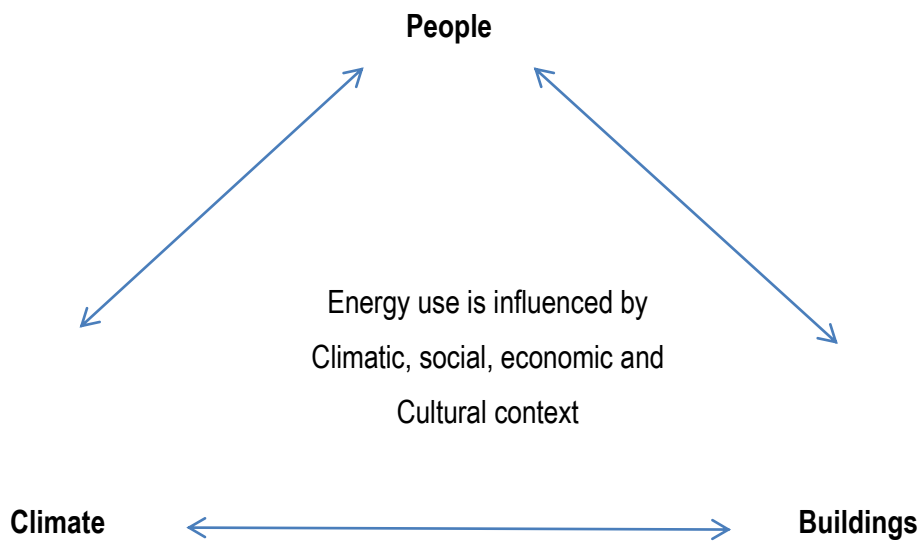
In the present case, the energy calculations are based on the predicted external temperature data, assuming that the other interactions, such as social behavior, economic conditions etc., remain constant.

ESP-r simulates building performance in a manner that:

a) is realistic and adheres closely to actual physical systems,

b) supports early-through-detailed design stage appraisals, and

c) enables integrated performance assessments in which no single issue is unduly prominent.

When hourly values are not available there are algorithms for generating hourly temperature values from daily values. These use the daily maximum temperature TMAX, and daily minimum temperature, TMIN [54]

The ESP-r energy modeling tool is ecploited for the building simulation and the calculation of the cooling and heating loads of a simple office building. ESP-r is a building simulation program which has been under development for more than 25 years. It is available at no cost under an Open Source license. ESP-r can simulate any element of the building envelope and the electrical-mechanical equipment for example rooms, stairways, doors, windows with different types of glass, internal-external or fixed or movable awnings, external

or internal walls etc. Users have the option to define the geometric complexity, and operational details of their models according to each project's requirements. The ESP-r operates through the information exchange between the sub models of the thermal zones, the air flow analysis between zones and within the area, the electricity and air flow systems etc., in order to take into account the interactions between the building's subsystems. At the same time it can cooperate with other modeling and simulation tools.
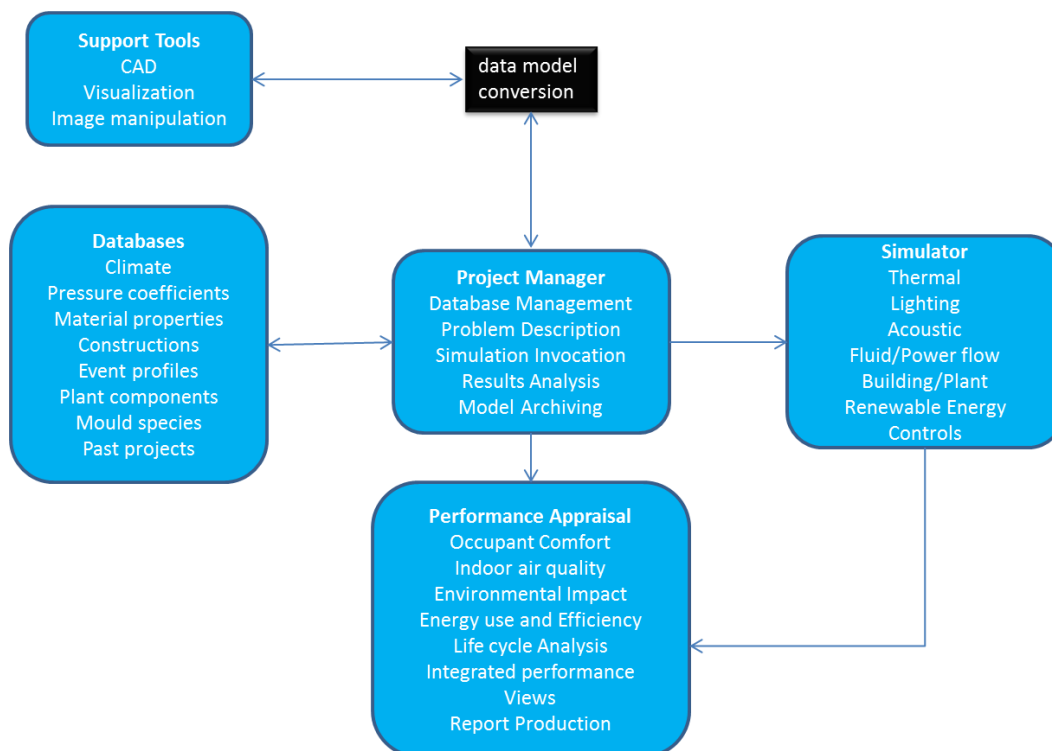
Figure 71. The principal components of the ESP-r system: a central project manager, an integrated simulator, support databases, a performance appraisal tool and support utilities for CAD and visualization

The following procedure is followed for a building simulation in ESP-r.

1. Thermal zones. Initially, the building is divided into zones which interact with each other as well as with the external environment. A thermal zone may consist of either a single space or a space module that operates under the same indoor climate. Each zone has independent heat gains and independent equipment and controls heating, cooling and ventilation. Finally, each zone can be linked to its neighboring areas through walls or other building elements with different thermal conductivities. The surfaces (horizontal and vertical) defined in the thermal zones, form the building model.

2. Thus, the simulation of the energy performance of a building requires knowledge of its dimensional and geometric characteristics of the orientation, thermal properties and radiation characteristics of the materials from which it is constructed.

3. Furthermore, a climate data record is defined. The selected data must provide hourly values for the following key climate parameters: total radiation (diffuse and direct), ambient temperature, wind direction and speed, total and diffuse light, relative humidity, air pressure and cloudiness.

ESP-r simulates building performance in a manner that: a) is realistic and adheres closely to actual physical systems, b) supports early-through-detailed design stage appraisals, and c) enables integrated performance assessments in which no single issue is unduly prominent.

ESP-r attempts to simulate the real world as rigorously as possible and to a level which is consistent with current best practice. By addressing all aspects simultaneously, ESP-r allows the designer to explore the complex relationships between a building's form, fabric, air flow, plant and control. ESP-r is based on a finite volume, conservation approach in which a problem (specified in terms of geometry, construction, operation, leakage distribution, etc.) is transformed into a set of conservation equations (for energy, mass, momentum, etc.) which are then integrated at successive time-steps in response to climate, occupant and control system influences. ESP-r comprises a central Project Manager around which are arranged support databases, a simulator, various performance assessment tools and a variety of third party applications for CAD, visualization and report generation.

In Table 17 the building characteristics are listed for the building model of the present study.

Table 17. Building characteristics

Type of Building	Office building		
Surface Area	80m^2		
Walls	Three layer brick-insulation-brick	Total Uvalue: 0.513W/m^{2}K	
Roof	Three layer plaster concrete insulation	Total Uvalue: 0.813W/m^{2}K	
Windows	North facing (33.33% coverage) double glazing windows	Uvalue: 0.505 W/m^{2}K	
Heating	Ideal load 3kW (set point 18.0^{o}C) from8:00 to 16:00		
Cooling	Ideal load 3kW (set point 26.0^{o}C) from8:00 to 16:00		
Casual gain Occupancy	0:00-8:00	0	0
	Time	Sensible (W)	Latent (W)
	8:00-12:00	225	165
	12:00-14:00	150	110
	14:00-16:00	225	165
	16:00-24:00	0	0
Small Power	8:00-16:00 258 (W) sensible		
Lights	10:00-14:00 288 (W) sensible		

	from November 1st - April		
Air changes per hour	0.3		

The ESP-r over other simulation software also offers higher accuracy utilizing methods of Computational Fluid Dynamics (CFD). By the use of CFD operating an internal space can be simulated with great precision. All the above functions (CFD, energy control systems, etc.) embedded in the program and does not require any use other third gear.

The ESP-r and can calculate a large set of different parameters on the building. Some of these are:

- Air temperature for each zone and surface

- Mean radiant temperature and dew point for each zone

- energy flow in the ground area:

→ infiltration

→ transfer air from adjacent zones

- Internal gains (heat):

→ Presence of people

→ Lighting

→ Device

→ For each surface (whole) but also on all surfaces together

- Energy flow for any surface because:

→ Education

→ Small, large (the building, sky) Wave Radiation

→ Storage

- Loads:

→ Sensible heat cooling, heating Load

→ Humidification-dehumidification

The building modeling methodology is divided in the following steps:

→ Developing the building in the ESP-r environment

→ Importing the structural characteristics

→ Setting the presence schedule

→ Importing the weather file

→ Setting the physical characteristics of the building materials

→ Setting the internal gains from users, lighting and equipment.
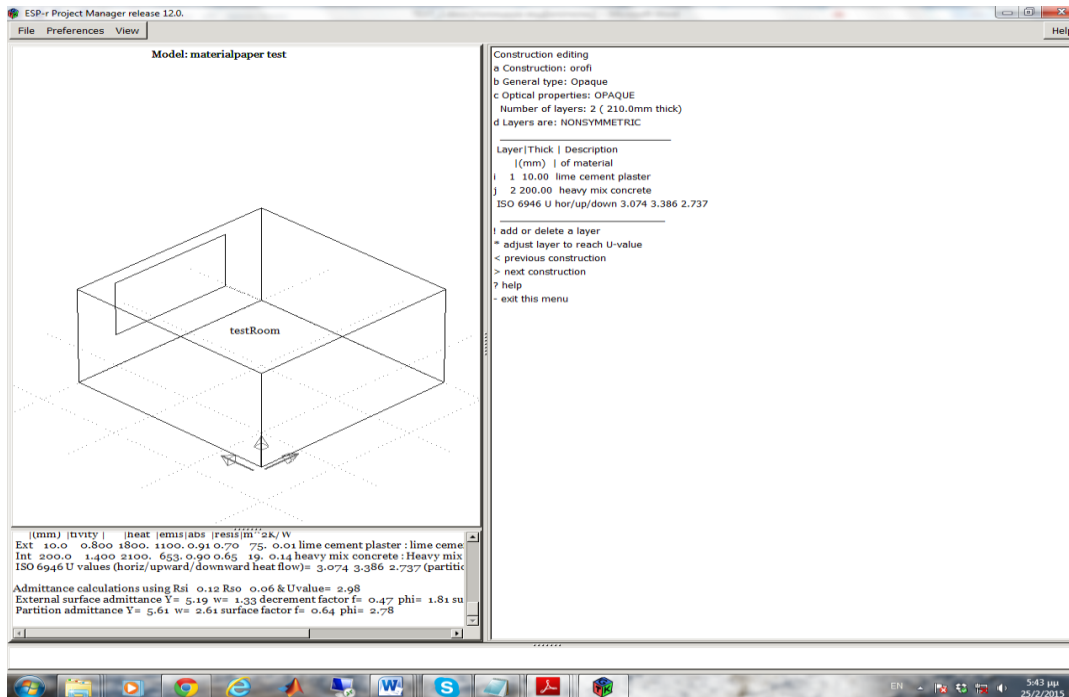
Figure 72. ESP-r model layout with the office building.

A model for prediction of the time temperature curve has been developed for the new forecast method. The temperature at each moment of the day is obtained using the prediction of the maximum and minimum daytime temperature. This provides various benefits when selecting the training days and in the training and forecasting phases, thus improving the relationship between expected consumption and temperatures. [50]

When hourly values are not available there are algorithms for generating hourly temperature values from daily values. These use the daily maximum temperature TMAX, and daily minimum temperature, TMIN [54]

$$T(t) = f_1 \cdot T_{MIN} + f_2 \cdot T_{MAX}$$

and
$$f_1 + f_2 = 1$$

where f_1 and f_2 are factors given in a table in the guide and T_{MIN} and T_{MAX} are the daily minimum and maximum temperatures respectively. These are related to sinusoidal interpolations and can be expressed more mathematically in the following equations:

for t<t$_{min}$:

$$f_1 = \frac{\cos\left(\frac{\pi(t_{min} - t)}{24} + t_{min} - t_{max}\right) + 1}{2}$$

Where t_{min} and t_{max} indicates the time corresponding to the maximum and minimum temperature of the day.

for $t_{min} < t < t_{max}$:

$$f_1 = \frac{\cos\left(\frac{\pi(t - t_{min})}{t_{max}} - t_{min}\right) + 1}{2}$$

for $t_{min} < t$:

$$f_1 = \frac{\cos\left(\frac{\pi(24 + t_{min} - t)}{24} + t_{min} - t_{max}\right) + 1}{2}$$

For a smoother transition between days the following equation was used:

$$T(t) = \left(\frac{Temp_{next} + Temp_{prev}}{2}\right) - \left(\frac{Temp_{next} - Temp_{prev}}{2}\right) \cdot \cos\left(\frac{\pi \cdot (t - t_{prev})}{(t_{next} - t_{prev})}\right)$$

Where Temp(next) is the next known temperature value, Temp(prev) is the previous known temperature value, t(next) the time for the next known temperature value, t(prev) the time for the previous known temperature value and t is the time. The hourly temperature data of a day with predicted Tmax = 15.75 °C and Tmin = 9.65 °C can be seen in Figure 73.
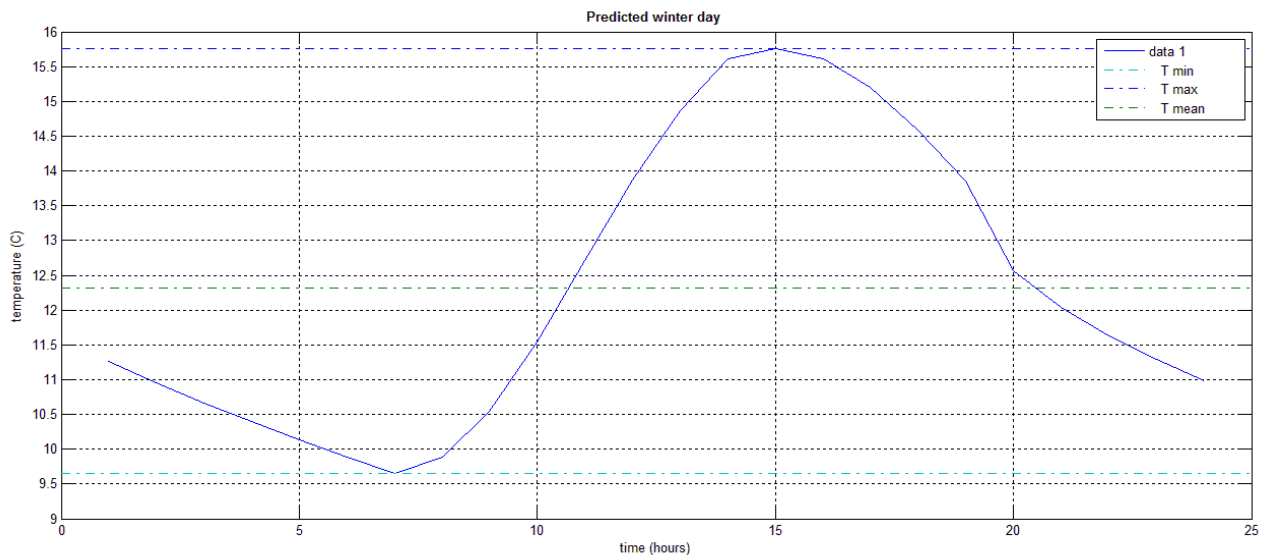

Figure 73. Hourly temperature values calculated according the maximum and minimum predicted temperature, in a winter day.

An algorithm in Matlab was developed for the calculation of the hourly temperature data taking as input the daily minimum and maximum previously predicted temperature data. Following, the weather files in the adequate format were created and inserted in the database of the ESP-r model.

First we begin with the calculation of the heating and cooling loads of the actual temperature data for the decade 2000-2009 Figure 74.
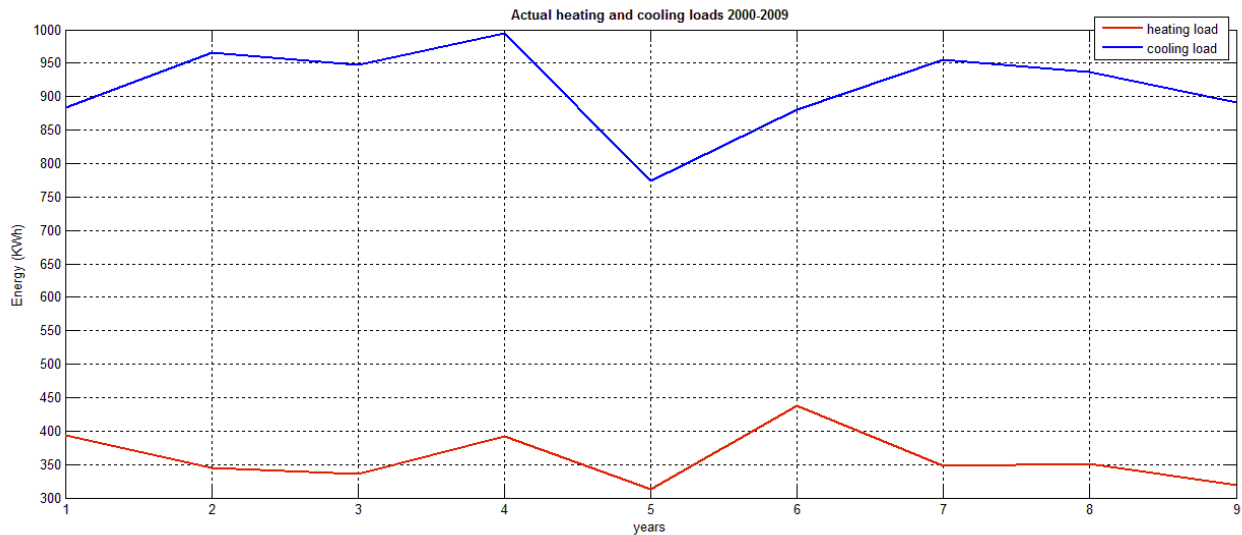
Figure 74. Actual heating and cooling loads of the decade 2000-2009

Then we proceed with the previously predicted temperature data, with the feed forward neural network. The internal temperature as it was calculated by the ESP-r model is shown in Figure 75. There exists a strong correlation between indoor and predicted outdoor temperature data. The high increase in the mean temperature is transferred in the internal building temperature.
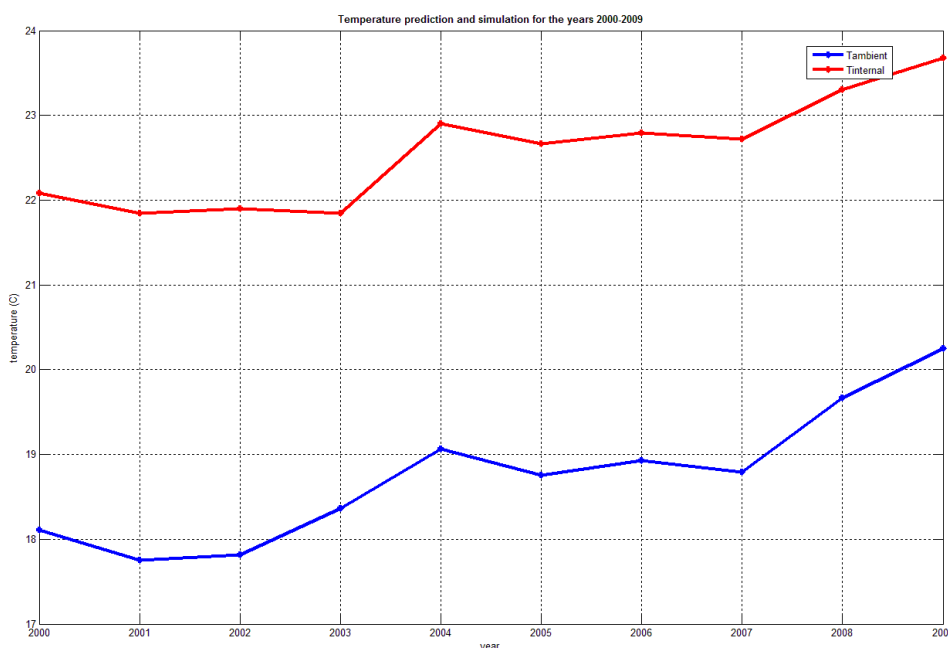
Figure 75 Outdoor and indoor mean yearly temperature of the decade 2000-2009 according to the feed forward network model predicted temperature data.

The reflection of the high temperature increase is fully represented in the models heating and cooling load calculations (Figure 76). There is an almost proportional increase in the cooling loads with the increase of the mean yearly temperature (Figure 75), while the opposite is observed regarding the heating loads which are inversely decreased. This cannot be considered as a representative result, ones the high increase in temperature and cooling loads is not realistic. As we see, the mean yearly temperature increase by 2°C in a decade, could result a full increase in the cooling loads by 30% (from 616kWh/year in 2000 to 916616kWh/year in 2009).
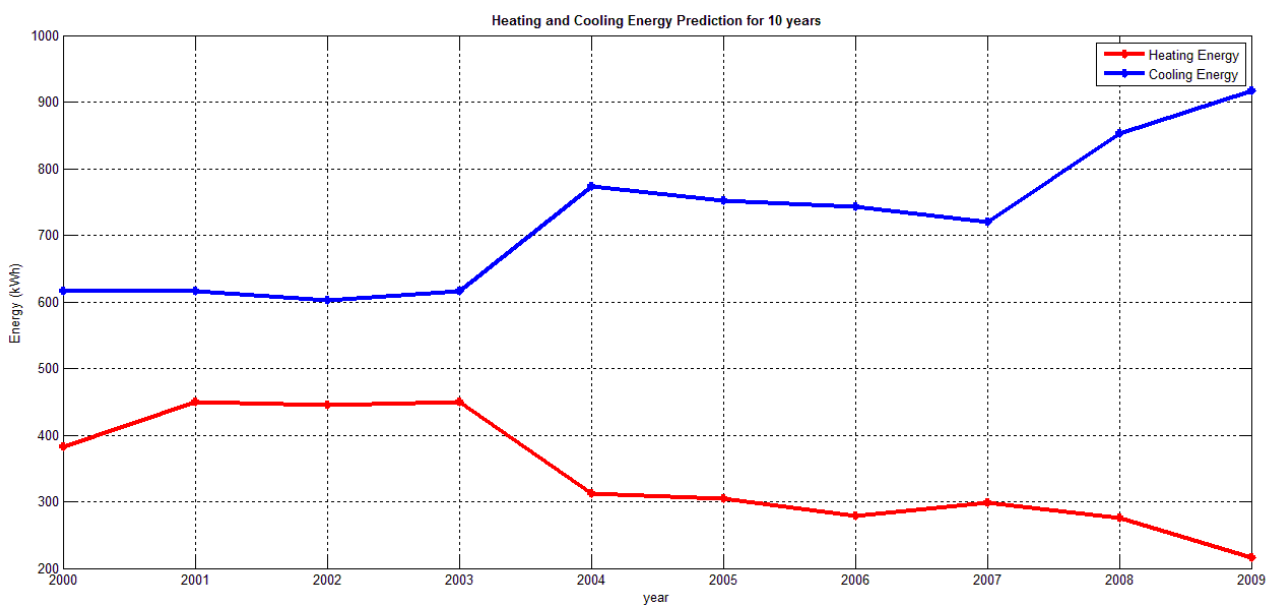

Figure 76. Heating and cooling loads of the decade 2000-2009 according to the feed forward network model predicted temperature data.

In Figure 77, there are the heating and cooling load calculations for the years 2000-2004, taking into account the NARX model developed and trained with 5-year training sets. As is can be seen, the heating load calculations resulted from the NARX model 5-year temperature prediction is closer to the actual energy consumption. Considering the cooling loads, there is an increase in the NARX model followed by a better correlation towards the actual ones. Nevertheless, the high cooling energy loads resulting from the actual temperature data, cannot be reached. This is due to the fact that there is lack in high temperature data, in our predictions, as this was already observed during the long term predictions using several types of neural networks. The small amount of higher temperatures in the training data sets, does not allow the accurate daily prediction of the upper temperatures, with result the underestimation of the cooling loads.
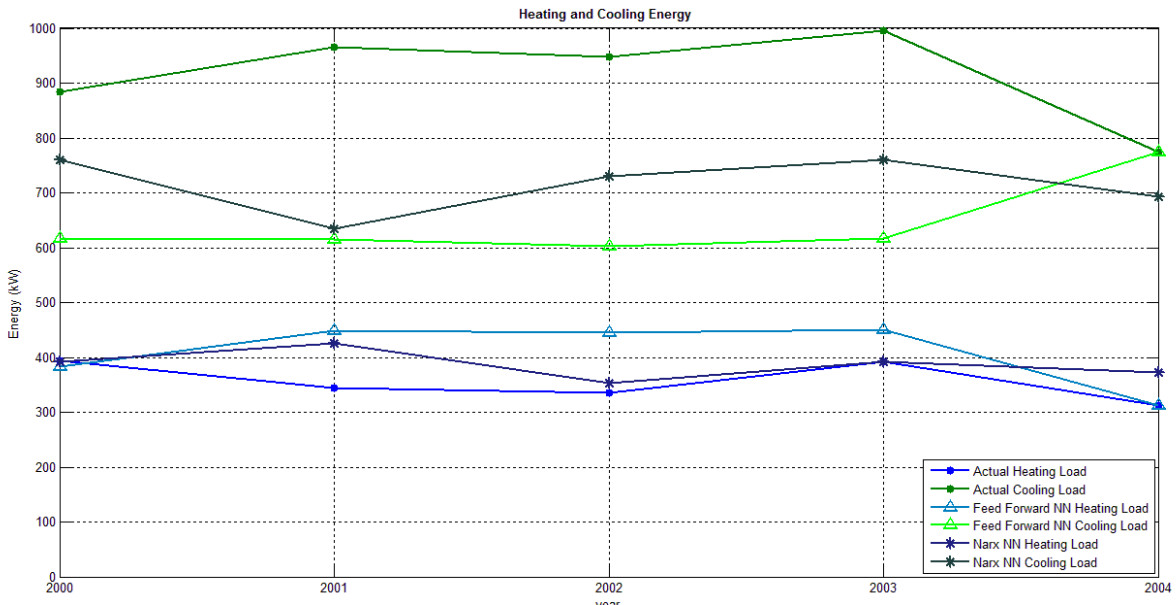
Figure 77. Prediction of Heating and Cooling Energy for the years 2000-2004

We proceed with the ten year calculation of the heating and cooling loads, taking into account the NARX model which gave the better results in the temperature prediction (Figure 49 to Figure 53). The ESP-r model results are depicted in Figure 78.
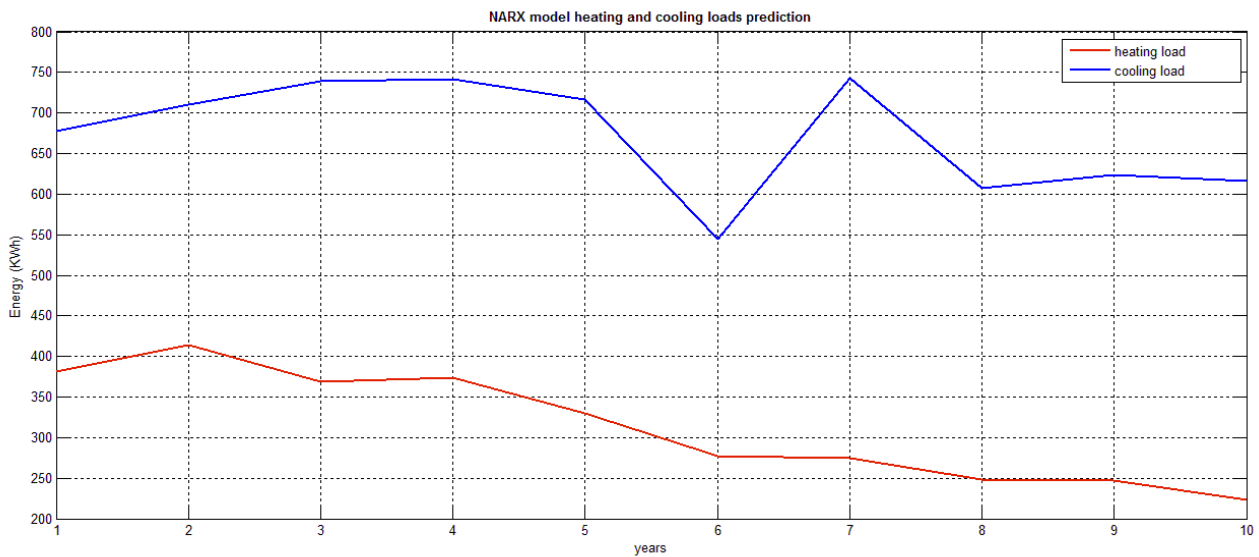

Figure 78. Heating and cooling loads of the decade 2010-2019 according to the NARX network model predicted temperature data.

5. Conclusions

This presented research work leads to the conclusion that outdoor air temperature prediction can be performed using neural networks, depending on the required statistical values. The performance of the neural networks has been evaluated using measurements collected from a local weather station in Heraklion. The annual performance is estimated using the statistical indicators R^2 and MSE, the mean, maximum and minimum temperature values of the predicted five or ten years period and the number of cooling degree days. The results indicate an acceptable performance of the neural networks to predict mean outdoor air temperature with a predictive horizon of 5-10 years. In terms of mean temperature data, the neural network can successfully approximate the temperature values and their seasonal variations. Furthermore, neural networks can fully simulate and predict the cooling degree days (set point 26 ^{o}C). Neural networks are proven appropriate for the forecasting of daily temperature time series based on previous minimum, maximum and mean temperatures. Nevertheless, it is, in general, difficult to define the learning rate of the developed neural network, as it is mostly acting like a "black box", with obvious inputs and outputs but with complex calculation procedures and intermediate correlations. Yet, neural networks are supreme mainly due to absence of other explanations of the perceived time series. Compared to the benchmark ARMA model, it is observed that neural networks can achieve better performances (R^2 and MSE) in the temperature data simulation.

The most suitable neural network is proved to be the nonlinear autoregressive network with exogenous inputs (NARX net). This is attributed to their dynamic learning capability, where the output is related with the previous inputs. The NARX network, as opposed to the feed forward networks, uses feedback connections with the previous data.

The one step long term (10 years) prediction resulted in a high trend followed by unrealistic temperature increases, which led subsequently to extreme cooling loads. For that reason, a subsequent prediction of temperature data is performed, for two five years periods. The first five years predicted values are used as an input for the forecasting of the second half of the decade 2010-2019.

Considering the building energy simulation model, a typical office building model is developed with good insulation characteristics. The ESP-r weather files are developed for the import of the predicted temperature data in the developed model. All results indicate a better correspondence of the model regarding the heating loads. The cooling loads did follow the fluctuations of the actual data, but were underrated because of the smaller predicted maximum temperature values.

Regarding further research in the area, the physical properties of the higher temperatures should be considered, by the development of an enhanced forecasting model. The forecasting study should either be focused on the degree days or on the individual minimum and maximum temperatures. As it is observed, in case of the degree days estimation, the neural networks are acceptable, because the study is handling an

unspecified set of temperature values above or under a set-point. But, when looking closer to the predicted ensemble over this set-point, the neural networks did not accomplish to "understand" the higher temperature variations resulting from the physical phenomena occurring in the surface layer and in urban environments. More investigation is needed for this prediction, which could be conducted integrating somehow the physical properties of temperature variations and probably followed by longer training intervals. Mesoscale modelling coupled with neural network models can be a challenging perspective for the combination of the physical characteristics of the boundary layer with modern computational techniques.

6. References

[1]   B. L. Meteorology and L. Prandtl, "A . Introduction to the Atmospheric Boundary Layer (ABL)," 2008. [Online]. Available: http://www.met.rdg.ac.uk/~swrhgnrj/teaching/MT36E/MT36E_BL_lecture_notes.pdf.

[2]   Vijek, "Velocity and Temperature boundary layer similarity - Boundary layer - Wikipedia, the free encyclopedia," *Created using Microsoft Powerpoint basedPreviously published: N/A. Licensed under CC BY-SA 3.0 via Wikimedia Commons*. [Online]. Available: http://commons.wikimedia.org/wiki/File:Velocity_and_Temperature_boundary_layer_similarity.png#medi aviewer/File:Velocity_and_Temperature_boundary_layer_similarity.png.

[3]   I. N. Harman, "Department of Meteorology The energy balance of urban areas," no. October, 2003.

[4]   V. C. K. Kakane and E. K. Agyei, "Determination of Surface Fluxes Using a Bowen Ratio System," vol. 9, 2006.

[5]   A.J.Dyer, "A review on flux profile relationships," *Csiro Div. Atmos. Physics, Aspendale, Victoria, Aust.*, vol. 7, pp. 363–372, 1974.

[6]   W. Kuttler, "Climate Change on the Urban Scale – Effects and Counter-Measures in Central Europe," in *Human and Social Dimensions of Climate Change*, vol. C, no. Table 1, N. Chhetri, Ed. CC BY 3.0 license. © The Author(s), 2012.

[7]   U.S. Environmental Protection Agency's Office of Atmospheric Programs, "Reducing Urban Heat Islands : Compendium of Strategies Urban Heat Island Basics," 2008.

[8]   M. K. Svensson and I. Eliasson, "Diurnal air temperatures in built-up areas in relation to urban planning," *Landsc. Urban Plan.*, vol. 61, no. 1, pp. 37–54, Sep. 2002.

[9]   H. Taha, D. Sailor, and S. Municipal, "High-Albedo Materials for Reducing Building Cooling Energy Use.," *Energy Environ. Div. Lawrence Berkeley Lab.*, 1992.

[10]   "Heat Island," *NASA_GHCC Project Atlanta*, 1999. [Online]. Available: http://weather.msfc.nasa.gov/urban/urban_heat_island.html.

[11]   T. R. O. J.A. Voogt, "Complete Urban Surface Temperatures," *Appl. Meteorol.*, vol. 36, pp. 1117–1132, 1997.

[12]   S.-B. Duan, Z.-L. Li, N. Wang, H. Wu, and B.-H. Tang, "Evaluation of six land-surface diurnal temperature cycle models using clear-sky in situ and satellite data," *Remote Sens. Environ.*, vol. 124, pp. 15–25, Sep. 2012.

[13]   F. Go, "Modelling of diurnal cycles of brightness temperature extracted from METEOSAT data," vol. 76, 2001.

[14]   A. Soux, J. A. Voogt, and T. R. Oke, "A MODEL TO CALCULATE WHAT A REMOTE SENSOR ' SEES ' OF AN," pp. 109–132, 2004.

[15]   E. al. János Unger, Tamás Gál, "AIR TEMPERATURE VERSUS SURFACE TEMPERATURE IN URBAN ENVIRONMENT," in *The seventh International Conference on Urban Climate, 29 June - 3 July, Yokohama, Japan*, 2009.

[16]   C. E. P. Brooks, "A period of warm winters in Europe," *Mon. Weather Rev.*, p. 29, 1923.

[17]   "The Modern Temperature Trend." [Online]. Available: http://www.aip.org/history/climate/20ctrend.htm#N_2_.

[18]   S. Shahid, S. Bin Harun, and A. Katimon, "Changes in diurnal temperature range in Bangladesh during the time period 1961–2008," *Atmos. Res.*, vol. 118, pp. 260–270, Nov. 2012.

[19]   T. Likso, "Diurnal Variation of Air Temperature in the Atmospheric Surface Layer," *Meteorol. Hydrol. Serv.*, vol. 71, no. 3, pp. 87–93.

[20]   D. R. Easterling, B. Horton, P. D. Jones, T. C. Peterson, T. R. Karl, D. E. Parker, M. J. Salinger, V. Razuvayev, N. Plummer, P. Jamason, and C. K. Folland, "Maximum and Minimum Temperature Trends for the Globe," vol. 277, no. July, pp. 364–367, 1997.

[21]   U. of C. Scientists, "Global Warming Effects on Food," 2011. [Online]. Available: http://www.climatehotmap.org/global-warming-effects/food.html. [Accessed: 02-Feb-2014].

[22]   J. Kapsomenakis, D. Kolokotsa, T. Nikolaou, M. Santamouris, and S. C. Zerefos, "Forty years increase of the air ambient temperature in Greece: The impact on buildings," *Energy Convers. Manag.*, vol. 74, pp. 353–365, Oct. 2013.

[23]   I. Eliasson, "The use of climate knowledge in urban planning," *Landsc. Urban Plan.*, vol. 48, pp. 31–44, 2000.

[24]   D. H. W. Li, L. Yang, and J. C. Lam, "Impact of climate change on energy use in the built environment in different climate zones – A review," *Energy*, vol. 42, no. 1, pp. 103–112, Jun. 2012.

[25]   M. Christenson, H. Manz, and D. Gyalistras, "Climate warming impact on degree-days and building energy demand in Switzerland," *Energy Convers. Manag.*, vol. 47, pp. 671–686, 2006.

[26]   K. Pilli-Sihvola, P. Aatola, M. Ollikainen, and H. Tuomenvirta, "Climate change and electricity consumption-Witnessing increasing or decreasing use and costs?," *Energy Policy*, vol. 38, no. 5, pp. 2409–2419, 2010.

[27]   a. R. Day, P. G. Jones, and G. G. Maidment, "Forecasting future cooling demand in London," *Energy Build.*, vol. 41, pp. 942–948, 2009.

[28]   C. Cartalis, a. Synodinou, M. Proedrou, a. Tsangrassoulis, and M. Santamouris, "Modifications in energy demand in urban areas as a result of climate changes: An assessment for the southeast Mediterranean region," *Energy Convers. Manag.*, vol. 42, pp. 1647–1656, 2001.

[29] S. Mirasgedis, Y. Sarafidis, E. Georgopoulou, V. Kotroni, K. Lagouvardos, and D. P. Lalas, "Modeling framework for estimating impacts of climate change on electricity demand at regional level: Case of Greece," *Energy Convers. Manag.*, vol. 48, pp. 1737–1750, 2007.

[30] M. Santamouris, N. Papanikolaou, I. Livada, I. Koronakis, C. Georgakis, a Argiriou, and D. . Assimakopoulos, "On the impact of urban climate on the energy consumption of buildings," *Sol. Energy*, vol. 70, no. 3, pp. 201–216, 2001.

[31] S. Hassid, M. Santamouris, N. Papanikolaou, a. Linardi, N. Klitsikas, C. Georgakis, and D. N. Assimakopoulos, "Effect of the Athens heat island on air conditioning load," *Energy Build.*, vol. 32, no. June 1997, pp. 131–141, 2000.

[32] J. G. Carter, G. Cavan, A. Connelly, S. Guy, J. Handley, and A. Kazmierczak, "Climate change and the city: Building capacity for urban adaptation," *Prog. Plann.*, Jul. 2014.

[33] S. Papantoniou, D. Kolokotsa, and A. Pouliezos, "Neuro-fuzzy model based predictive algorihm for environmental management of buildings." 3rd International Conference on Industrial and Hazardous Waste Management, Chania, pp. 1–8, 2012.

[34] A. H. Nury, M. Koch, and M. J. B. Alam, "Time Series Analysis and Forecasting of Temperatures in the Sylhet Division of Bangladesh," pp. 1–4, 2011.

[35] G. Jürgen, Kirchgässner Wolters, *Introduction to Modern Time Series Analysis*. Springer, 2007.

[36] I. Rojas, O. Valenzuela, F. Rojas, a. Guillen, L. J. Herrera, H. Pomares, L. Marquez, and M. Pasadas, "Soft-computing techniques and ARMA model for time series prediction," *Neurocomputing*, vol. 71, no. 4–6, pp. 519–537, Jan. 2008.

[37] M. Ghiassi, H. Saidane, and D. K. Zimbra, "A dynamic artificial neural network model for forecasting time series events," *Int. J. Forecast.*, vol. 21, pp. 341–362, 2005.

[38] F. Tseng, H. Yu, and G. Tzeng, "Combining neural network model with seasonal time series ARIMA model," vol. 69, no. 12, pp. 71–87, 2002.

[39] H. K. Elminir, Y. a. Azzam, and F. I. Younes, "Prediction of hourly and daily diffuse fraction using neural network, as compared to linear regression models," *Energy*, vol. 32, no. 8, pp. 1513–1523, Aug. 2007.

[40] H. N. Koivo, "NEURAL NETWORKS : Basics using MATLAB Neural Network Toolbox By," pp. 1–59, 2008.

[41] W. Duch and N. Jankowski, "Transfer functions : hidden possibilities for better neural networks .," no. April, pp. 81–94, 2001.

[42] L. Suganthi and A. a. Samuel, "Energy models for demand forecasting—A review," *Renew. Sustain. Energy Rev.*, vol. 16, no. 2, pp. 1223–1240, Feb. 2012.

[43] A. L. S. Maia, F. D. a. T. de Carvalho, and T. B. Ludermir, "Forecasting models for interval-valued time series," *Neurocomputing*, vol. 71, no. 16–18, pp. 3344–3352, Oct. 2008.

[44]   G. P. Zhang, "Time series forecasting using a hybrid ARIMA and neural network model," *Neurocomputing*, vol. 50, pp. 159–175, Jan. 2003.

[45]   C. N. Babu and B. E. Reddy, "A moving-average filter based hybrid ARIMA–ANN model for forecasting time series data," *Appl. Soft Comput.*, vol. 23, pp. 27–38, Oct. 2014.

[46]   World Meteorogical Organization, "2014 on course to be one of hottest, possibly hottest, on record," *Press Release No. 1009*, 2014. [Online]. Available: http://www.wmo.int/pages/mediacentre/press_releases/pr_1009_en.html. [Accessed: 04-Feb-2015].

[47]   K. Gobakis, D. Kolokotsa, a. Synnefa, M. Saliari, K. Giannopoulou, and M. Santamouris, "Development of a model for urban heat island prediction using neural network techniques," *Sustain. Cities Soc.*, vol. 1, no. 2, pp. 104–115, Jul. 2011.

[48]   I. Kaastra and M. Boyd, "Designing a neural network for forecasting financial and economic time series," *Neurocomputing*, vol. 10, no. 3, pp. 215–236, Apr. 1996.

[49]   A. W. Moore, "Regression and Classification with Neural Networks," 2003.

[50]   C. Roldán-Blay, G. Escrivá-Escrivá, C. Álvarez-Bel, C. Roldán-Porta, and J. Rodríguez-García, "Upgrade of an artificial neural network prediction method for electrical consumption forecasting using an hourly temperature curve model," *Energy Build.*, vol. 60, pp. 38–46, May 2013.

[51]   L. Pérez-Lombard, J. Ortiz, and C. Pout, "A review on buildings energy consumption information," *Energy Build.*, vol. 40, no. 3, pp. 394–398, Jan. 2008.

[52]   D. Urge-Vorsatz, K. Petrichenko, M. Staniec, and J. Eom, "Energy use in buildings in a long-term perspective," *Curr. Opin. Environ. Sustain.*, vol. 5, no. 2, pp. 141–151, Jun. 2013.

[53]   J. He, A. Hoyano, and T. Asawa, "A numerical simulation tool for predicting the impact of outdoor thermal environment on building energy performance," *Appl. Energy*, vol. 86, no. 9, pp. 1596–1605, Sep. 2009.

[54]   D. H. C. Chow and G. J. Levermore, "New algorithm for generating hourly temperature values using daily maximum, minimum and average values from climate models," *Build. Serv. Eng. Res. Technol.*, vol. 28, no. 3, pp. 237–248, Aug. 2007.